Rosa Monteiro

Writing 3D *in vitro* models of human tendon within a biomimetic fibrillar support platform

UMinho | 2022

Universidade do Minho
Escola de Engenharia
Instituto de Investigação em Biomateriais,
Biodegradáveis e Biomiméticos

Rosa da Conceição Freitas Monteiro

Writing 3D *in vitro* models of human tendon within a biomimetic fibrillar support platform

julho de 2022

Universidade do Minho
Escola de Engenharia
Instituto de Investigação em Biomateriais,
Biodegradáveis e Biomiméticos

Rosa da Conceição Freitas Monteiro

Writing 3D *in vitro* models of human tendon within a biomimetic fibrillar support platform

Dissertação de Mestrado

Ciclo de Estudos Conducentes ao Grau de Mestre em

Engenharia Biomédica

Ramo Biomateriais, Reabilitação e Biomecânica

Trabalho efetuado sob a orientação de

Professora Doutora Maria Manuela Estima Gomes

e co-orientação de

Doutor Rui Miguel Andrade Domingues

julho de 2022

Agradecimentos

Chegada ao final desta longa jornada, não posso deixar de agradecer a todos os que contribuíram para a concretização e realização deste projeto.

Antes de mais, agradeço ao Professor Rui Reis pela oportunidade e privilégio de desenvolver a minha dissertação no Instituto de Investigação em Biomateriais, Biodegradáveis e Biomiméticos (I3Bs), da Universidade do Minho.

Agradeço à minha orientadora, Professora Manuela Gomes, pela oportunidade de desenvolver a dissertação sob sua orientação, e integrar esta equipa de investigação fantástica. Obrigada pela sua confiança, e por todo o seu tempo e disponibilidade!

Ao meu coorientador, Rui Domingues, pela gigantesca paciência e disponibilidade para me tirar todas as dúvidas, mesmo que pela milésima vez. Serei eternamente grata por todo o conhecimento que me transmitiu, por me ter acompanhado ao longo de todo este percurso, por me ajudar sempre a encontrar uma solução, mesmo quando parecia não haver nada a fazer, e claro, pelas horas exaustivas no confocal, que quase sempre acabaram por valer muito a pena!

Um agradecimento ao projeto MagTendon que financiou todo este projeto de investigação.

A todos os colegas do laboratório com quem tive a oportunidade de trabalhar! À Eduarda, pela boa disposição e por estar sempre pronta para ajudar e a dar força e motivação para continuar em frente. A todo o staff I3Bs, mas em especial à Teresa, por estar sempre lá para me ajudar e para alegrar o dia.

À Mahwish, para quem não chegam as palavras para agradecer tudo o que fez por mim. Obrigada por me teres transmitido tudo o que sei hoje! Obrigada por estares sempre lá para mim e por nunca te queixares, mesmo quando já não aguentavas estar de pé após infinitas horas de trabalho. (NÃO) Vou ter saudades das nossas noitadas até às 6 h da manhã, mas que valeram muito a pena, e que sem elas este trabalho não estaria concluído.

À Library Crew, por todos os momentos de boa disposição e desabafos. Obrigada por estarem sempre lá para me animarem e darem uma palavra de motivação. Ao João Pedro, Margarida e Mário, e à nova geração, Diogo e Filipa, levo-vos comigo, e espero que a vida vos sorria muito!

A todos os professores que passaram pelo meu percurso, desde o primeiro ano da primária até ao último ano da universidade. Foram vocês que construíram em mim, desde pequenina, esta vontade

de explorar e ir mais além, sem nunca ficar satisfeita. São vocês que constroem os bons profissionais que nos tornamos um dia, cada um com o seu pequeno ou grande contributo.

Ao Marc, por ter sido o meu pilar ao longo deste percurso, por me motivar cada dia a seguir os meus sonhos com garra e determinação, sem nunca baixar os braços. Obrigada por me dares sempre a mão e me puxares para cima, principalmente quando eu não me conseguia levantar sozinha.

Às minhas irmãs, que sempre foram à minha frente a mostrar-me o melhor caminho a seguir (ou até mesmo o que não seguir), porque é isso o que as irmãs mais velhas fazem.

Aos meus pais, que com tanto esforço e dedicação conseguiram que eu alcançasse tudo aquilo que tenho hoje, e que sempre me apoiaram em todo o percurso da minha vida sem que nada me faltasse. Sem eles, nada disto seria possível. Um infinito obrigada!

E por fim, às minhas duas estrelinhas mais brilhantes que sempre torceram por mim, mas que infelizmente partiram este ano sem me poderem ver concluir esta etapa. À minha avó de coração, que sempre me apoiou e deu motivação para continuar, e que me deu forças para nunca desistir, mesmo quando as coisas pareciam muito difíceis. E ao meu melhor amigo Rui, que cresceu comigo, foi o meu parceiro de carteira e da vida, e que a vida nos decidiu tirar num ato tão injusto e cruel mesmo depois de tanta luta. Sei que onde vocês os dois estiverem, estão muito orgulhosos e vão continuar a cuidar de mim em todas as fases da minha vida.

Foram várias as batalhas e turbulências que tive de enfrentar durante o desenvolvimento desta dissertação. Foram duras perdas pessoais, e quando começava a ver luz ao fundo do túnel um problema de saúde que me deixou temporariamente imobilizada e que muito me assustou. Mas Deus não nos dá um fardo maior do que aquele que podemos carregar, e esta dissertação é a prova de que com muita dedicação, resiliência, e rodearmo-nos de pessoas boas é a chave para o sucesso, e que em momento algum devemos baixar os braços. É com nostalgia que termino desta longa viagem que tanto me fez crescer e evoluir, tanto a nível pessoal como profissional, e que culminou neste bonito projeto do qual me orgulho tanto.

"Põe quanto és, no mínimo que fazes"

DECLARAÇÃO DE INTEGRIDADE

Declaro ter atuado com integridade na elaboração do presente trabalho académico e confirmo que não recorri à prática de plágio nem a qualquer forma de utilização indevida ou falsificação de informações ou resultados em nenhuma das etapas conducente à sua elaboração.
Mais declaro que conheço e que respeitei o Código de Conduta Ética da Universidade do Minho.

STATEMENT OF INTEGRITY

I hereby declare having conducted this academic work with integrity. I confirm that I have not used plagiarism or any form of undue use of information or falsification of results along the process leading to its elaboration.
I further declare that I have fully acknowledged the Code of Ethical Conduct of the University of Minho.

Resumo

As patologias do tendão são doenças altamente debilitantes, para as quais os tratamentos atuais permanecem desafiadores e têm resultados de recuperação pouco relevantes. Deste modo, modelos *in vitro* relevantes, que permitam o estudo da tendinopatia e a testagem de novas abordagens regenerativas para desenvolver melhores tratamentos são altamente necessários. Neste trabalho, propomos o fabrico automatizado de sistemas microfisiológicos bioimpressos em 3D (MPS), incorporados numa plataforma de suporte fibrilar biomimética baseada na automontagem de nanocristais de celulose (CNCs). A matriz extracelular descelularizada do tendão (dECM) foi usada para produzir biotinta que recapitula de perto as pistas biofísicas e bioquímicas do nicho de células do tendão e, assim, autoinduz a diferenciação tenogénica de células-estaminais derivadas do tecido adiposo humano (hASCs). Dois MPS foram desenvolvidos: um sistema de monocultura que recria os padrões celulares e o fenótipo do tendão; e um sistema multicelular, com a incorporação de células endoteliais para estudar a comunicação entre o tendão e o sistema vascular, que desempenha papéis críticos na tendinopatia e no desenvolvimento do tendão. Ambos os MPS mostraram alta viabilidade celular, proliferação e alinhamento durante a cultura até 21 dias, e o hidrogel de dECM induziu a diferenciação de células-estaminais em direção à linhagem tenogénica, mostrado pela expressão de marcadores relacionados com o tendão, como Scleraxis (SCX) e Tenomodulin (TNMD). Notavelmente, as células endoteliais migram em direção ao compartimento do tendão, mostrando a atração química existente entre os dois compartimentos, mas não o invadiram. A comunicação com células endoteliais parece aumentar a diferenciação tenogénica das hASCs. No geral, o sistema proposto pode ser promissor para o fabrico automatizado de modelos organotípicos de tendão-num-chip que será uma nova ferramenta valiosa para estudar a fisiologia e as patologias do tendão, bem como o efeito de medicamentos para o tratamento de tendinopatias.

Palavras-chave: Matriz extracelular descelularizada, nanocristais de celulose, tendão-num-chip, tendinopatia, sistemas microfisiológicos

Abstract

Tendon pathologies are highly debilitating diseases, for which current treatments remains challenging, and has poor recovery outcomes. Therefore, relevant *in vitro* models allowing to study tendinopathies and test new regenerative approaches to develop better treatments are highly needed. Here we propose the automated fabrication of 3D bioprinted microphysiological systems (MPS) embedded into a biomimetic fibrillar support platform based on self-assembling of cellulose nanocrystals (CNCs). Tendon decellularized extracellular matrix (dECM) was used to produce bioink that closely recapitulate the biophysical and biochemical cues of tendon cell niche, and thus self-induce the tenogenic differentiation of human adipose derived stem cells (hASCs). Two MPS were developed: a monoculture system that recreates the cellular patterns and phenotype of tendon core; and a multicellular system, incorporating endothelial cells to study the crosstalk between the tendon and the vascular compartments, which plays critical roles in tendinopathy and tendon development. Both MPS showed high cell viability, proliferation, and alignment during culture up to 21 days, and the dECM hydrogel induced stem cell differentiation towards tenogenic lineage, as shown by the expression of tendon-related markers such as Scleraxis (SCX) and Tenomodulin (TNMD). Remarkably, endothelial cells migrate towards tendon compartment, showing the existing chemoattraction between the two compartments, but did not invade it. The crosstalk with endothelial cells seem to boost hASCs tenogenesis. Overall, the proposed system might be promising for the automated fabrication of organotypic tendon-on-chip models that will be a valuable new tool to study tendon physiology and pathologies, as well as the effect of drugs for the treatment of tendinopathy.

Keywords: Decellularized extracellular matrix, cellulose nanocrystals, tendon-on-chip, tendinopathy, microphysiological systems

Table of contents

List of abbreviations

#	
%	Percentage
3D	Three Dimensional
α-MEM	Alpha minimum essential medium
°	Degree
°C	Degree Celsius
µm	Micrometer
µL	microliter
A	
A/A	Antibiotic/Antimycotic
AA	Acetic Acid
AB	Alcian Blue
ASCs	Adipose Tissue-Derived Stem Cells
ATCC	NIH 3T3 murine embryonic fibroblast cells
B	
BMSCs	Bone marrow derived stem cells
BSA	Bovine Albumin Serum
C	
Ca	Calcium
$CaCl_2$	Calcium Chloride
CAD	Computer-Aided Design
CD31	Cluster of differentiation 31
CLM	Confocal laser microscopy
CNCs	Cellulose Nanocrystals
CO2	Carbon Dioxide
COL1A1	Alpha-1 type I collagen
COL3A1	Alpha-1 type III collagen
Cps	Cycles per second
D	
d	Day
DAPI	4,6 Diamidino - 2 - Phenylindole
dECM	Decellularized Extracellular Matrix
DI	deionized water
DMEM	Dulbecco's Modified Medium
DNA	Deoxyribonucleic Acid
DNase	Deoxyribonuclease
dsDNA	Double Stranded Deoxyribonucleic
E	
EDTA	Ethylenediamine tetraacetic acid
EGF	Epithelial Growth Factor
ECM	Extracellular matrix
F	
F	Forward Primer
FBS	Fetal Bovine Serum
FGF	Fibroblast Growth Factor
FITC	Fluorescein isothiocyanate
G	
g	Grams
G	Gravitational Force Unit
GAGs	Glycosaminoglycans
GAPDH	Glyceraldehyde phosphate dehydrogenase
GELMA	Gelatin Methacryloyl
GF	Growth Factors
H	
h	Hour
H&E	Hematoxylin and Eosin

hASCs	Human Adipose Derived Stem Cells
HCl	Hydrochloric acid
hTDCs	Human Tendon Derived Cells
HUVECs	Human Umbilical Vein Endothelial Cells
Hz	Hertz

I

ICC	Immunocytochemistry
IGF	Insulin Growth Factor

K

kDa	Kilodalton
kV	Kilovolts

M

M	Molar
MCC	Microcrystalline Cellulose
mg	Miligrams
Mg^{2+}	Magnesium ion
min	Minutes
mL	mililiters
mM	millimolar
MPS	Microphysiological Systems
MSCs	Mesenchymal Stem Cells
MT	Mason's Trichrome
MWCO	Molecular Weight Cut-Off

N

NaCl	Sodium Chloride
NaOH	Sodium Hydroxide
ng	Nanograms
nm	Nanometers

O

OoC	Organ-On-Chip

P

PAA	Peracetic Acid
PBS	Phosphate Buffered Saline
PCL	Polycaprolactone
PCR	Polymerase Chain Reaction
PDGF	Platelet Derived Growth Factor
PDMS	Polydimethylsiloxane
PEG	Poly(Ethylene Glycol)
PI	Propidium Iodide
PL	Platelet Lysate
PMSF	Phenylmethylsulphonyl fluoride

R

R	Reverse Primer
RNA	Ribonucleic Acid
RNase	Ribonuclease
rpm	Revolutions per minute
RT	Room temperature
RT-PCR	Reverse Transcriptase PCR

S

s	Seconds
SCX	Scleraxis bHLH transcription factor
SDS	Sodium Dodecyl Sulphate
SEM	Scanning Electron Microscopy
SRP	Sirius Red Picrate
stl	Stereolithograthy file format

T

TDCs	tendon-derived stem cells
TERM	Tissue Engineering and Regenerative Medicine
TGF-β	Transforming Growth Factor Beta
TnBP	tri-n-butyl phosphate
TNC	Tenascin-C

TNMD	Tenomodulin

V

V/mL	Volume Per Milliliters
v/v	Volume concentration (volume per volume)
VEGF	Vascular Endothelial Growth Factor
VEGF-A	Vascular Endothelial Growth Factor-A

W

w/v	Mass Concentration (weight per volume)
wt. %	weight percent

List of Figures

Chapter I. General Introduction

Chapter II. Materials and Methods

Chapter III. Writing 3D in vitro models of human tendon within a biomimetic fibrillar support platform

List of Tables

Chapter I. General Introduction

Chapter II. Materials and Methods

Chapter I.

General Introduction

Chapter I. General Introduction

Chapter I. General Introduction

I.1. Tendon physiology and pathology

Tendon is a highly and dense organized tissue that connects the muscle to the bone and is subjected to extreme mechanical forces during its activity [1]. Tendon has an important role in the production of movement, transmitting muscle contraction forces to the skeleton, maintaining the stability of the joints [2]. Tendon structure is mainly composed of aligned and crosslinked type-I collagen fibers that are maintained by a stromal, mostly fibroblastic cell population (tenocytes) [1].

The extracellular matrix (ECM) of tendons makes up about 80% of the tendon structure and is composed by non-cellular components, such as collagen, proteoglycans, water, and other non-collagenous proteins, such as elastin, fibronectin and integrins [2]. Collagen is the most abundant component of the tendon, representing about 60-85% of its dry-weight, where type I collagen is the most abundant (≈95%), followed by type III collagen (3%) and other types in small levels (2%) like type V, XI, XII and XIV collagens [2]. The ground substance that surrounds collagen consists of proteoglycans, glycoproteins and glycosaminoglycans (GAGs) which are highly viscous and hydrophilic, giving tendon the viscoelastic properties to resist compressive forces [2], [3]. Elastic fibers allow long-range deformability and passive recoil, ensuring the flexibility and extensibility of tendons [3].

Mature and healthy tendons are characterized by low cellular density, and the cellular component is composed by approximately 90-95% of tenoblasts and tenocytes, which are specialized fibroblast-like cells that produce collagen [2], [3]. The remaining cell types include synovial cells present in tendon sheaths, chondrocytes present in enthesis, and endothelial cells and smooth muscle cells found in vessels [2]. Tenoblasts are spindle-shaped cells, with high level of metabolic activity, and are the immature precursors of tenocytes. When they start to maturate to become tenocytes, their shape becomes flat and elongated, their metabolism rate decreases, and their energy production switches from aerobic to predominantly anaerobic metabolic pathway [2]. Structurally, the tendon unit is formed by collagen organized from the nano to the microscale (figure I.1) into microfibrils, fibrils, fibers and fascicles [2]. The fascicles are packed together and separated by the endotenon or interfascicular matrix, a fine connective tissue that contains the blood vessels, lymphatics and nerves, and are all enclosed by the epitenon [4].

Tendinopathy describes a complex multifaceted pathology of the tendon, and is characterized by pain, loss of function, and reduce exercise tolerance [5]. A diseased tendon is characterized by fragmented collagen fibers, disorganized collagen bundles, accumulation of GAGs and increased microvasculature associated with neoinnervation, leading to adverse changes in the material properties of the tendon [5]. This neovascularization and subsequent increase of oxygen and nutrients supply has been shown as a trigger of degenerative ECM remodeling within the tissue stroma [4]. The healing processes typically follows three phases, namely inflammation, proliferation and remodeling [2]. In the most cases of tendinopathy, the injuries are associated with overuse, resulting in multiple overlapping pathological processes, leading to pain, diffuse or localized swelling, loss of tissue integrity and impaired performance [5].

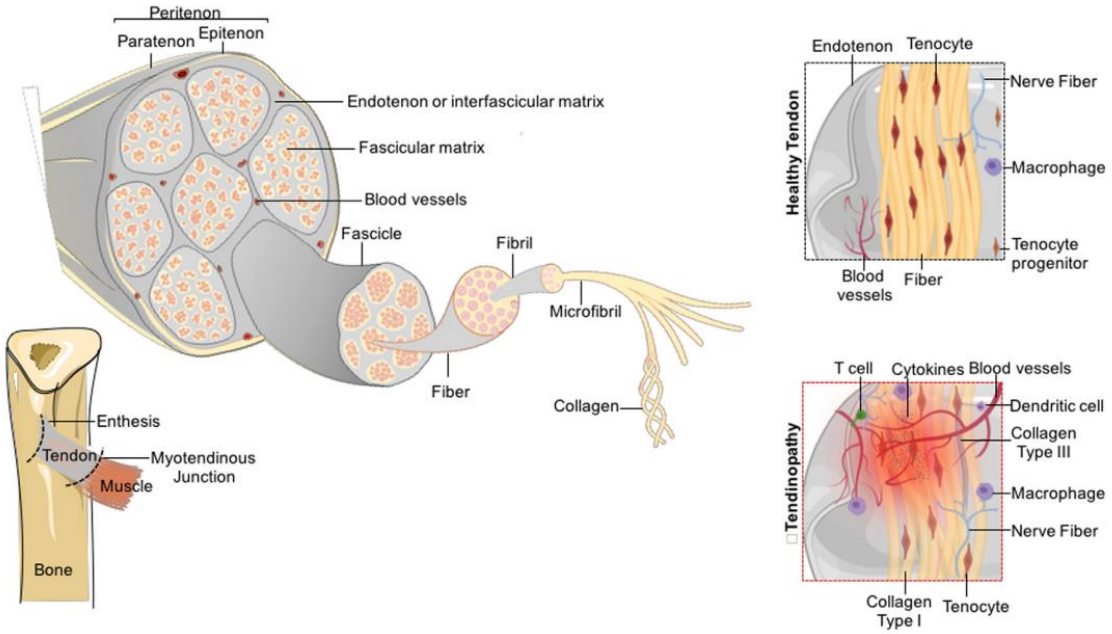

Figure I.1. Tendon structure. Hierarchical anisotropic structure of tendon from the nano (collagen molecules) to the macroscale (tissue). Healthy tendons suffer cellular and molecular alterations during tendinopathy (adapted from [4]).

Until now, clinical treatment of tendinopathy relies on physiotherapy with exercise-based strategies, use of anti-inflammatory drugs, injection therapy like corticosteroid or platelet-rich plasma injections, extracorporeal shockwave therapy, or surgery in extreme cases [6], [7]. To the date, treatment of tendinopathy remains challenging and has poor recovery outcomes, resulting in prolonged patient suffering and substantial loss of personal productivity [6]. As so, it is highly

needed to develop new and effective treatments to bring a better life for patients that suffer from tendinopathy disease.

I.2. Reliable models for the study of tendon physiology and pathophysiology

The main barrier to the advance of scientific and clinical approaches in the tendon field has been the persistent lack of valid models of human tendon disease, essential to clarify basic cellular mechanisms and to test novel therapeutic treatments [8]. These models are included in a range of *in vivo* and *in vitro* models, from animal models to 2D cell culture models.

Animal models sounds appealing for the study of tendon repair as they have interplay between tissues and cell-system interaction (lymph, nerve, vessel, among others). However, these models are limited in their availability and ability to capture human features of tendon disease as they fail to mimic the intrinsic repair capacity of adult human tendon tissue, and they also represent a high cost approach with low throughput, with the addition of considerable ethical and time constraints [8].

On the other hand, 2D cell culture models are less complex than *in vivo* models, and are commonly used to study cell behavior due to their practicability, high-throughput and cost-effectiveness [9]. These models are a simple way to study the basic morphology, gene expression and differentiation, allowing the researchers to capture clinical an biological relevant effects of human individuality that varies by donor-to-donor [8], [9]. For example, after observing T cells signatures in human tendinopathy, a recent work explored the interaction between T cells and tenocytes, by direct and indirect (transwell) coculture, to understand their interaction and contribution in tissue remodeling and inflammation [10]. The results showed that the interaction between the two types of cells induced the expression of inflammatory cytokines/ chemokines in tenocytes and altered the collagen composition, favoring collagen type III, and self-amplified T cell activation via an auto-regulatory feedback loop [10]. However, 2D cell culture models fail in representing the biomechanical and biophysical environment of native tendons. Moreover, another huge concern arises when we talk about tenocytes cultures, since the increasing of cell passage results in loss of spindle-like morphology and, consequently, their functionality [11].

Tendon explant models have been used as another approach to study tendon tissue, where intact native tissue samples are dissected and cultured *ex vivo*. This method allows the study of

cell-ECM interactions in a near-physiological environment within intact tissue architecture, and have been used for structure and function characterization of tendon tissue, to study cell-mediated processes and to investigate crosstalk mechanisms [9], [12]. The explant model was also used to study the bi-directional crosstalk occurring between stem cells and the native tendon niche by using an indirect (transwell) system for coculturing human tendon explants and human adipose derived stem cells (hASCs), showing that the tendon explant had a significant influence in tissue architecture and secretion of ECM remodeling enzymes, inducing the hASCs commitment towards tenogenic phenotype [13]. The main limitations of tendon explants are the loss of homeostasis, the viability is time-dependent, it's difficult to standardize, there is no (neuro-)vascular supply, and it has poor translatability to human [8], [9].

Mimicking the tendon environment and tendinopathy situation remains challenging, and the lack of representative models have been leading to the demand for new representative models, where 3D *in vitro* models has been pointed as the main solution.

3D *in vitro* models can recreate the physiological context of the tissue, and adequately recreate neo-tendon formation after an acute injury, study the interactions between recruited tendon cells and an implanted biomaterial, or the crosstalk between tendon fibroblasts and other cell types as immune and stem cells [8]. 3D *in vitro* models allow the recreation of tissue environments with the construction of more representative mechanistic insights of innate tissue cellular interactions [4]. These models enable the recreation of more complex systems with the incorporation of multi-cellular environment and incorporation of human cells, it can recreate the 3D architecture of the tissue, has an increased representability of tissues, captures human individuality, and helps in the reduction of animal testing [4]. The 3D *in vitro* models that have been used/studied so far include: cell sheets, which takes advantage of ECM deposition by the cells themselves, preserving cell-to-cell contact to produce self-assembled microtissues [14]; collagen structures, where collagen-based hydrogels allows the easy production of anisotropic cellular constructs [15]–[18]; fibrous scaffolds, produced by both natural and synthetic fibrous material platforms, such as collagen, chitosan, silk fibroin and PCL [19]–[22], by different techniques like electrospinning or wet spinning [23]–[26]; lastly, bioprinted constructs have emerged as a very powerful alternative to obtain biologically and physiologically relevant spatial architectures with multiple cells and/or biomaterials, which can lead, eventually, to the construction of 3D living constructs that resemble the native tissues in many aspects [4], [27]. This last technology is the focus of this thesis and therefore, will be further described below.

I.3. Bioprinting 3D *in vitro* models

Microphysiological systems (MPS) are proposed as an improved tool to recapitulate the physiology of human organs or tissues *in vitro*, which might help to predict *in vivo* responses using an *in vitro* assay [28]. One of the main types of MPS that are gaining great attention are the organs-on-chip (OoC) models, used for modeling diseases and test new drugs [29]. Microfluidic devices are commonly made of polydimethylsiloxane (PDMS), a material easy to mold, biocompatible and transparent. However, its soft lithography-based microfabrication process involves stacking and bonding different layers together, which limits the 3D complexity of the constructs and increases the final cost [12].

3D Bioprinting has emerging as an alternative to solve the fabrication barrier associated with MPS, allowing low-cost, rapid, one-step, and truly 3D fabrication of microfluidic devices, which may result into more complex multicellular *in vitro* models [29]. This promising technology allow the replication of tissue-tissue interfaces due to its inherent capability to distribute heterogeneous bioinks with cells, biomaterials and growth factors in a defined spatiotemporal manner relevant to biological architectures, manufacturing living tissues and organs in three dimensions [12], [27]. Biofabricated 3D *in vitro* models offer a great opportunity to investigate the physiological and pathological processes of tissues or organs, as well as to perform drug screening and toxicological studies [12].

Many bioprinting technologies have been developed and adapted to manufacture tissues or organs, and these technologies are classified in several groups whose nomenclature use to be associated with the mechanism behind the bioprinting technique [27]. The most commonly used 3D Bioprinting method is the extrusion-based printing that consists of depositing cell-laden bioinks, layer-by-layer, to obtain a 3D tissue-like structure [4], [9]. These pressure-assisted systems are largely used as they are more low-cost than the other printing systems, are commercially available, and use to be equipped with one or more cartridges/print-heads that allow the dispensing of different combination of cells and biomaterials by applying gas pressure [27]. In these systems, the resolution is defined by the type of the material, pressure, nozzle diameter, and deposition speed [27]. However, bioinks have innate weak mechanical properties, which also compromises the size and shape fidelity of the bioprinted constructs. 3D printing within suspension baths has been proposed as a solution to this problem, providing a platform for the patterning of mechanically

weak bioinks into complex and well-defined structures, preventing not only the settling and collapse of the bioink, but also dehydration of printed material and embedded cells [30].

A recent work [31] reported the development of a microparticulate formulation of alginate microparticles in xanthan gum-supplemented growth medium that allowed the printing of a small-scale human heart with major blood vessels. After printing, each ventricle was injected with blue and red dyes to demonstrate the integrity of the different compartments and the ability to manipulate and perfuse the printed hearts [31].

A platform or support bath that could allow more biomimetic cell-cell and cell-matrix crosstalk would contribute to the construction of complex 3D *in vitro* models with higher physiological relevance. Based on this, a recent work from our group [32] reported the development of a self-assembled nanoparticle-based fibrillar platform for the embedded 3D bioprinting of miniaturized tissues. This system creates an alternative to the organs-on-chip (OoC) models housed in the typical plastic platforms commonly used for microfluidic device fabrication, and proposes a platform that combines the concept of 3D free-form bioprinting in suspension baths, with the controlled self-assembly of plant-derived cellulose nanocrystals (CNCs) as building blocks to fabricate cell-laden constructs embedded within its own fibrillar device [32]. This CNCs fibrillar matrix platform has the ability to hold the print of different viscosity bioinks with different patterns, with high printing resolution and transparency, when compared with the commonly used agarose support bath. It also enables the printing of perfusable channels and allows structure removal by enzymatic hydrolysis of CNCs with cellulase, showing as an example the complete recovering of a butterfly after printing (figure I.2). Most importantly, this platform has unique fibrillar properties that match the native ECM dimensions present in the nature. *In vivo*, the ECM fibrils of parenchyma and stromal tissues varied from 10 to 230 nm, depending on tissue type, while the dense 3D networks of basement membranes have a pore size ranging from about 10 to 130 nm. In comparison, the entangled fibrils of these system have a mean diameter of 28.5 ± 11.3 nm and mean pore size of 76.7 ± 17.8 nm matching the native ECM properties [32].

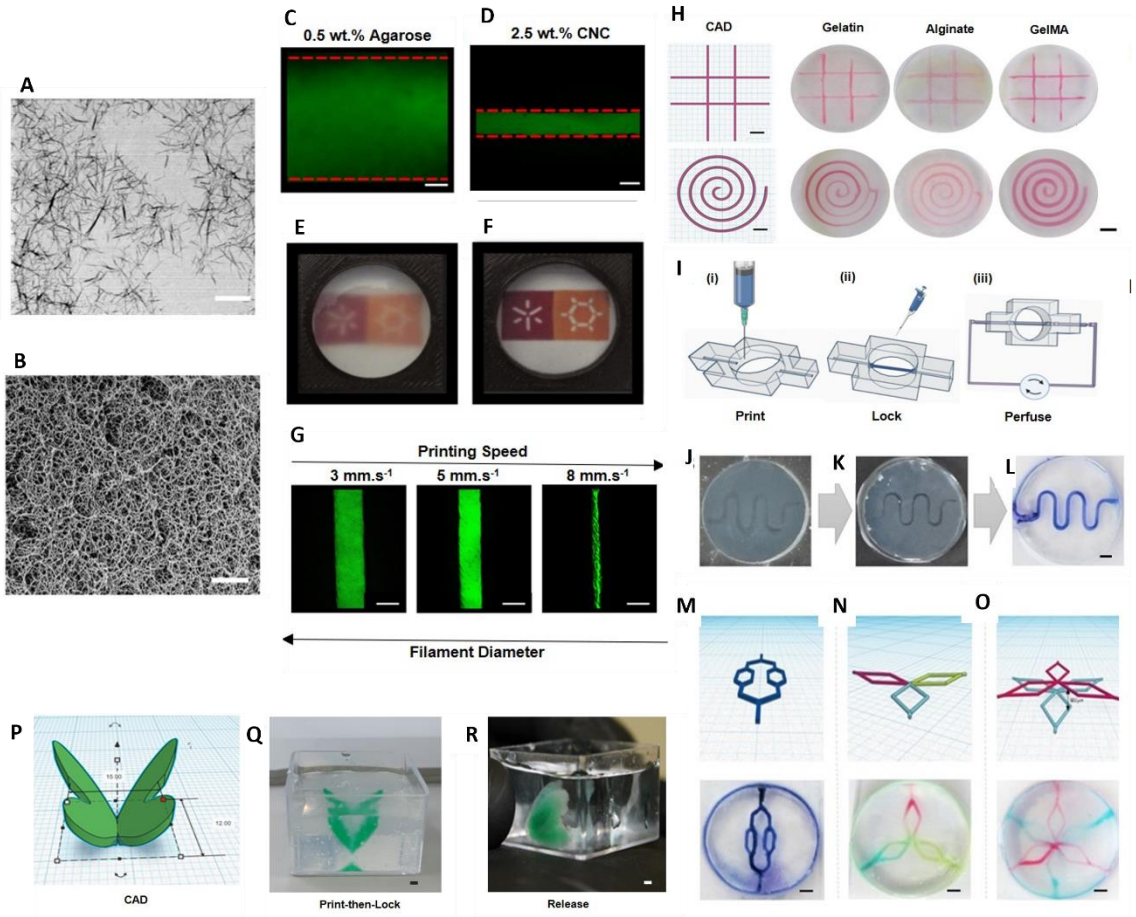

Figure I.2. CNCs support media development. Scanning electron microscopy (SEM) images of A) CNC showing its rod-shaped morphology, and B) self-assembled hydrogel showing hierarchical arrangements of CNC into fibrillar networks (scale bar: 200 nm). Confocal images comparing the resolution of fluorescently labeled (FITC) gelatin ink printed within C) 0.5 wt% agarose slurry and D) 2.5 wt% CNC colloidal suspension (scale bar: 250 µm). Photographs showing the optical transparency of E) agarose bath, and F) CNC colloidal suspension. G) Resolution of FITC-labeled gelatin 5 wt% ink printed at a constant pressure of 5 kPa and variable speed of 3, 5, and 8 $mm.s^{-1}$ with a 30G nozzle (scale bar: 150 µm). H) CAD design and respective photographs of two-layered linear patterns and a continuously extruded spiral printed in CNC colloidal matrix with 5 wt% gelatin (GelTG, enzymatic crosslinking), 2 wt% alginate (ionic-crosslinking) and 5 wt% GelMA (photo-crosslinking) (scale bar: 500 µm). I) Illustration of the process for direct 3D printing perfusable channels within CNC fibrillar matrix: i) print channel circuit with fugitive ink, ii) lock structure inducing self-assembly of the CNC with Ca^{2+}, (iii) perfusion of the self-standing embedded channel after purging the sacrificial ink. J) Photograph of a printed and locked sinusoidal filament with Pluronic F-127 fugitive ink, K) its liquefication at 4 °C, and L) perfusion of the hollow channel with water (added food color for visualization). CAD models and respective perfusion of resulting

microfluidic chip with M) bifurcated design, N) independent inlets and bifurcations with common convergence point (water with different food colors is perfused to aid the visualization of each channel independently), O) multilayered channels separated by a depth distance of 500 μm (water is perfused with blue food color in the bottom layer and red in the top layer to aid visualization, scale bars in J, K, L, M, N, O: 1 mm). P) CAD model of a butterfly, and Q) respective 3D printed and locked structure (height 15 mm and width 12 mm, wings with 1.5 mm thickness on the bottom and 0.5 mm on top). R) Released structure immersed in PBS after enzymatic hydrolysis of CNC matrix with cellulase. (Adapted from [32])

Overall, this platform does not require specific microfabrication processes, equipment or skills, and has many advantages as high throughput, reproducibility, and scalability for the manufacturing of miniaturized multicellular systems with complex bioinspired 3D architectures, and can be a promising platform for the automated biofabrication of *in vitro* tissue/organ models [32].

One of the main concerns in bioprinting is the selection of adequate bioinks. These bioinks should be selected, and/or designed and prepared according to the target tissue or organ, considering the bioprinting technique to be used. The commonly used bioinks can be derived either from natural or synthetic polymers, where hydrogels have been gaining force as the ideal materials for cell culture and encapsulation, even with soft mechanical properties and hydrated state, that can be complemented with the concept of support baths [27]. Hydrogels provide an excellent environment for stimuli responsiveness, integration of complex biochemical/biomechanical signals, and recapitulation of the soft tissues natural environment [27]. Many hydrogels have been proposed for bioprinting, namely natural polymers such alginate [33]–[40], agarose [41]–[44], hyaluronic acid (HA) [40], [45]–[53], chitosan [54]–[60], gelatin [35], [55], [61]–[66], collagen [67]–[70], silk [71]–[76] and gelatin methacryloyl (GelMA) [47], [77], [78], or synthetic hydrogels like poly(ethylene glycol) (PEG) [79]. In tendon related bioprinting, the most commonly used hydrogels so far are gelatin methacryloyl (GelMA) [80] and collagen [15], [81].

However, despite the wide variety of hydrogel formulations available for bioprinting, there is still not an "ideal" bioink that is both easily and consistently printable and capable of mimicking the cell microenvironment [27]. Decellularized extracellular matrix (dECM) hydrogels are emerging as a valuable approach for bioink formulation as dECM bioinks exhibit higher levels of

biofunctionality for the generation of inherent environmental niches than other available hydrogels, with high regenerative potential, preserving the main biochemical and biophysical cues of the respective niches [82]. dECM hydrogel formulations can be derived from different tissues/organs, depending on the field of interest, and can be derived from kidney [83]–[85], heart [82], [86]–[88], cornea [89], muscle [90], [91], liver [82], [92], skin [93], [94], brain [95], [96], intestinal tissue [82], [97]–[99], muscle [100], [101], bone [22], tendon [22], [102]–[106], among others.

I.4. Decellularized extracellular matrix for tendon cell culture

Extracellular matrix (ECM) is a 3D network that provides a microenvironment for cell homeostasis, ingrowth, tissue formation and repair [107]. ECM is tissue/organ-specific derived, and cell-ECM interactions are fundamental in cell behavior, function and fates modulation [108]. Decellularized ECM has become an attractive material for several tissue engineering strategies due to the retention of biochemical cues that influences cells growth and differentiation, and dECM bioinks have the ability to recapitulate a cell-supportive microenvironment niche in bioprinted constructs [109]. ECM is a non-cellular 3D macromolecular network, composed by collagens, proteoglycans/glycosaminoglycans, elastin, fibronectin, laminins, among several other glycoproteins, and is a highly dynamic structural network that is in constant remodeling mediated by matrix-degrading enzymes during normal and pathological conditions [110]. Collagen is the most dominant and abundant protein in mammals ECM [111], representing 70% of tendon ECM dry weight, with the prevalence of collagen type I (95%), followed by collagen type III (3%), and small levels (2%) of collagen type V, XI, XII and XIV [2].

Trough cell-ECM communication, ECM has the ability to regulate stem-cell fate with its structural support, biochemical composition, growth factors, and biochemical factors [109]. Stem-cell niches retain the stemness of adult stem cells in a quiescent state and, when a tissue is injured, the surrounding microenvironment induces stem cells to promote either self-renewal or differentiation to form new tissues [109]. During tissue repair, ECM regulates stem-cell behavior with structural support and biochemical, growth factor and biomechanical regulation. In one hand, the porosity, mechanical properties and cell-matrix communication of ECM provides structural support for the regulation of cell adhesion, growth, differentiation and formation of 3D tissue structures [112]. Secondly, biochemical signaling of stem-cells is regulated by integrins that regulate cell proliferation, adhesion, migration and differentiation [113]. On the other hand, ECM is a reservoir of growth factors that induce stem-cell self-renewal, survival and differentiation [114].

Finally, ECM topography, microstructure, stiffness and elasticity induces stem-cell biomechanical regulation by modulating cells shape with tissue elongation and cell-ECM interaction [115]–[118].

I.4.1. Decellularization methods

Decellularization is a term that refers to the treatment or process that efficiently eliminates the cellular and nuclear constituents of ECM, while preserving essential components, biological activity and the mechanical integrity of the prepared dECM-based materials [119]. The removal of all the cellular content is important, as xenografts and allografts can induce host inflammatory and immune response due to their cellular antigens [120].

A successful decellularization can be achieved through a series of physical, chemical or enzymatic treatments but, an effective and robust decellularization protocol involves a combination of all three of these [119].

Physical decellularization methods involve freezing and thawing, pressure or mechanical force, mechanical agitation, poly(ethylene glycol) (PEG), supercritical CO_2 and sonication [119]. Specifically, freeze-thaw cycles aim to disrupt the cell membrane trough intracellular ice crystals, provoking cell lysis, while pressure or mechanical force leads to cellular disintegration, and mechanical agitation can lead to cellular disruption alone or in combination with a chemical method [121]. PEG, with different molecular weights, destabilizes the cellular membrane through PEG amphiphilic properties, causing cell lysis [122]. The efficiency of physical methods relies on factors such as tissue thickness, ECM density and degree of cellularity, and alone use to be inadequate to achieve an effective decellularization [119].

Chemical treatments promote hydrolytic degradation of biomolecules, disrupt cellular membranes, and solubilize the bonds accountable for intercellular and extracellular connections, leading to an effective removal of cellular content. These treatments include the use of acids and bases, detergents, hypo- and hypertonic solutions, chelating agents, and solvents. Acid-base treatments are highly effective in solubilizing cytoplasmatic components, disrupting the nucleic acids and protein denaturing, by causing hydrolytic degradation of the biomolecules, but can disrupt and eliminate collagens, GAGs, and growth factors. The treatment with ionic (SDS), nonionic (Triton X-100) and zwitterionic detergents can effectively remove cytoplasmatic and nuclear material from the tissue. Ionic detergents like SDS are highly ionic and actuate by solubilizing the cytoplasmic and nuclear components of ECM, but it also tends to denature proteins by disrupting

protein-protein interactions and can be very disruptive to ECM if not used carefully. On the other hand, nonionic detergents are widely used for tissue decellularization due to their relatively less or mild detrimental effects than ionic treatments on tissue structure. These nonionic detergents cause the disruption of lipid-lipid and lipid-protein interactions of the cell membrane with limited impact on protein-protein interactions of the ECM, and Triton X-100 use to be pointed as the gold standard of nonionic detergents. Zwitterionic detergents exhibits both properties of nonionic and ionic detergents but are more likely to denature proteins than nonionic detergents alone. Hypertonic (NaCl) and hypotonic (Tris-HCl) solutions causes osmotic shock in the cells and the disruption of DNA-protein interactions, causing cell lysis with minimal alterations in the matrix molecules and its architecture. Solvents like alcohols and acetone lyses the cells by dehydration, solubilization and removal of lipids, and, finally, chelating agents such as EDTA or EGTA disrupts cell-ECM adhesion by binding to divalent cations such as Ca^{2+} and Mg^{2+} which are necessary for cell attachment to collagen and fibronectin. [119], [120]

Finally, enzymatic treatments include the use of nucleases, proteases, dispase, collagenase, calcium chelating agents, lipase and thermolysin for cleaving proteins and cellular bonds that account for intercellular and extracellular connections and disruption of cell adhesion to the ECM, providing high specificity for removal of cellular residues and efficient cell disruption. Trypsin is a serine protease, a highly specific proteolytic enzyme that cleaves the peptide bonds present on the carbon side of lysine and arginine, with maximal enzymatic activity at 37°C. Many reported decellularization procedures considered the exposure to trypsin as an initial step in tissue decellularization for complete elimination of cell nuclei from dense tissues and better preservation of GAG content. Nucleases such as RNase and DNase aid in the hydrolysis of ribonucleotide and deoxyribonucleotide chains, fragmenting RNA and DNA sequences. [119], [120]

After decellularization, besides the complete removal of cellular content, it is also important to assure that none detergent or enzyme remains present, as it can negatively affect cell viability.

There are some criteria that define if a tissue was properly decellularized or not. One of the criteria in based on DNA quantification, where the tissue is accepted as decellularized if there is less than 50 ng dsDNA per mg dry weight of dECM, or less than 200 base pair (bp) DNA fragment length, and the absence of nuclear material in dECM tissue sections as unveiled by histological and immunohistochemical analysis such as H&E and DAPI staining [123]–[125]. The preservation of the main components of the ECM structure can also be assessed trough quantitative or image-

based analysis by staining the tissue sections, for example, with H&E, Masson's Trichrome, Alcian Blue, Toluidine blue and Picro Sirius [119]. In H&E staining, while hematoxylin is used to assess the nuclear content, the eosin is used to assess the non-nucleic ECM architecture [119]. Alcian Blue and Toluidine Blue are used to evaluate the preservation of GAG content within the decellularized tissue, and Mason's Trichrome can assess not only the preservation of the collagenous structure, but also the presence of cytoplasmic molecules [126], [127]. Finally, Picro Sirius staining is a special good staining to differentiate the collagen with the use of polarized light, where the collagen type I stains in red and the collagen type III with green [128].

ECM tissues can be obtained from human or animal sources. The main concern while using animal sources are the risk of xenozoonoses, but they kept being an appropriate solution to overcome the shortage of human tissues [120].

Tendon tissues have been decellularized from different sources such as human [106], [129], [130], bovine [24], [102], [131], [132], equine [133], [134] and porcine [22], [81], [103]–[105], [135], [136]. It is important to select the appropriate animal source, as each animal has its pros and cons. Pig has been the major tissue source in general tissues, but also specifically in tendon dECM, as this animal source is sustainable, easily available, have higher breeding potential, short gestation period and rapid growth, and also show some anatomical and physiological similarities to humans [104], [112], [119]. One of the main concerns of using porcine sources is the immune rejection of porcine antigens caused by alpha-gal (α-gal) epitope [112], [119]. Luckily, cloning technology is able to eliminate the gene encoding α-galactosyltransferase, generating α-gal-knockout pigs [119], and making pigs a safe source of tissues.

I.4.2. Development of dECM based bioinks

For subsequent use, namely in the development of hydrogels/bioinks, decellularized tissue ECM, is usually freeze-dried and milled to obtain a homogeneous power, and subsequently enzymatically digested at low pH while stirring, to yield a viscous solution. The choice of the solubilization protocol is crucial, and involves two important steps: (1) solubilization of the dECM proteins, and (2) temperature and neutralization pH needed to induce the spontaneous reformation of the intramolecular bons of the solubilized dECM proteins [137]. The most prevalent method used to form an ECM hydrogel trough dECM powder solubilization is achieved by pepsin digestion,

also known as dECM digestion [137]. Pepsin is an enzyme derived from porcine gastric juices and has been used to solubilize acid-insoluble collagen [138]. This enzyme actuates by cleaving the telopeptide bonds of the collagen triple helix structure to unravel collagen fibril aggregates [139].

The osmotic pressure and stiffness of the obtained bioink are important factors that can affect the biological functions of cells, and the choice of the acidic solution can affect the overall properties of the final bioink. A recent study compared three types of commonly used acidic solutions in the development of tendon derived dECM bioink for 3D Bioprinting: 0.5 M acetic acid (AA), 0.1 M hydrochloric acid (HCl) and 0.02 M HCl [105]. This study found that the low pH value of 0.1 M HCl could accelerate the digestion process of the dECM powders, leading to a much softer and weaker dECM hydrogels with formation of smaller fragments of collagen fibrils and molecules, and also more unstable as they shrink significantly during the culture time when compared with the other two types of acid [105]. On the other hand, 0.5 M AA dECM bioink led to much lower cellular viability rate due to its hyperosmotic state [105]. Finally, the dECM bioink prepared with 0.02 M HCl presented a less digested state, didn't shrink, presented good cell viability, and showed better printability, being suitable to be used in the creation of complex tissue constructs [105].

ECM solubilization is considered complete only when a homogenous gel is formed with no visible particles [140]. Different digestion time can also affect the properties of the final hydrogel. Another recent study tested the printability of a porcine tendon derived hydrogel by digesting dECM with 0.1 M HCl pepsin containing solution, and evaluated the hydrogel with 3 h, 12 h, and 72 h of digestion, referred to as high, medium and low viscosity slurry, respectively [104]. The analyses showed that from 6 h to 24 h the digested material become clearer and more transparent, and from 24 h to 72 h there was no change in the general morphology as time progressed, but at 72 h of digestion the hydrogel became liquid. The incomplete digestion of the dECM powders after 3 h of digestion showed no collagen fibers formation. After 12 h of digestion, collagen fibers were formed when the pH value was neutralized, but after increasing the temperature to 37 °C, fibers were no longer formed. In the low viscosity slurry with 72 h of digestion, no visible fibers were found when the hydrogel was neutralized, but after the temperature was raised to 37 °C, a gradual process of fibers formation was observed. In terms of printability, the 12 h state was impossible to print, while in the 3 h state the cells viability was less than 70 % after printing, and less than 40% after 3 days of printing. Finally, the 72h state showed good printability, with 90 % of cells viability after printing [104].

Thus, the process of dECM hydrogel/bioink development should be carefully designed, selecting optimum pepsin concentration, acid type and respective concentration, and digestion time, in order to achieve an extrudable hydrogel favorable for both bioprinting and for cells survival and proliferation.

A simple resume of the main studies using tendon dECM is presented in the Table I.1, namely the tendon ECM sources commonly used, decellularization methods, dECM solubilization (when applied), the aim of each study, and the main and most relevant results obtained.

Table I.1. Summary table of studies reported in the literature using tendon dECM.

Tendon source	Cell type	Decellularization approach	dECM solubilization	Aim of the study	Relevant results	Ref
Porcine	BMSCs	Acetone, 3 x 30 min 60/40 (v/v) Hexane: Acetone, 24 h 70 % Ethanol, O.N. 0.25% Trypsin-EDTA, O.N 2% SDS, 96 h Distilled water, 1 week	3 mg/mL pepsin 0.1 M HCl 30 mg/mL dECM 3, 12 and 72 h digestion	Study of the digestion time influence in extrusion-based 3D cell printing. dECM encapsulated with BMSCs to study the cell viability for different viscosity bioinks.	The solution couldn't be extruded with 12 h of digestion, and the 3 h digested solution showed better printability than 72 h digested solution. the Tendon-derived dECM bioink showed more gene expression associated with tendon formation, compared with alginate bioink	[104]
Porcine	BMSCs	0.25% trypsin-EDTA, 48h 0.5% SDS + 0.5% TritonX-100, 48h 0.1% peracetic acid in 4% ethanol, 4h Distilled water, 1 week	3 mg/mL pepsin 0.5 M Acetic Acid (AA), 0.1 M HCl, 0.02 M HCl 72 h 30 mg/mL dECM	Comparison of three different acidic solutions in dECM bioink properties	0.1 M HCl condition revealed more digested state, but more unstable hydrogel with high contraction. 0.5 M AA and 0.02 M HCl conditions showed better printability with no contraction. HCl conditions showed good cell viability, but AA showed low cell viability. The softest 0.1 M HCl condition showed the highest tenogenic ability.	[105]
Bovine	ATCC	Frozen in 10 mM Tris-HCL in PBS) and thaw in 1.5 M NaCl in 50 mM Tris-HCl, 5x 0.05% Trypsin-EDTA, 30 min 2% SDS, 4 days PBS, 1 week	1 mg/mL pepsin dECM: pepsin ratio of 10:1 0.01 M HCl 48 h	Development of a biocompatible, biomimetic and bioprintable ECM hydrogel from bovine Achilles tendon.	The developed dECM bioink showed good cell viability and tendon lineage-specific morphology in the early days of culture	[102]

Table I.1. Summary table of studies reported in the literature using tendon dECM. (continued)

Tendon source	Cell type	Decellularization approach	dECM solubilization	Aim of the study	Relevant results	Ref
Porcine	BMSCs	5 freeze-thaw cycles 1% Triton 100-X, 48 h Benzonase in 50 mM Tris/ 1mM $MgCl_2$, 24 h 2.7 mM EDTA, 3 h 50 mM Tris/1.5 M NaCl, O.N. 70% Ethanol, 30 min 1% Triton 100-X, 48 h Benzonase in 50 mM Tris/ 1mM $MgCl_2$, 24 h PBS, 5 days	—	Decellularization of porcine Achilles tendon to *in vitro* and *in vivo* studies.	Decellularized tendons supported stem cell proliferation, induced early tenogenic differentiation and induced anti-inflammatory response in macrophages. *In vivo* experiments showed that 6 weeks after implantation, decellularized tendons integrated with host tendon without signs of tissue rejection	[103]
Porcine	BMSCs	0.5 % Trypsin/ 25 mM EDTA, 6 h 2% Triton X-100, 3 days 50 U/mL DNase, 2 days 0.1% peracetic acid in 40% ethanol, 3 h PBS, 3 days	0.5 M AA with pepsin for 3-4 days	3D cell-printing of a tendon-bone interface (TBI) using tendon and bone dECM bioinks encapsulated with BMSCs	The compositionally reverse gradients of tissue specific dECM bioinks offered coax region-specific differentiation of encapsulated BMSCs for TBI formation *in vitro*. *In vivo* studies showed highly arranged collagen orientation a biomechanical strength in a rat chronic tear model.	[22]
Bovine	Mouse MSC	1% Triton X-100 + 5 mM EDTA + 0.5 mM PMSF, 24h 200 U/mL DNase + 50 U/mL RNase, 12h PBS, 5x	3 M urea, 3 days Dialysis, 3 days	Development of tendon ECM modified bioactive eletrospun fibers to promote MSC tenogenic differentiation. The obtained solubilized dECM (sdECM) was added into the shell layer of CTS/PLGA ultrafine fibers	The ultrafine fibers modified with sdECM were more cytocompatible and capable of inducing a predominant tenogenic phenotype of mouse MSCs, with enhanced expression of tendon markers. This inductive effect was enhanced when unilateral mechanical loading was applied *in vivo*.	[24]

Table I.1. Summary table of studies reported in the literature using tendon dECM. (continued)

Tendon source	Cell type	Decellularization approach	dECM solubilization	Aim of the study	Relevant results	Ref
Porcine	ATCC	3 Freeze-Thaw cycles Acetone, 1 h PBS + aprotinin (10 KIU/mL), 5x 0.5 mg/mL gentamicin sulfate + 0.05 mg/mL vancomycin hydrochloride + 0.2 mg/mL polymyxin B, 1h 0.1% SDS, 24 h PBS + aprotinin, 71h 1U/mL benzonase, 2h 2.7 mM EDTA, 3x 50 mM Tris/ 1.5 M NaCl, 18h 0.1% peracetic acid, 3h PBS, 1 week	———	Decellularization of porcine superflexor tendon as a potential anterior cruciate ligament replacement	The decellularized tendon was biocompatible *in vitro* and *in vivo* after implantation in a mouse subcutaneous model for 12 weeks. Cells of a fibroblastic and macrophage morphology were observed penetrating the implanted decellularized tissue.	[135]
Rats	———	6 Freeze-Thaw cycles 50 U/mL DNase I and 1 U/mL RNase A, 24h 75% ethanol, 1h PBS, 5x	———	Fabrication of decellularized autologous ECM scaffolds by implanting a PCL template subcutaneously in rats for 4 weeks, forming PCL-Cell-ECM composites. The composites were explanted, the PCL removed. The Cell-ECM compounds were decellularized (aECM) and re-implanted	aECM scaffolds supported tendon remodeling and achieved enhanced restoration of functional and mechanical properties to Achilles tendon defects in rat models	[21]

Table I.1. Summary table of studies reported in the literature using tendon dECM. (continued)

Tendon source	Cell type	Decellularization approach	dECM solubilization	Aim of the study	Relevant results	Ref
Bovine	———	1st group: PBS, 24h 2nd goup: 5 Freeze-Thaw cycles, 100 µg/mL RNase and 150 IU/mL DNase 3rd group: 2% SDS, 0.05% trypsin-EDTA for 10 min, DNase for 30 min and 95% ethanol for 2h	———	Development of a naturally derived tendon tissue engineering scaffold with the preservation of the native ultrastructure, tensile strength and biochemical composition of tendon ECM.	SDS was better than freeze and thaw technique in terms of effective decellularization, and the structure and alignment of collagen fibers were preserved in SDS group	[131]
Porcine	Human tenocytes	1% SDS + 0.2% sodium azide + 5 mM EDTA, 24 h 0.05 % trypsin/0.053 mM EDTA, 24 h 3% Triton-X 100, 24h 70% ethanol, 30 min Distilled water, 24h	———	Implanting decellularized porcine Achilles tendons recellularized with human tenocytes into nude mice to obtain tendon-like tissue formation	dECM lost some GAGs and structure, but could be recellularized *in vitro* with human tenocytes, although the cell distribution remained inhomogeneous with accumulation at the margins of the constructs. *In vivo*, the dECM constructs revealed no inflammation and a more homogenous cell distribution and suggested the formation of a tendon-like tissue *in vivo*.	[136]
Equine	BMSCs	1st group: PBS (control) 2nd group: 1% TnBP 3rd group: 1% SDS + 0.5% Triton X-100 4th group: 1% SDS 5th group: 2% SDS All groups: 0.05% Trypsin-EDTA, 10 min DNase I, 30 min 95% Ethanol, 2h	———	Optimization of a biologically derived scaffold for tendon tissue engineering using equine flexor digitorum superficialis tendons, with evaluation of changes in scaffold composition and ultrastructure	The protocol based on 2% SDS in conjunction with trypsinization, DNase I, and ethanol sterilization induced practical acellularity without compromising functionality.	[133]

Table I.1. Summary table of studies reported in the literature using tendon dECM. (continued)

Tendon source	Cell type	Decellularization approach	dECM solubilization	Aim of the study	Relevant results	Ref
Human	hASCs	0.1 % EDTA, 4h 0.1 % SDS + 0.1 % EDTA, 24 h Wash with PBS	1 mg/mL pepsin 0.02 M HCl 10, 20 and 30 mg/mL dECM 12-72 h digestion	Development of a biocompatible ECM hydrogel from human tendons as a potential scaffold to be delivered percutaneously into a zone of tendon injury	The gel displayed promising characteristics and biocompatibility both *in vivo* as well as after being reseeded *in vitro*. This gel has potential to facilitate the regeneration of new tendon tissue *in vivo*.	[106]
Rabbits	BMSCs	PBS, 3 x 30 min 5 Freeze-thaw cycles 0.1 % SDS, 4 h PBS, 12 h	———	Development of a book-shaped decellularized scaffold derived from New Zealand white rabbits to repair 1 mm Achilles tendon defect	The scaffold could promote the regeneration of type I collagen at the wound site, and promoted healing after Achilles tendon injury, with stem cells enhancing the effect, being differentiated into tenocytes.	[141]
Equine	Equine MSC	Tris Buffer, 48 h Group 1: 5 Freeze-Thaw cycles + 1 % Triton X-100 Group 2: 5 Freeze-Thaw cycles + 1 % SDS Group 3: 1 % Triton X-100 Group 4: 1 % SDS Washing 48h	———	Assess the effect of repetitive freeze-thaw cycles and two different detergents on decellularization effectiveness and cytocompatibility in large tendons	The decellularization was significantly more effective when including freeze-thaw cycles in the protocols. All the protocols were cytocompatible but cell distribution tended to be better in scaffolds decellularized with freeze-thaw cycles combined with Triton X-100 instead of SDS.	[142]
Human	———	0.1 % EDTA + 0.1 % SDS, 24 h 5 % PAA, 6 h PBS, 24 h	———	Evaluate the immunogenicity and strength of tendon grafts when implanted into an immunocompetent rat model	The decellularization protocol was successful, with removal of cellular antigens, decreasing immune response when placed into Wistar Rats	[130]

Table I.1. Summary table of studies reported in the literature using tendon dECM. (continued)

Tendon source	Cell type	Decellularization approach	dECM solubilization	Aim of the study	Relevant results	Ref
Human	Human dermal fibroblasts	Group 1: control Group 2: 1% Triton X-100 Group 3: 1% TnBP Group 4: 1% SDS Group 5: 0.1 % SDS Group 2-5 with a pretreatment with 0.1 % EDTA, 4 h, a treatment of 24 h, and post-treatment with PBS, 1h	———	Development of a tissue-engineered flexor tendon scaffold for clinical use in individuals with loss of flexor tendons, by comparison of 4 decellularization methods and their compatibility with allogenic human cells.	Only SDS treatments significantly decreased DNA content, showed no decrease in GAGs or collagen after SDS treatment and present good biocompatibility after re-seeding with human cells. This provides a promising scaffold for future human flexor tendon tissue engineering studies.	[129]
Porcine	MSCs	1 % Triton X-100, 3 days 200 U/mL DNase and 50 U/mL RNase, 24h Wash with PBS, 6x	10 % dECM 3 M Urea 3 days Dialysis, 2 days	Evaluation of the potential of decellularized mesenchymal tissue ECMs from various mesenchymal tissues in musculoskeletal tissue engineering approaches, due to tissue-specific bioactivity	Decellularization was successful and each tissue exhibited variations in their growth factor distribution and on cell culture appeared to promote cell differentiation toward specified used ECM tissue phenotype.	[81]
Bovine	BMSCs TDCs	5 Freeze-Thaw cycles 100 µg/mL RNase and 150 IU/mL DNase, 12 h PBS, 30 min	———	Assess the effect of stem cell ECM-modified decellularized tendon-slices (ECM-DTSs) on BMSCs migration.	ECM-DTSs enhanced BMSCs migration, led to early cytoskeletal changes, and is pointed as a novel strategy to recruit stem cells.	[132]
Rabbits	———	0.1 % EDTA + 10 K IU/mg aprotinin, 24h 0.5 % SDS, 24 h 1 % Triton X-100, 24 h PBS, 3 days	———	Development of a decellularized tendon scaffold for allograft transplantation in rotator cuff tears.	The decellularized tendon scaffold maintained the most important biomechanical characteristics and permitted cell infiltration when implanted *in vivo*.	[143]

BMSCs, bone marrow mesenchymal stem cells; ATCC, NIH 3T3 murine embryonic fibroblast cells; MSC, mesenchymal stem cells; TDCs, tendon-derived stem cells; PMSF, phenylmethylsulphonyl fluoride; hASCs, human adipose derived stem cells; TnBP, tri-n-butyl phosphate; PAA, peracetic acid.

I.5. Tendon-on-Chip model development

Organ-on-chip technology is unlikely to replace animal testing in the near future. However, organs-on-chip can generate independent data sets that can be used to augment various stages of drug discover and/or to decipher tissue/organ biological mechanisms, and if these systems prove to be able to consistently and accurately predict the effects of drugs in pathologies, it will be possible to achieve very impactful paradigm shift in preclinical drug-testing towards *in vitro* 3D human tissue models [144].

Tendinopathy is a multifaceted pathology, characterized by modifications in tendon microstructure, cellularity and collagen composition [4]. Healing mechanisms are far from being completely understood, and current treatments have poor recovery outcomes, so it's highly needed to develop relevant *in vitro* models that enable to study the complex multicellular crosstalk occurring in tendon microenvironments, and also test new treatments [4].

It's referred that a representative *in vitro* tendinopathy model should be vascularized and mimic the hierarchical structure of tendon niche, with elongated cells being organized in a parallel fashion [9]. In more detail, to mimic the tendon pathophysiology *in vitro*, the following requirements should be fulfilled: (i) representative cellular growth as demonstrated by the spindle-shape morphology and tenocyte marker expression, (ii) production of ECM and cell-matrix interactions, (iii) supporting nanometric and axially aligned structure (anisotropy), (iv) responsive to physiological levels of uniaxial strain, (v) neurovascular supply, and (vi) mimicking micro-damage like acute injuries and chronic overuse [9]. In tendon tissue engineering, the most obvious cell type to utilize are tenocytes, as they are the most abundant cell type *in vivo* tendon [9]. The interaction between resident cells (tenocytes, tendon stem cells, or MSCs), immune cells, growth factors and cytokines is crucial to gain new insights [145]. *In vivo*, these immunomodulatory cells/molecules are partially provided through the blood stream, reason why the incorporation of vascular supply, or at least endothelial cells is mandatory, although it remains a major challenge in tissue engineering [146]. When tenocytes are cultured together with HUVECs and AT-MSCs, the expression of tenogenic markers was upregulated, showing that tenocytes profit from the providing vascularization [147].

Even if the system lacks of microfluidic flow, it can be considered to be an organ-on-a-chip device, according to a recent definition, since the platform has a significant engineering component and spatially guides cell confinement [144], [148].

Herein we propose to ally the ECM mimetic properties of CNCs platform [32], to be used as a support bath/chip platform, with the unique features of tendon dECM hydrogels, that better mimics the tendon microenvironment, for the freeform 3D Bioprinting of humanized tendon-on-chip models. In one hand, this CNCs platform will allow us to recreate the tendon microenvironment with the desired patterns, surrounded by an ECM mimetic fibrillar material, with the possibility to assess multicellular crosstalk with relevant tendon cell populations. On the other hand, extracellular matrix plays a critical role in bioinstructing cellular self-assembly and spatial (re)configuration processes that culminate in the *in vitro* generation and maturation of human organoids [149]. With the unique features of dECM hydrogels and CNCs platform, this microphysiological system will allow cell-cell and cell-matrix interactions to occur in a more relevant physical and biological context.

I.6. References

[1] T. Stauber *et al.*, "Extrinsic Macrophages Protect While Tendon Progenitors Degrade: Insights from a Tissue Engineered Model of Tendon Compartmental Crosstalk," *Adv. Healthc. Mater.*, vol. 10, no. 20, p. 2100741, Oct. 2021, doi: 10.1002/adhm.202100741.

[2] C. Lee, "Tendon physiology and repair," *Orthop. Trauma*, vol. 35, no. 5, pp. 274–281, Oct. 2021, doi: 10.1016/j.mporth.2021.07.003.

[3] D. Docheva, S. A. Müller, M. Majewski, and C. H. Evans, "Biologics for tendon repair," *Adv. Drug Deliv. Rev.*, vol. 84, pp. 222–239, Apr. 2015, doi: 10.1016/j.addr.2014.11.015.

[4] M. Gomez-Florit, C. J. Labrador-Rached, R. M. A. Domingues, and M. E. Gomes, "The Tendon Microenvironment: Engineered In Vitro Models to Study Cellular Crosstalk," *Adv. Drug Deliv. Rev.*, vol. 185, p. 114299, 2022, doi: 10.1016/j.addr.2022.114299.

[5] N. L. Millar *et al.*, "Tendinopathy," *Nat. Rev. Dis. Prim.*, vol. 7, no. 1, p. 1, Dec. 2021, doi: 10.1038/s41572-020-00234-1.

[6] J. G. Snedeker and J. Foolen, "Tendon injury and repair – A perspective on the basic mechanisms of tendon disease and future clinical therapy," *Acta Biomater.*, vol. 63, pp. 18–36, Nov. 2017, doi: 10.1016/j.actbio.2017.08.032.

[7] "Tendinopathy," *Nat. Rev. Dis. Prim.*, vol. 7, no. 1, p. 2, Dec. 2021, doi: 10.1038/s41572-020-00242-1.

[8] S. L. Wunderli, U. Blache, and J. G. Snedeker, "Tendon explant models for physiologically relevant in vitro study of tissue biology – a perspective biology – a perspective," *Connect. Tissue Res.*, vol. 61, no. 3–4, pp. 262–277, 2020, doi: https://doi.org/10.1080/03008207.2019.1700962.

[9] M. Meeremans, G. R. Van de Walle, S. Van Vlierberghe, and C. De Schauwer, "The Lack of a Representative Tendinopathy Model Hampers Fundamental Mesenchymal Stem Cell Research," *Front. cell Dev. Biol.*, vol. 9, p. 651164, May 2021, doi: 10.3389/fcell.2021.651164.

[10] E. Garcia-Melchor *et al.*, "Novel self-amplificatory loop between T cells and tenocytes as a driver of chronicity in tendon disease," *Ann. Rheum. Dis.*, vol. 80, no. 8, pp. 1075–1085, Aug. 2021, doi: 10.1136/annrheumdis-2020-219335.

[11] L. Yao, C. S. Bestwick, L. A. Bestwick, N. Maffulli, and R. M. Aspden, "Phenotypic Drift in Human Tenocyte Culture," *Tissue Eng.*, vol. 12, no. 7, pp. 1843–1849, Jul. 2006, doi: 10.1089/ten.2006.12.1843.

[12] S. Piluso *et al.*, "Mimicking the Articular Joint with In Vitro Models," *Trends Biotechnol.*, vol. 37, no. 10, pp. 1063–1077, Oct. 2019, doi: 10.1016/j.tibtech.2019.03.003.

[13] R. Costa-Almeida, D. Berdecka, M. T. Rodrigues, R. L. Reis, and M. E. Gomes, "Tendon explant cultures to study the communication between adipose stem cells and native tendon niche.," *J. Cell. Biochem.*, vol. 119, no. 4, pp. 3653–3662, Apr. 2018, doi: 10.1002/jcb.26573.

[14] Y. Haraguchi *et al.*, "Fabrication of functional three-dimensional tissues by stacking cell sheets in vitro," *Nat. Protoc.*, vol. 7, no. 5, pp. 850–858, 2012, doi: 10.1038/nprot.2012.027.

[15] J. L. Puetzer, T. Ma, I. Sallent, A. Gelmi, and M. M. Stevens, "Driving Hierarchical Collagen Fiber Formation for Functional Tendon, Ligament, and Meniscus Replacement," *Biomaterials*, vol. 269, no. August, p. 120527, Feb. 2021, doi: 10.1016/j.biomaterials.2020.120527.

[16] M. L. Bayer *et al.*, "The initiation of embryonic-like collagen fibrillogenesis by adult human tendon fibroblasts when cultured under tension," *Biomaterials*, vol. 31, no. 18, pp. 4889–4897, 2010, doi: https://doi.org/10.1016/j.biomaterials.2010.02.062.

[17] V. S. Nirmalanandhan, M. Rao, M. S. Sacks, B. Haridas, and D. L. Butler, "Effect of length of the engineered tendon construct on its structure–function relationships in culture," *J. Biomech.*, vol. 40, no. 11, pp. 2523–2529, 2007, doi: https://doi.org/10.1016/j.jbiomech.2006.11.016.

[18] R. Gehwolf *et al.*, "Global Responses of Il-1β-Primed 3D Tendon Constructs to Treatment with

Pulsed Electromagnetic Fields," *Cells*, vol. 8, no. 5, 2019, doi: 10.3390/cells8050399.

[19] P. J. Yang and J. S. Temenoff, "Engineering Orthopedic Tissue Interfaces," *Tissue Eng. Part B Rev.*, vol. 15, no. 2, pp. 127–141, 2009, doi: 10.1089/ten.teb.2008.0371.

[20] Y. J. No, M. Castilho, Y. Ramaswamy, and H. Zreiqat, "Role of Biomaterials and Controlled Architecture on Tendon/Ligament Repair and Regeneration," *Adv. Mater.*, vol. 32, no. 18, p. 1904511, 2020, doi: https://doi.org/10.1002/adma.201904511.

[21] W. Li *et al.*, "Subcutaneously engineered autologous extracellular matrix scaffolds with aligned microchannels for enhanced tendon regeneration: Aligned microchannel scaffolds for tendon repair," *Biomaterials*, vol. 224, no. September, 2019, doi: 10.1016/j.biomaterials.2019.119488.

[22] S. Chae, Y. Sun, Y.-J. Choi, D.-H. Ha, I. Jeon, and D.-W. Cho, "3D cell-printing of tendon-bone interface using tissue-derived extracellular matrix bioinks for chronic rotator cuff repair," *Biofabrication*, vol. 13, no. 3, p. 035005, Jul. 2021, doi: 10.1088/1758-5090/abd159.

[23] C. Rinoldi, E. Kijeńska-Gawrońska, A. Khademhosseini, A. Tamayol, and W. Swieszkowski, "Fibrous Systems as Potential Solutions for Tendon and Ligament Repair, Healing, and Regeneration," *Adv. Healthc. Mater.*, vol. 10, no. 7, p. 2001305, 2021, doi: https://doi.org/10.1002/adhm.202001305.

[24] T. Tu *et al.*, "Tendon ECM modified bioactive electrospun fibers promote MSC tenogenic differentiation and tendon regeneration," *Appl. Mater. Today*, vol. 18, p. 100495, 2020, doi: 10.1016/j.apmt.2019.100495.

[25] M. M. Smoak, K. J. Hogan, K. J. Grande-allen, and A. G. Mikos, "Bioinspired electrospun dECM scaffolds guide cell growth and control the formation of myotubes," 2021.

[26] M. Santschi, A. Vernengo, D. Eglin, M. D'Este, and K. Wuertz-Kozak, "Decellularized matrix as a building block in bioprinting and electrospinning," *Curr. Opin. Biomed. Eng.*, vol. 10, pp. 116–122, 2019, doi: 10.1016/j.cobme.2019.05.003.

[27] C. Mota, S. Camarero-Espinosa, M. B. Baker, P. Wieringa, and L. Moroni, "Bioprinting: From Tissue and Organ Development to in Vitro Models," *Chem. Rev.*, vol. 120, no. 19, pp. 10547–10607, Oct. 2020, doi: 10.1021/acs.chemrev.9b00789.

[28] J. Parrish, K. Lim, B. Zhang, and M. Radisic, "New Frontiers for Biofabrication and Bioreactor Design in Microphysiological System Development," *Trends Biotechnol.*, vol. 37, no. 12, pp.

1327–1343, 2019, doi: 10.1016/j.tibtech.2019.04.009.

[29] V. Mehta and S. N. Rath, "3D printed microfluidic devices: a review focused on four fundamental manufacturing approaches and implications on the field of healthcare," *Bio-Design Manuf.*, vol. 4, no. 2, pp. 311–343, Jun. 2021, doi: 10.1007/s42242-020-00112-5.

[30] A. McCormack, C. B. Highley, N. R. Leslie, and F. P. W. Melchels, "3D Printing in Suspension Baths: Keeping the Promises of Bioprinting Afloat," *Trends Biotechnol.*, vol. 38, no. 6, pp. 584–593, 2020, doi: https://doi.org/10.1016/j.tibtech.2019.12.020.

[31] N. Noor, A. Shapira, R. Edri, I. Gal, L. Wertheim, and T. Dvir, "3D Printing of Personalized Thick and Perfusable Cardiac Patches and Hearts," *Adv. Sci.*, vol. 6, no. 11, p. 1900344, 2019, doi: https://doi.org/10.1002/advs.201900344.

[32] S. M. Bakht, M. Gomez-Florit, T. Lamers, R. L. Reis, R. M. A. Domingues, and M. E. Gomes, "3D Bioprinting of Miniaturized Tissues Embedded in Self-Assembled Nanoparticle-Based Fibrillar Platforms," *Adv. Funct. Mater.*, vol. 31, no. 46, 2021, doi: 10.1002/adfm.202104245.

[33] H. W. Ooi, C. Mota, A. T. ten Cate, A. Calore, L. Moroni, and M. B. Baker, "Thiol–Ene Alginate Hydrogels as Versatile Bioinks for Bioprinting," *Biomacromolecules*, vol. 19, no. 8, pp. 3390–3400, Aug. 2018, doi: 10.1021/acs.biomac.8b00696.

[34] S. Hafeez *et al.*, "Viscoelastic Oxidized Alginates with Reversible Imine Type Crosslinks: Self-Healing, Injectable, and Bioprintable Hydrogels," *Gels*, vol. 4, no. 4, 2018, doi: 10.3390/gels4040085.

[35] T. Jiang *et al.*, "Engineering bioprintable alginate/gelatin composite hydrogels with tunable mechanical and cell adhesive properties to modulate tumor spheroid growth kinetics," *Biofabrication*, vol. 12, no. 1, p. 15024, 2019, doi: 10.1088/1758-5090/ab3a5c.

[36] A. Habib, V. Sathish, S. Mallik, and B. Khoda, "3D Printability of Alginate-Carboxymethyl Cellulose Hydrogel," *Materials* , vol. 11, no. 3. 2018, doi: 10.3390/ma11030454.

[37] S. Sakai *et al.*, "Visible Light-Induced Hydrogelation of an Alginate Derivative and Application to Stereolithographic Bioprinting Using a Visible Light Projector and Acid Red," *Biomacromolecules*, vol. 19, no. 2, pp. 672–679, Feb. 2018, doi: 10.1021/acs.biomac.7b01827.

[38] F. Olate-Moya, L. Arens, M. Wilhelm, M. A. Mateos-Timoneda, E. Engel, and H. Palza, "Chondroinductive Alginate-Based Hydrogels Having Graphene Oxide for 3D Printed Scaffold

Fabrication," *ACS Appl. Mater. Interfaces*, vol. 12, no. 4, pp. 4343–4357, Jan. 2020, doi: 10.1021/acsami.9b22062.

[39] L. K. Narayanan, P. Huebner, M. B. Fisher, J. T. Spang, B. Starly, and R. A. Shirwaiker, "3D-Bioprinting of Polylactic Acid (PLA) Nanofiber–Alginate Hydrogel Bioink Containing Human Adipose-Derived Stem Cells," *ACS Biomater. Sci. Eng.*, vol. 2, no. 10, pp. 1732–1742, Oct. 2016, doi: 10.1021/acsbiomaterials.6b00196.

[40] C. Antich *et al.*, "Bio-inspired hydrogel composed of hyaluronic acid and alginate as a potential bioink for 3D bioprinting of articular cartilage engineering constructs," *Acta Biomater.*, vol. 106, pp. 114–123, 2020, doi: https://doi.org/10.1016/j.actbio.2020.01.046.

[41] A. Nadernezhad, N. Khani, G. A. Skvortsov, and B. Toprakhisar, "Multifunctional 3D printing of heterogeneous hydrogel structures," *Nat. Publ. Gr.*, no. March, pp. 1–12, 2016, doi: 10.1038/srep33178.

[42] G. R. López-Marcial, A. Y. Zeng, C. Osuna, J. Dennis, J. M. García, and G. D. O'Connell, "Agarose-Based Hydrogels as Suitable Bioprinting Materials for Tissue Engineering," *ACS Biomater. Sci. Eng.*, vol. 4, no. 10, pp. 3610–3616, Oct. 2018, doi: 10.1021/acsbiomaterials.8b00903.

[43] Y. Gu, B. Schwarz, A. Forget, A. Barbero, I. Martin, and V. P. Shastri, "Advanced Bioink for 3D Bioprinting of Complex Free-Standing Structures with High Stiffness," *Bioengineering*, vol. 7, no. 4, 2020, doi: 10.3390/bioengineering7040141.

[44] A. Forget *et al.*, "Mechanically Tunable Bioink for 3D Bioprinting of Human Cells," *Adv. Healthc. Mater.*, vol. 6, no. 20, p. 1700255, Oct. 2017, doi: https://doi.org/10.1002/adhm.201700255.

[45] C. B. Highley, C. B. Rodell, and J. A. Burdick, "Direct 3D Printing of Shear-Thinning Hydrogels into Self-Healing Hydrogels," *Adv. Mater.*, vol. 27, no. 34, pp. 5075–5079, Sep. 2015, doi: https://doi.org/10.1002/adma.201501234.

[46] J. A. Burdick and G. D. Prestwich, "Hyaluronic Acid Hydrogels for Biomedical Applications," *Adv. Mater.*, vol. 23, no. 12, pp. H41–H56, Mar. 2011, doi: https://doi.org/10.1002/adma.201003963.

[47] M. E. Prendergast, M. D. Davidson, and J. A. Burdick, "A biofabrication method to align cells within bioprinted photocrosslinkable and cell-degradable hydrogel constructs via embedded fibers," *Biofabrication*, vol. 13, no. 4, 2021, doi: 10.1088/1758-5090/ac25cc.

[48] I. Noh, N. Kim, H. N. Tran, J. Lee, and C. Lee, "3D printable hyaluronic acid-based hydrogel for its potential application as a bioink in tissue engineering," *Biomater. Res.*, vol. 23, no. 1, p. 3, 2019, doi: 10.1186/s40824-018-0152-8.

[49] A. Skardal, J. Zhang, L. McCoard, X. Xu, S. Oottamasathien, and G. D. Prestwich, "Photocrosslinkable Hyaluronan-Gelatin Hydrogels for Two-Step Bioprinting," *Tissue Eng. Part A*, vol. 16, no. 8, pp. 2675–2685, 2010, doi: 10.1089/ten.tea.2009.0798.

[50] J. Lee, S.-H. Lee, B. S. Kim, Y.-S. Cho, and Y. Park, "Development and Evaluation of Hyaluronic Acid-Based Hybrid Bio-Ink for Tissue Regeneration," *Tissue Eng. Regen. Med.*, vol. 15, no. 6, pp. 761–769, 2018, doi: 10.1007/s13770-018-0144-8.

[51] D. Petta, U. D'Amora, L. Ambrosio, D. W. Grijpma, D. Eglin, and M. D'Este, "Hyaluronic acid as a bioink for extrusion-based 3D printing," *Biofabrication*, vol. 12, no. 3, p. 32001, 2020, doi: 10.1088/1758-5090/ab8752.

[52] A. Skardal, J. Zhang, and G. D. Prestwich, "Bioprinting vessel-like constructs using hyaluronan hydrogels crosslinked with tetrahedral polyethylene glycol tetracrylates," *Biomaterials*, vol. 31, no. 24, pp. 6173–6181, 2010, doi: https://doi.org/10.1016/j.biomaterials.2010.04.045.

[53] T. B. Ngo, B. S. Spearman, N. Hlavac, and C. E. Schmidt, "Three-Dimensional Bioprinted Hyaluronic Acid Hydrogel Test Beds for Assessing Neural Cell Responses to Competitive Growth Stimuli," *ACS Biomater. Sci. Eng.*, vol. 6, no. 12, pp. 6819–6830, Dec. 2020, doi: 10.1021/acsbiomaterials.0c00940.

[54] Q. Wu, D. Therriault, and M.-C. Heuzey, "Processing and Properties of Chitosan Inks for 3D Printing of Hydrogel Microstructures," *ACS Biomater. Sci. Eng.*, vol. 4, no. 7, pp. 2643–2652, Jul. 2018, doi: 10.1021/acsbiomaterials.8b00415.

[55] K. D. Roehm and S. V Madihally, "Bioprinted chitosan-gelatin thermosensitive hydrogels using an inexpensive 3D printer," *Biofabrication*, vol. 10, no. 1, p. 15002, Nov. 2017, doi: 10.1088/1758-5090/aa96dd.

[56] Q. Wu, M. Maire, S. Lerouge, D. Therriault, and M.-C. Heuzey, "3D Printing of Microstructured and Stretchable Chitosan Hydrogel for Guided Cell Growth," *Adv. Biosyst.*, vol. 1, no. 6, p. 1700058, Jun. 2017, doi: https://doi.org/10.1002/adbi.201700058.

[57] L. Zhou *et al.*, "3D printing of high-strength chitosan hydrogel scaffolds without any organic

solvents," *Biomater. Sci.*, vol. 8, no. 18, pp. 5020–5028, 2020, doi: 10.1039/D0BM00896F.

[58] A. Sadeghianmaryan *et al.*, "Extrusion-based printing of chitosan scaffolds and their in vitro characterization for cartilage tissue engineering," *Int. J. Biol. Macromol.*, vol. 164, pp. 3179–3192, 2020, doi: https://doi.org/10.1016/j.ijbiomac.2020.08.180.

[59] F. Pahlevanzadeh *et al.*, "Three-Dimensional Printing Constructs Based on the Chitosan for Tissue Regeneration: State of the Art, Developing Directions and Prospect Trends," *Materials (Basel).*, vol. 13, no. 11, 2020, doi: 10.3390/ma13112663.

[60] M. Rahimnejad, T. Labonté-Dupuis, N. R. Demarquette, and S. Lerouge, "A rheological approach to assess the printability of thermosensitive chitosan-based biomaterial inks," *Biomed. Mater.*, vol. 16, no. 1, p. 15003, 2020, doi: 10.1088/1748-605x/abb2d8.

[61] B. J. Klotz, D. Gawlitta, A. J. W. P. Rosenberg, J. Malda, and F. P. W. Melchels, "Gelatin-Methacryloyl Hydrogels: Towards Biofabrication-Based Tissue Repair," *Trends Biotechnol.*, vol. 34, no. 5, pp. 394–407, May 2016, doi: 10.1016/j.tibtech.2016.01.002.

[62] S. Bertlein *et al.*, "Thiol–Ene Clickable Gelatin: A Platform Bioink for Multiple 3D Biofabrication Technologies," *Adv. Mater.*, vol. 29, no. 44, p. 1703404, Nov. 2017, doi: https://doi.org/10.1002/adma.201703404.

[63] D. J. Choi, Y. Kho, S. J. Park, Y.-J. Kim, S. Chung, and C.-H. Kim, "Effect of cross-linking on the dimensional stability and biocompatibility of a tailored 3D-bioprinted gelatin scaffold," *Int. J. Biol. Macromol.*, vol. 135, pp. 659–667, 2019, doi: https://doi.org/10.1016/j.ijbiomac.2019.05.207.

[64] N. Contessi Negrini, N. Celikkin, P. Tarsini, S. Farè, and W. Święszkowski, "Three-dimensional printing of chemically crosslinked gelatin hydrogels for adipose tissue engineering," *Biofabrication*, vol. 12, no. 2, p. 25001, 2020, doi: 10.1088/1758-5090/ab56f9.

[65] A. Leucht, A.-C. Volz, J. Rogal, K. Borchers, and P. J. Kluger, "Advanced gelatin-based vascularization bioinks for extrusion-based bioprinting of vascularized bone equivalents," *Sci. Rep.*, vol. 10, no. 1, p. 5330, 2020, doi: 10.1038/s41598-020-62166-w.

[66] R. Schwartz, M. Malpica, G. L. Thompson, and A. K. Miri, "Cell encapsulation in gelatin bioink impairs 3D bioprinting resolution," *J. Mech. Behav. Biomed. Mater.*, vol. 103, p. 103524, 2020, doi: https://doi.org/10.1016/j.jmbbm.2019.103524.

[67] N. Diamantides, C. Dugopolski, E. Blahut, S. Kennedy, and L. J. Bonassar, "High density cell seeding affects the rheology and printability of collagen bioinks," *Biofabrication*, vol. 11, no. 4, p. 45016, 2019, doi: 10.1088/1758-5090/ab3524.

[68] E. O. Osidak *et al.*, "Viscoll collagen solution as a novel bioink for direct 3D bioprinting," *J. Mater. Sci. Mater. Med.*, vol. 30, no. 3, p. 31, 2019, doi: 10.1007/s10856-019-6233-y.

[69] S. Zhang, D. Huang, H. Lin, Y. Xiao, and X. Zhang, "Cellulose Nanocrystal Reinforced Collagen-Based Nanocomposite Hydrogel with Self-Healing and Stress-Relaxation Properties for Cell Delivery," *Biomacromolecules*, vol. 21, no. 6, pp. 2400–2408, Jun. 2020, doi: 10.1021/acs.biomac.0c00345.

[70] Y. B. Kim, H. Lee, and G. H. Kim, "Strategy to Achieve Highly Porous/Biocompatible Macroscale Cell Blocks, Using a Collagen/Genipin-bioink and an Optimal 3D Printing Process.," *ACS Appl. Mater. Interfaces*, vol. 8, no. 47, pp. 32230–32240, Nov. 2016, doi: 10.1021/acsami.6b11669.

[71] M. K. Włodarczyk-Biegun and A. del Campo, "3D bioprinting of structural proteins," *Biomaterials*, vol. 134, pp. 180–201, 2017, doi: https://doi.org/10.1016/j.biomaterials.2017.04.019.

[72] A. Bandyopadhyay and B. B. Mandal, "A three-dimensional printed silk-based biomimetic tri-layered meniscus for potential patient-specific implantation," *Biofabrication*, vol. 12, no. 1, p. 15003, 2019, doi: 10.1088/1758-5090/ab40fa.

[73] M. J. Rodriguez, J. Brown, J. Giordano, S. J. Lin, F. G. Omenetto, and D. L. Kaplan, "Silk based bioinks for soft tissue reconstruction using 3-dimensional (3D) printing with in vitro and in vivo assessments," *Biomaterials*, vol. 117, pp. 105–115, 2017, doi: https://doi.org/10.1016/j.biomaterials.2016.11.046.

[74] Z. Li *et al.*, "Addition of Platelet-Rich Plasma to Silk Fibroin Hydrogel Bioprinting for Cartilage Regeneration," *Tissue Eng. Part A*, vol. 26, no. 15–16, pp. 886–895, Feb. 2020, doi: 10.1089/ten.tea.2019.0304.

[75] Z. Zheng *et al.*, "3D Bioprinting of Self-Standing Silk-Based Bioink," *Adv. Healthc. Mater.*, vol. 7, no. 6, p. 1701026, Mar. 2018, doi: https://doi.org/10.1002/adhm.201701026.

[76] S. Gupta, H. Alrabaiah, M. Christophe, M. Rahimi-Gorji, S. Nadeem, and A. Bit, "Evaluation of silk-based bioink during pre and post 3D bioprinting: A review," *J. Biomed. Mater. Res. Part B Appl. Biomater.*, vol. 109, no. 2, pp. 279–293, Feb. 2021, doi: https://doi.org/10.1002/jbm.b.34699.

[77] P. N. Bernal *et al.*, "Volumetric Bioprinting of Organoids and Optically Tuned Hydrogels to Build Liver-Like Metabolic Biofactories," *Adv. Mater.*, 2022, doi: 10.1002/adma.202110054.

[78] H. Ravanbakhsh *et al.*, "Freeform cell-laden cryobioprinting for shelf-ready tissue fabrication and storage," *Matter*, vol. 5, no. 2, pp. 573–593, 2022, doi: 10.1016/j.matt.2021.11.020.

[79] J. Zhu, "Bioactive modification of poly(ethylene glycol) hydrogels for tissue engineering," *Biomaterials*, vol. 31, no. 17, pp. 4639–4656, 2010, doi: https://doi.org/10.1016/j.biomaterials.2010.02.044.

[80] Z. Luo *et al.*, "Vertical Extrusion Cryo(bio)printing for Anisotropic Tissue Manufacturing," *Adv. Mater.*, vol. 34, no. 12, pp. 1–13, 2022, doi: 10.1002/adma.202108931.

[81] H. Hanai, G. Jacob, S. Nakagawa, R. S. Tuan, and D. E. Heath, "Potential of Soluble Decellularized Extracellular Matrix for Musculoskeletal Tissue Engineering – Comparison of Various Mesenchymal Tissues," vol. 8, no. November, pp. 1–15, 2020, doi: 10.3389/fcell.2020.581972.

[82] B. Kang *et al.*, "Facile Bioprinting Process for Fabricating Size-Controllable Functional Microtissues Using Light-Activated Decellularized Extracellular Matrix-Based Bioinks," *Adv. Mater. Technol.*, vol. 2100947, pp. 1–13, 2021, doi: 10.1002/admt.202100947.

[83] M. Ali, A. K. PR, J. J. Yoo, F. Zahran, A. Atala, and S. J. Lee, "A Photo-Crosslinkable Kidney ECM-Derived Bioink Accelerates Renal Tissue Formation," *Adv. Healthc. Mater.*, vol. 8, no. 7, p. 1800992, Apr. 2019, doi: https://doi.org/10.1002/adhm.201800992.

[84] K. T. Lawlor *et al.*, "Cellular extrusion bioprinting improves kidney organoid reproducibility and conformation," *Nat. Mater.*, vol. 20, no. 2, pp. 260–271, 2021, doi: 10.1038/s41563-020-00853-9.

[85] R. Sobreiro-Almeida, M. Gómez-Florit, R. Quinteira, R. L. Reis, M. E. Gomes, and N. M. Neves, "Decellularized kidney extracellular matrix bioinks recapitulate renal 3D microenvironment in vitro," *Biofabrication*, vol. 13, no. 4, p. 45006, 2021, doi: 10.1088/1758-5090/ac0fca.

[86] F. Pati *et al.*, "Printing three-dimensional tissue analogues with decellularized extracellular matrix bioink," *Nat. Commun.*, vol. 5, pp. 1–11, 2014, doi: 10.1038/ncomms4935.

[87] J. M. Singelyn and K. L. Christman, "Modulation of Material Properties of a Decellularized Myocardial Matrix Scaffold," *Macromol. Biosci.*, vol. 11, no. 6, pp. 731–738, Jun. 2011, doi: https://doi.org/10.1002/mabi.201000423.

[88] S. B. Seif-Naraghi, D. Horn, P. J. Schup-Magoffin, and K. L. Christman, "Injectable extracellular matrix derived hydrogel provides a platform for enhanced retention and delivery of a heparin-binding growth factor," *Acta Biomater.*, vol. 8, no. 10, pp. 3695–3703, 2012, doi: https://doi.org/10.1016/j.actbio.2012.06.030.

[89] J. Fernández-Pérez and M. Ahearne, "The impact of decellularization methods on extracellular matrix derived hydrogels," *Sci. Rep.*, vol. 9, no. 1, p. 14933, 2019, doi: 10.1038/s41598-019-49575-2.

[90] Y.-J. Choi *et al.*, "A 3D cell printed muscle construct with tissue-derived bioink for the treatment of volumetric muscle loss," *Biomaterials*, vol. 206, pp. 160–169, 2019, doi: https://doi.org/10.1016/j.biomaterials.2019.03.036.

[91] X. Zhang, D. Wang, K. K. Mak, R. S. Tuan, and D. F. E. Ker, "Engineering Musculoskeletal Grafts for Multi-Tissue Unit Repair: Lessons From Developmental Biology and Wound Healing," *Front. Physiol.*, vol. 12, no. August, Aug. 2021, doi: 10.3389/fphys.2021.691954.

[92] A. Ravichandran, B. Murekatete, and D. Moedder, "Photocrosslinkable liver extracellular matrix hydrogels for the generation of 3D liver microenvironment models," *Sci. Rep.*, pp. 1–12, 2021, doi: 10.1038/s41598-021-94990-z.

[93] V. Lee *et al.*, "Design and Fabrication of Human Skin by Three-Dimensional Bioprinting," *Tissue Eng. Part C Methods*, vol. 20, no. 6, pp. 473–484, Nov. 2013, doi: 10.1089/ten.tec.2013.0335.

[94] B. S. Kim *et al.*, "3D cell printing of in vitro stabilized skin model and in vivo pre-vascularized skin patch using tissue-specific extracellular matrix bioink: A step towards advanced skin tissue engineering," *Biomaterials*, vol. 168, pp. 38–53, 2018, doi: https://doi.org/10.1016/j.biomaterials.2018.03.040.

[95] A.-N. Cho *et al.*, "Microfluidic device with brain extracellular matrix promotes structural and functional maturation of human brain organoids," *Nat. Commun.*, vol. 12, no. 1, p. 4730, 2021, doi: 10.1038/s41467-021-24775-5.

[96] C. J. Medberry *et al.*, "Hydrogels derived from central nervous system extracellular matrix," *Biomaterials*, vol. 34, no. 4, pp. 1033–1040, 2013, doi: https://doi.org/10.1016/j.biomaterials.2012.10.062.

[97] L. R. Madden *et al.*, "Bioprinted 3D Primary Human Intestinal Tissues Model Aspects of Native

Physiology and ADME/Tox Functions," *iScience*, vol. 2, pp. 156–167, Apr. 2018, doi: 10.1016/j.isci.2018.03.015.

[98] S. Rajasekar *et al.*, "IFlowPlate—A Customized 384-Well Plate for the Culture of Perfusable Vascularized Colon Organoids," *Adv. Mater.*, vol. 32, no. 46, p. 2002974, Nov. 2020, doi: 10.1002/adma.202002974.

[99] T. J. Keane *et al.*, "Preparation and characterization of a biologic scaffold and hydrogel derived from colonic mucosa," *J. Biomed. Mater. Res. Part B Appl. Biomater.*, vol. 105, no. 2, pp. 291–306, Feb. 2017, doi: https://doi.org/10.1002/jbm.b.33556.

[100] D. Boso, E. Maghin, E. Carraro, M. Giagante, P. Pavan, and M. Piccoli, "Extracellular Matrix-Derived Hydrogels as Biomaterial for Different Skeletal Muscle Tissue Replacements," *Mater. (Basel, Switzerland)*, vol. 13, no. 11, p. 2483, May 2020, doi: 10.3390/ma13112483.

[101] J. A. DeQuach *et al.*, "Injectable skeletal muscle matrix hydrogel promotes neovascularization and muscle cell infiltration in a hindlimb ischemia model," *Eur. Cell. Mater.*, vol. 23, pp. 400–412, Jun. 2012, doi: 10.22203/ecm.v023a31.

[102] B. Toprakhisar, A. Nadernezhad, E. Bakirci, N. Khani, G. A. Skvortsov, and B. Koc, "Development of Bioink from Decellularized Tendon Extracellular Matrix for 3D Bioprinting," *Macromol. Biosci.*, vol. 18, no. 10, p. 1800024, Oct. 2018, doi: 10.1002/mabi.201800024.

[103] A. Dede Eren *et al.*, "Decellularized Porcine Achilles Tendon Induces Anti-inflammatory Macrophage Phenotype In Vitro and Tendon Repair In Vivo," *J. Immunol. Regen. Med.*, vol. 8, no. January, p. 100027, Jun. 2020, doi: 10.1016/j.regen.2020.100027.

[104] F. Zhao *et al.*, "Digestion degree is a key factor to regulate the printability of pure tendon decellularized extracellular matrix bio-ink in extrusion-based 3D cell printing," *Biofabrication*, vol. 12, no. 4, p. 045011, Jul. 2020, doi: 10.1088/1758-5090/aba411.

[105] F. Zhao *et al.*, "Comparison of three different acidic solutions in tendon decellularized extracellular matrix bio-ink fabrication for 3D cell printing," *Acta Biomater.*, vol. 131, no. xxxx, pp. 262–275, Sep. 2021, doi: 10.1016/j.actbio.2021.06.026.

[106] S. Farnebo *et al.*, "Design and Characterization of an Injectable Tendon Hydrogel: A Novel Scaffold for Guided Tissue Regeneration in the Musculoskeletal System," *Tissue Eng. Part A*, vol. 20, no. 9–10, pp. 1550–1561, May 2014, doi: 10.1089/ten.tea.2013.0207.

[107] M. C. Prewitz *et al.*, "Tightly anchored tissue-mimetic matrices as instructive stem cell microenvironments.," *Nat. Methods*, vol. 10, no. 8, pp. 788–794, Aug. 2013, doi: 10.1038/nmeth.2523.

[108] S. Sart, S. N. Agathos, and Y. Li, "Engineering stem cell fate with biochemical and biomechanical properties of microcarriers.," *Biotechnol. Prog.*, vol. 29, no. 6, pp. 1354–1366, 2013, doi: 10.1002/btpr.1825.

[109] C. Liu, M. Pei, Q. Li, and Y. Zhang, "Decellularized extracellular matrix mediates tissue construction and regeneration," *Front. Med.*, vol. 16, no. 1, pp. 56–82, 2022, doi: 10.1007/s11684-021-0900-3.

[110] A. D. Theocharis, S. S. Skandalis, C. Gialeli, and N. K. Karamanos, "Extracellular matrix structure.," *Adv. Drug Deliv. Rev.*, vol. 97, pp. 4–27, Feb. 2016, doi: 10.1016/j.addr.2015.11.001.

[111] S. Ricard-Blum, "The collagen family," *Cold Spring Harb. Perspect. Biol.*, vol. 3, no. 1, pp. a004978–a004978, Jan. 2011, doi: 10.1101/cshperspect.a004978.

[112] D. Choudhury, H. W. Tun, T. Wang, and M. W. Naing, "Organ-Derived Decellularized Extracellular Matrix : A Game Changer for Bioink Manufacturing ?," *Trends Biotechnol.*, vol. 36, no. 8, pp. 787–805, 2018, doi: 10.1016/j.tibtech.2018.03.003.

[113] K. R. Legate, S. A. Wickström, and R. Fässler, "Genetic and cell biological analysis of integrin outside-in signaling.," *Genes Dev.*, vol. 23, no. 4, pp. 397–418, Feb. 2009, doi: 10.1101/gad.1758709.

[114] S. J. Morrison and A. C. Spradling, "Stem cells and niches: mechanisms that promote stem cell maintenance throughout life.," *Cell*, vol. 132, no. 4, pp. 598–611, Feb. 2008, doi: 10.1016/j.cell.2008.01.038.

[115] A. J. Engler, S. Sen, H. L. Sweeney, and D. E. Discher, "Matrix elasticity directs stem cell lineage specification.," *Cell*, vol. 126, no. 4, pp. 677–689, Aug. 2006, doi: 10.1016/j.cell.2006.06.044.

[116] P. M. Gilbert *et al.*, "Substrate elasticity regulates skeletal muscle stem cell self-renewal in culture.," *Science*, vol. 329, no. 5995, pp. 1078–1081, Aug. 2010, doi: 10.1126/science.1191035.

[117] M. Hirata and T. Yamaoka, "Effect of stem cell niche elasticity/ECM protein on the self-beating

cardiomyocyte differentiation of induced pluripotent stem (iPS) cells at different stages.," *Acta Biomater.*, vol. 65, pp. 44–52, Jan. 2018, doi: 10.1016/j.actbio.2017.10.032.

[118] J. M. Muncie, N. M. E. Ayad, J. N. Lakins, X. Xue, J. Fu, and V. M. Weaver, "Mechanical Tension Promotes Formation of Gastrulation-like Nodes and Patterns Mesoderm Specification in Human Embryonic Stem Cells.," *Dev. Cell*, vol. 55, no. 6, pp. 679-694.e11, Dec. 2020, doi: 10.1016/j.devcel.2020.10.015.

[119] B. S. Kim, S. Das, J. Jang, and D.-W. Cho, "Decellularized Extracellular Matrix-based Bioinks for Engineering Tissue- and Organ-specific Microenvironments," *Chem. Rev.*, vol. 120, no. 19, pp. 10608–10661, Oct. 2020, doi: 10.1021/acs.chemrev.9b00808.

[120] F. Kabirian and M. Mozafari, "Decellularized ECM-derived bioinks : Prospects for the future," vol. 171, no. February 2019, pp. 108–118, 2020, doi: 10.1016/j.ymeth.2019.04.019.

[121] T. W. Gilbert, T. L. Sellaro, and S. F. Badylak, "Decellularization of tissues and organs," *Biomaterials*, vol. 27, no. 19, pp. 3675–3683, 2006, doi: https://doi.org/10.1016/j.biomaterials.2006.02.014.

[122] E. Uchimura *et al.*, "Novel method of preparing acellular cardiovascular grafts by decellularization with poly(ethylene glycol)," *J. Biomed. Mater. Res. Part A*, vol. 67A, no. 3, pp. 834–837, Dec. 2003, doi: https://doi.org/10.1002/jbm.a.10097.

[123] S. F. Badylak, "Xenogeneic extracellular matrix as a scaffold for tissue reconstruction," *Transpl. Immunol.*, vol. 12, no. 3, pp. 367–377, 2004, doi: https://doi.org/10.1016/j.trim.2003.12.016.

[124] P. M. Crapo, T. W. Gilbert, and S. F. Badylak, "An overview of tissue and whole organ decellularization processes," *Biomaterials*, vol. 32, no. 12, pp. 3233–3243, 2011, doi: https://doi.org/10.1016/j.biomaterials.2011.01.057.

[125] A. J. Vernengo, S. Grad, D. Eglin, M. Alini, and Z. Li, "Bioprinting Tissue Analogues with Decellularized Extracellular Matrix Bioink for Regeneration and Tissue Models of Cartilage and Intervertebral Discs," vol. 1909044, 2020, doi: 10.1002/adfm.201909044.

[126] S. L. Wilson, L. E. Sidney, S. E. Dunphy, J. B. Rose, and A. Hopkinson, "Keeping an Eye on Decellularized Corneas: A Review of Methods, Characterization and Applications," *J. Funct. Biomater.*, vol. 4, no. 3, pp. 114–161, 2013, doi: 10.3390/jfb4030114.

[127] Y. Luo, D. Lou, L. Ma, and C. Gao, "Optimizing detergent concentration and processing time to

balance the decellularization efficiency and properties of bioprosthetic heart valves," *J. Biomed. Mater. Res. Part A*, vol. 107, no. 10, pp. 2235–2243, Oct. 2019, doi: https://doi.org/10.1002/jbm.a.36732.

[128] L. C. Junqueira and J. Carneiro, *Basic Histology*, 3rd ed. Rio de Janeiro: Guanabara, 1974.

[129] B. C. Pridgen *et al.*, "Flexor Tendon Tissue Engineering: Acellularization of Human Flexor Tendons with Preservation of Biomechanical Properties and Biocompatibility," *Tissue Eng. Part C Methods*, vol. 17, no. 8, pp. 819–828, Aug. 2011, doi: 10.1089/ten.tec.2010.0457.

[130] S. S. Raghavan *et al.*, "Human Flexor Tendon Tissue Engineering: Decellularization of Human Flexor Tendons Reduces Immunogenicity In Vivo," *Tissue Eng. Part A*, vol. 18, no. 7–8, pp. 796–805, Apr. 2012, doi: 10.1089/ten.tea.2011.0422.

[131] M. A. Bhat *et al.*, "Preparation and Functional Characterization of Decellularized Bovine Tendon Scaffolds for Tendon Tissue Engineering," *J. Anim. Res.*, vol. 5, no. 4, p. 921, 2015, doi: 10.5958/2277-940X.2015.00152.7.

[132] X. Yao *et al.*, "Stem Cell Extracellular Matrix-Modified Decellularized Tendon Slices Facilitate the Migration of Bone Marrow Mesenchymal Stem Cells," *ACS Biomater. Sci. Eng.*, vol. 5, no. 9, pp. 4485–4495, Sep. 2019, doi: 10.1021/acsbiomaterials.9b00064.

[133] D. W. Youngstrom, J. G. Barrett, R. R. Jose, and D. L. Kaplan, "Functional Characterization of Detergent-Decellularized Equine Tendon Extracellular Matrix for Tissue Engineering Applications," vol. 8, no. 5, 2013, doi: 10.1371/journal.pone.0064151.

[134] P. Aeberhard *et al.*, "Efficient decellularization of equine tendon with preserved biomechanical properties and cytocompatibility for human tendon surgery indications," *Artif. Organs*, vol. 44, no. 4, pp. 161–171, Apr. 2020, doi: 10.1111/aor.13581.

[135] G. Jones, A. Herbert, H. Berry, J. H. Edwards, J. Fisher, and E. Ingham, "Decellularization and Characterization of Porcine Superflexor Tendon: A Potential Anterior Cruciate Ligament Replacement," *Tissue Eng. Part A*, vol. 23, no. 3–4, pp. 124–134, Feb. 2017, doi: 10.1089/ten.tea.2016.0114.

[136] A. Lohan, B. Kohl, C. Meier, and G. Schulze-tanzil, "Tenogenesis of Decellularized Porcine Achilles Tendon Matrix Reseeded with Human Tenocytes in the Nude Mice Xenograft Model," pp. 1–18, 2018, doi: 10.3390/ijms19072059.

[137] L. T. Saldin, M. C. Cramer, S. S. Velankar, L. J. White, and S. F. Badylak, "Extracellular matrix hydrogels from decellularized tissues: Structure and function," *Acta Biomater.*, vol. 49, pp. 1–15, Feb. 2017, doi: 10.1016/j.actbio.2016.11.068.

[138] E. J. Miller, "Structural studies on cartilage collagen employing limited cleavage and solubilization with pepsin.," *Biochemistry*, vol. 11, no. 26, pp. 4903–4909, Dec. 1972, doi: 10.1021/bi00776a005.

[139] D. J. S. Hulmes, "Collagen Diversity, Synthesis and Assembly BT - Collagen: Structure and Mechanics," P. Fratzl, Ed. Boston, MA: Springer US, 2008, pp. 15–47.

[140] D. O. Freytes, J. Martin, S. S. Velankar, A. S. Lee, and S. F. Badylak, "Preparation and rheological characterization of a gel form of the porcine urinary bladder matrix," *Biomaterials*, vol. 29, no. 11, pp. 1630–1637, 2008, doi: https://doi.org/10.1016/j.biomaterials.2007.12.014.

[141] S. Xie *et al.*, "Book-shaped decellularized tendon matrix scaffold combined with bone marrow mesenchymal stem cells-sheets for repair of achilles tendon defect in rabbit," *J. Orthop. Res.*, vol. 37, no. 4, pp. 887–897, Apr. 2019, doi: 10.1002/jor.24255.

[142] J. Burk *et al.*, "Freeze-Thaw Cycles Enhance Decellularization of Large Tendons," *Tissue Eng. Part C Methods*, vol. 20, no. 4, pp. 276–284, Apr. 2014, doi: 10.1089/ten.tec.2012.0760.

[143] A. de Lima Santos *et al.*, "A new decellularized tendon scaffold for rotator cuff tears – evaluation in rabbits," *BMC Musculoskelet. Disord.*, vol. 21, no. 1, p. 689, Dec. 2020, doi: 10.1186/s12891-020-03680-w.

[144] B. Zhang, A. Korolj, B. F. L. Lai, and M. Radisic, "Advances in organ-on-a-chip engineering," *Nat. Rev. Mater.*, vol. 3, no. 8, pp. 257–278, 2018, doi: 10.1038/s41578-018-0034-7.

[145] S. Caddeo, M. Boffito, and S. Sartori, "Tissue Engineering Approaches in the Design of Healthy and Pathological In Vitro Tissue Models," *Front. Bioeng. Biotechnol.*, vol. 5, 2017, doi: 10.3389/fbioe.2017.00040.

[146] H. Tempfer and A. Traweger, "Tendon Vasculature in Health and Disease," *Front. Physiol.*, vol. 6, 2015, doi: 10.3389/fphys.2015.00330.

[147] S. Wu, Y. Wang, P. N. Streubel, and B. Duan, "Living nanofiber yarn-based woven biotextiles for tendon tissue engineering using cell tri-culture and mechanical stimulation," *Acta Biomater.*, vol.

62, pp. 102–115, 2017, doi: https://doi.org/10.1016/j.actbio.2017.08.043.

[148] Y. Zhao *et al.*, "Engineering microenvironment for human cardiac tissue assembly in heart-on-a-chip platform," *Matrix Biol.*, vol. 85–86, pp. 189–204, 2020, doi: 10.1016/j.matbio.2019.04.001.

[149] B. S. Moura, M. V Monteiro, L. P. Ferreira, P. Lavrador, V. M. Gaspar, and J. F. Mano, "Advancing Tissue Decellularized Hydrogels for Engineering Human Organoids," *Adv. Funct. Mater.*, p. 2202825, May 2022, doi: 10.1002/adfm.202202825.

Chapter II.

Materials and Methods

Chapter II. Materials and Methods

Under the scope of this thesis, we ambitioned to develop tendon-on-chip models that comply with the requirements of tendon tissue and organs-on-chip. Therefore, we intended to recreate the native tendon niche and reproduce the interaction between this tissue and the vascular system. In this section, we describe in detail the materials that were selected for this study, and the experimental procedures developed throughout this thesis, to allow their understanding and reproducibility, achieving the main objectives proposed by this thesis.

II.1. Materials

In tissue engineering strategies and organs-on-chip development, it is important to select the adequate materials to recreate the native microenvironment of the tissue/organ of interest. For this purpose, a detailed description of the materials used in this study, as well as the motivation behind their selection is herein described in this section.

II.1.1. Decellularized extracellular matrix (dECM) hydrogel

In biomaterials-based regenerative medicine strategies, it is important to use materials that can recreate the specific cellular niche of the target tissue. Decellularized extracellular matrix (dECM) have been extensively used in the regenerative medicine field, as this material can exert synergistic effects by triggering tissue-specific differentiation processes that can recreate original cellular functions. Trough cell-ECM communication, ECM has the ability to regulate stem-cell fate with its structural support, biochemical composition, growth factors, and biochemical factors [1]. In tendon tissues, collagen represents 70% of tendon ECM dry weight, with the prevalence of collagen type I (95%), followed by collagen type III (3%), and small levels (2%) of collagen type V, XI, XII and XIV [2]. This makes dECM-based bioinks hydrogels with superior potential to recapitulate tissue-specific microenvironmental niches when compared with other protein-based bioinks such as collagen or gelatin [1], [3]. ECM-derived biomaterials are a complex mixture of extracellular components and cellular material that can represent a source of host reactivity, causing immune rejection and inflammatory response [3], [4]. To remove the cellular material, the tissue is submitted to a process of decellularization that involves physical, chemical, and enzymatic treatments to efficiently eliminate its cellular content while preserving the essential components of the ECM. Physical treatments of decellularization include freeze-thaw cycles, pressure or mechanical force, mechanical agitation, sonication, or supercritical CO_2 [5], [6]. On the other hand, chemical treatments are usually

based on different soaking cycles with acids or bases, detergents, hypotonic and hypertonic solutions, chelating agents and solvents, while enzymatic treatments involve the use of nucleases and proteases to cleave proteins and cellular bonds [1], [3], [7]–[10]. An efficient and robust decellularization protocol should include a combination of physical, chemical, and enzymatic approaches, and should have a good balance between nuclear content removal and preservation of the major ECM components.

It is important to select the appropriate animal source since each species has advantages and disadvantages related with its inherent biological specificities. Tissues from porcine, bovine, caprine, cercopithecine, lapine and murine origin are the mostly widely used animal sources to develop dECM. Although bovine Achilles tendon has been a common choice for tendon decellularization [11]–[14], pig has been the major tissue source not only for preparing tendon dECM, but also for other organs/tissues in general, as this animal source is sustainable, easily available, have higher breeding potential, short gestation period and rapid growth, and also show some anatomical and physiological similarities to humans [3], [15]–[22].

Another important aspect of using decellularized tissues in this filed are the concerns related with its potential immunogenicity. dECM derived biomaterials should not be cytotoxic or induce any immunological response. In this regard, one of the main concerns of using tissues from porcine origin is the immune rejection of porcine antigens caused by alpha-gal (α-gal) epitope [3], [21]. Luckily, cloning technology is able to eliminate the gene encoding α-galactosyltransferase, generating α-gal-knockout pigs, which would overcome this translational barrier [3]. After decellularization, besides the complete removal of nuclear content, it is also important to ensure that no detergent or enzyme residues remains present, as it can negatively affect cell viability.

Herein, the decellularization process was optimized to obtain a well-preserved tendon dECM from porcine flexor tendons, which were then used to develop a hydrogel suitable for bioprinting, as will be further described in the methods section.

II.1.2. Cellulose Nanocrystals (CNCs)

Cellulose is one of the most abundant renewable organic biomaterial on the nature, produced from plants, marine animals and bacteria [23]–[27]. Despite of its source, cellulose is characterized as a high molecular weight homopolymer of β-1,4-linked anhydro-D-glucose units, in which every monomer

is corkscrewed 180° relatively to its neighbors, and the repeat segment is a dimer of glucose, known as cellobiose [24].

Cellulose nanocrystals (CNCs) are most commonly produced from lignocellulosic sources such as wood pulp, grasses and cotton [25]. The high-ordered assembly in wood and the chemical interactions between its hydrophilic and hydrophobic components modulate the interactions with water [27]. CNCs are highly crystalline nanoparticles typically produced by acid hydrolysis, causing the selective chemical degradation of the amorphous regions, isolating rod-shaped crystalline regions [26]. The most commonly used method for production of CNCs is by sulfuric acid hydrolysis, where cellulose chains undergo two simultaneous chemical reactions, as demonstrated in figure II.1: hydrolysis of glycosidic bonds and esterification of surface hydroxyl groups [25]. The hydrolysis of glycosidic bonds occurs rapidly in the less-ordered regions of cellulose, decreasing the length of cellulose chains, until mostly remaining the more resistant crystalline regions, while simultaneously it occurs the esterification of hydroxyl groups forming sulfate half-ester groups on its surface [25]. These two reactions result in rod-shaped CNCs with high aspect ratio and a high crystallinity index, showing high colloidal stability in aqueous suspensions due to the electrostatic repulsion forces between nanoparticles, [25], [26].

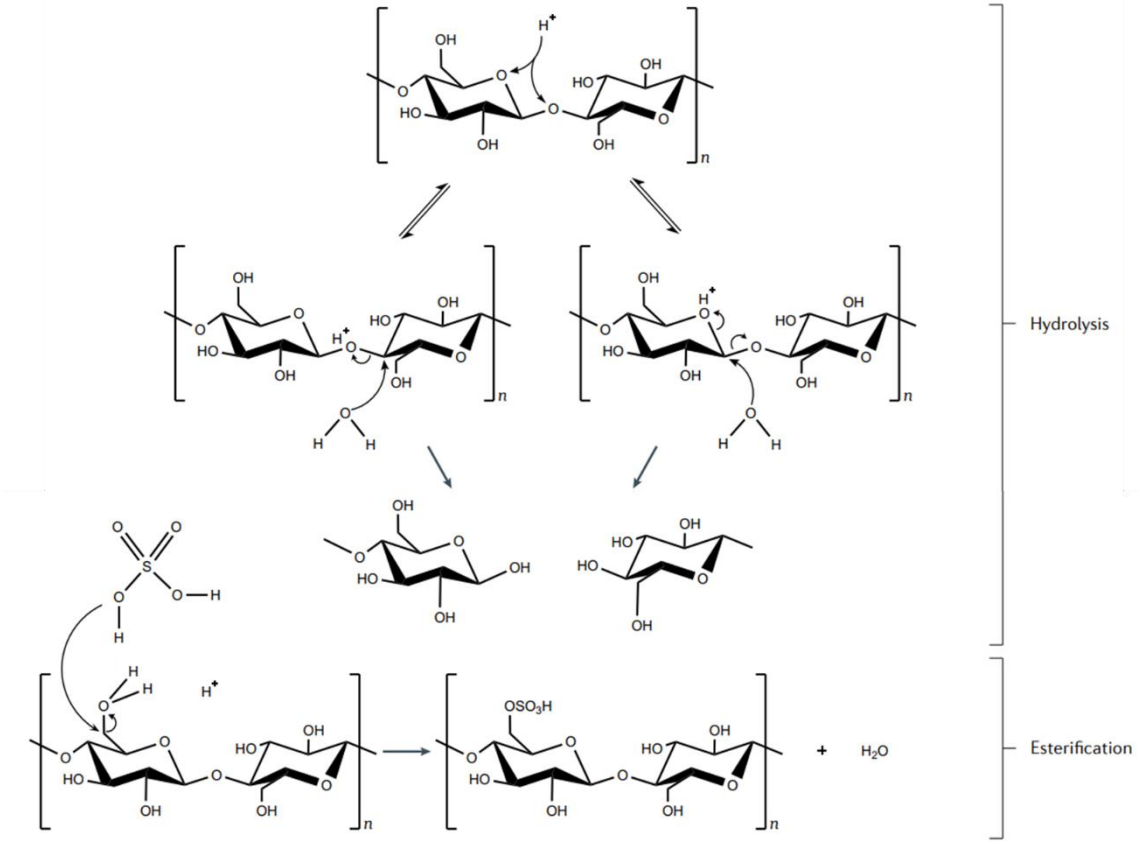

Figure II.1. Mechanism for hydrolysis and esterification of cellulose subjected to concentrated sulfuric acid, to produce CNCs (adapted from [25]).

Fibrillar hydrogels are formed in a hierarchical process, and the mechanism of gel formation depends on the types of building blocks (e.g., colloidal particles or molecules as peptides or block copolymers) [26]. CNCs have typical length between 100-300 nm and diameter between 5-30 nm, depending on their origin. These particles can associate side-by-side, end-to-end, into fibers with a range of diameters, with high self-assembled aqueous stability supported by the balance of van der Walls attraction and electrostatic repulsion, as well as intra- and intermolecular hydrogen bonds [25], [26].

As a high-quality nanomaterial, CNCs has been used for several applications as materials for biomedical devices, electronics and sensors, high-viscosity fluids and polymer composites, but specially, this material has been gaining attention in the field of tissue engineering and regenerative medicine (TERM) strategies [25], [28]. One of the possible applications is to be used as fluid gel to assist embedded 3D bioprinting strategies. Embedded bioprinting concepts refer to printing bioinks into a prepared reservoir made of fluid media, providing a physically supportive bath that avoids the collapse of the printed structure induced by gravity. This embedding material should be biocompatible and have appropriate rheological behavior to allow the printing of the bioink [3]. A recent work developed by our group has proposed CNCs as building blocks for a "print-then-lock" approach resulting in an ECM mimetic fibrillar support material. This strategy explored the concept of 3D Bioprinting within suspension baths made of CNC fluid gel to biofabricate hierarchical living constructs for developing physiologically relevant 3D *in vitro* models [29]. In this system CNCs were produced from microcrystalline cellulose by sulfuric acid hydrolysis, resulting in rod-shaped nanocrystals with dimensions of 173.4 ± 16.1 nm in length and 4.9 ± 1.8 nm in width, and then uses a biocompatible bivalent ion (Ca^{2+}) to control the rheological behavior and induce the self-assembly of these colloidal suspension [29]. The addition of Ca^{2+} ions reduce the Debye length of nanoparticles and consequently causes their lateral aggregation by dominant attractive interactions (e.g., Van der Waals forces and hydrogen bonding), as show in figure II.2 [29].

The CNCs fluid gel at 2.5 wt.% with 2×10^{-3} M Ca^{2+} solution presents shear-thinning and self-healing behavior, which allows the fluid gel to rapidly recover from a predominantly viscous to a predominantly elastic state after disruption by an external mechanical stimulus (e.g., nozzle) [29]. These properties allow the printing of different viscosity bioinks, retaining the printed patterns with good shape fidelity and high resolution [29]. After printing, the structure is locked with an excess of Ca^{2+} (7.5×10^{-3} M), resulting in stable hydrogels with a well-developed hierarchical fibrillar architecture as show in Figure II.2, whose entangled fibrils have a mean diameter of 28.5 ± 11.3 nm and mean pore size of 76.7 ± 17.8 nm, matching the corresponding dimensions found in native ECMs [29].

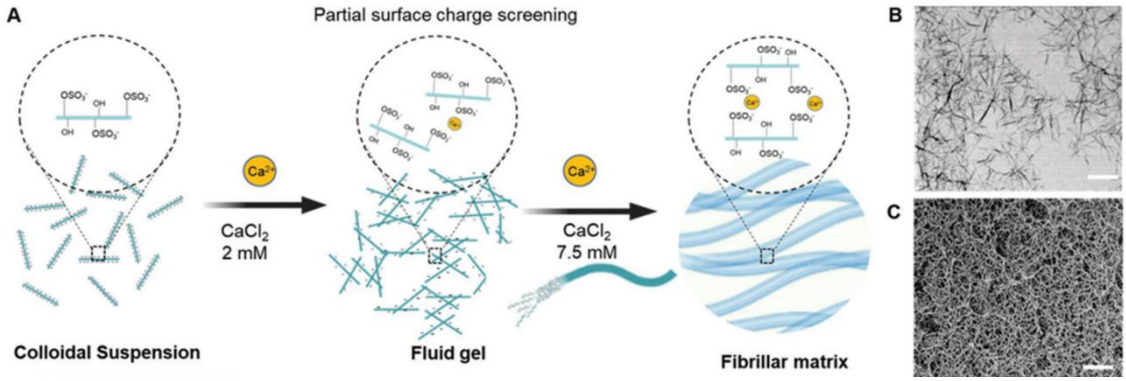

Figure II.2. A) Schematic illustration of the transformation of a colloidal suspension of CNC into a fluid gel by partial surface charge screening on the addition of Ca^{2+} ions followed by its locking into fibrillar matrix by CNC self-assembly induced by the addition of excess cations. Scanning electron microscopy images (SEM) of B) CNC showing its rod-shaped morphology, and C) self-assembled hydrogel showing hierarchical arrangements of CNC into fibrillar networks (scale bar: 200 nm) (Adapted from [29]).

The present work aims to explore this CNC-based platform for the development of 3D bioprinted human tendon models. The proposed concept consists on printing tendon dECM-based bioink within this transparent print-then-lock system, obtaining high-resolution printing with the desired 3D patterns housed within the CNC fibrillar matrix to support its long-term *in vitro* maturation.

II.1.3. Platelet Lysate (PL)

Platelet Lysate (PL) is a source of growth factors (GFs) involved in essential stages of wound healing and regenerative processes such as chemotaxis, cell proliferation and differentiation. Various GFs are present in its composition, including platelet derived growth factor (PDGF), vascular endothelial growth factor (VEGF), transforming growth factor-β (TGF-β), fibroblast growth factor (FGF), insulin growth factor (IGF), epithelial growth factor (EGF), among others, along with adhesive proteins such as fibrin, fibrinogen, fibronectin, and vitronectin, which play an important role in the formation of ECM and in the adhesion and migration of cells [30]–[34]. PL can be obtained from platelet concentrates by cryogenic disruption of platelets, and exhibits several advantages, including: i) the possibility of either autologous or allogenic application, ii) modulation of inflammatory processes and wound healing, iii) PL is a solution that hardly forms spontaneously a gel or retracts as the clot and platelet debris are removed during PL processing, iv) the freeze/thaw cycles are easy to standardize and do not requires the addition of any clot activator to release the platelet factors, v) it can be frozen and stored for further use, and vi) the concentration of the

GFs and cytokines is highly reproducible between batches (when we have polled batches from several donors), which can contribute for more predictable outcomes [32], [35].

PL has been widely used in tissue engineering strategies, as it is safe, easily obtainable from the blood of the patient, and is a cost-effective source of bioactive molecules [31], [33]. In a previous work developed by our group, PL was used as a bioink for the encapsulation of endothelial cells, and showed highly inductive cell proliferation properties, with formation of extensive cell-to-cell contacts [29]. It has been previously described that a combination of growth factors can synergistically induce angiogenesis and long-lasting functional vessels compared with a single growth factor and, in an animal study, the controlled release of PL was effective in encouraging angiogenesis in a critical limb ischemia [36]. In another study, a controlled release of PL proteins from genipin-crosslinked PL patches supported the activity of human tendon-derived cells (hTDCs), which showed an up-regulation of tenogenic genes and deposition of tendon-related extracellular matrix proteins, suggesting that PL support the activity of native tendon cells, being those proposed for tendon regeneration applications [32].

In this work, we propose the use of PL to provide support for the endothelial cells, and we apply this bioink in the development of the multicellular systems, in order to evaluate the cellular crosstalk between endothelial cells and tendon core compartment.

II.2. Methods

II.2.1. Porcine tendons decellularization and processing

Porcine trotters were obtained from a local slaughterhouse and the flexor *profundus* tendons were immediately harvested under aseptic conditions, following a previously optimized harvesting protocol [37]. After dissection, the tendons were cut in small pieces and frozen at -80 °C for further decellularization.

The decellularization procedure was based on the protocol developed by B. Toprakhisar et. al. [13], with some modifications. In general, it consisted of successive soaking cycles performed under sterile conditions and kept in an orbital shaker at 4 °C unless otherwise is referred. The used reagents Phosphate Buffered Saline (PBS), Tris, NaCl, EDTA, TrisHCl, $MgCl_2$, $CaCl_2$, Triton X-100 and Sodium Dodecyl Sulfate (SDS) were purchased from Sigma-Aldrich, Trypsin from Thermo Fisher and DNase I from VWR.

Tendons samples were first subjected to five cycles of freeze-thaw in liquid nitrogen and PBS at 37 °C, respectively, and then incubated in a solution of 50 mM Tris/ 1.5 M NaCl (pH=7.6) overnight. The tissue samples were then incubated at 37 °C in a solution of 0.5% (v/v) Trypsin/ 5mM EDTA (in PBS) (pH=7.6), and then immersed in a 2% SDS + 2% Triton X-100 solution (w/v and v/v respectively, in PBS) for 2 days. Upon this, the tendon samples were rinsed with PBS and then incubated in 10 mM Tris + 1% Triton X-100 for 1 day. Subsequently, the samples were incubated in DNase (200 U/mL) at 37 °C overnight, and finally washed with PBS containing antibiotic for one week to remove any remaining detergent or enzyme.

After decellularization, the tendon samples were freeze-dried and milled in a cryogenic grinder (SPEX SamplePrep) during 2 min, with a rate of 20 cps (cycles per second), resulting in a homogeneous powder of porcine tendon decellularized extracellular matrix (dECM). The dECM was then stored at -20°C until further use. The multiple processing steps starting from the tendon dissection until the final milled powder can be seen in the figure II.3.

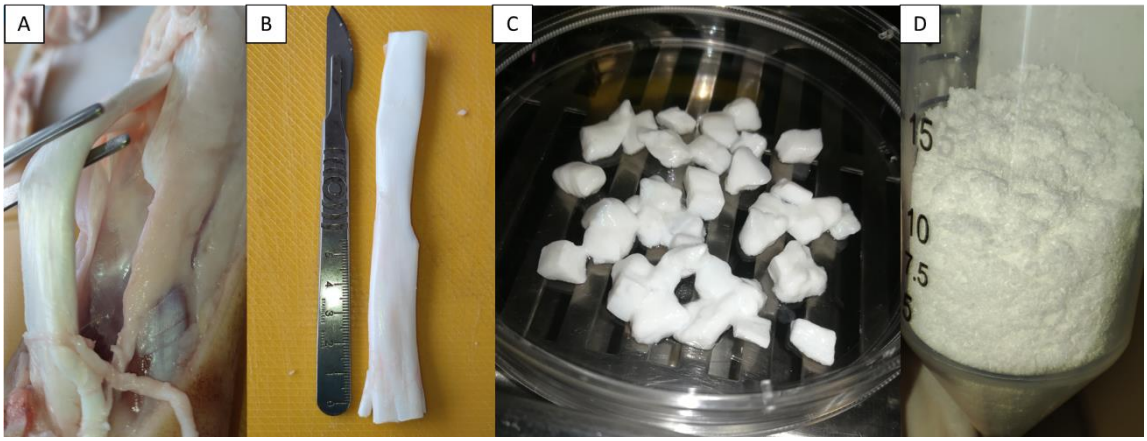

Figure II.3. Schematic representation of decellularization process of porcine flexor *profundus* tendon. Initial tendon harvesting (A) and after dissection (B). Tendon appearance after the decellularization process (C), and the homogeneous dECM powder after cryo-milling (D).

II.2.2. Tendon decellularized extracellular matrix characterization

II.2.2.1. DNA quantification

After decellularization, it is mandatory to evaluate the presence of residual cellular material. DNA quantification in dECM is usually performed to evaluate the effectiveness of decellularization. The samples

are considered completely decellularized when they have less than 50 ng dsDNA per mg of dry ECM weight, and nuclear material is not detected in the samples by DAPI or Hematoxylin and Eosin staining [8], [21], [38].

To measure the double-stranded DNA (dsDNA), both native and decellularized tendon pieces were freeze dried and then cryogenic milled as previously described, in order to obtain a homogeneous powder. The powder was digested for 6h at 56 °C with proteinase K and the remaining DNA extraction was performed using DNeasy blood and tissue kit (Qiagen) according to manufacturer's instructions. Each sample (N=3) was derived from different decellularization batches and weighed before the digestion step. The extracted DNA was measured using Nanodrop spectrophotometer (Thermo Fisher Scientific).

II.2.2.2. Histological staining

Histological analysis was performed to assess the removal of genetic material from the tissue, as well to understand the impact of decellularization on the preservation of important components of the matrix, such as collagen and GAG's. In this work Hematoxylin and eosin (H&E), 4,6-diamidino-2-phenylindole (DAPI), Masson's Trichrome (MT), Alcian Blue (AB) and Sirius Red Picrate (SRP) stainings were performed. H&E is a widely used histological staining in which hematoxylin stains the nucleus of the cells in purple, and the eosin stains the collagen and the cytoplasm in pink [39]. This staining is used to assess if the nuclear material is completely removed after decellularization, with preservation of ECM. DAPI is a fluorescent dye that strongly binds to cell's DNA, showing the presence or absence of nucleus in the tissue before and after decellularization. MT staining was performed using a commercially available kit which uses four different stains: Weigert's iron hematoxylin for nuclei, picric acid for erythrocytes, a mixture of acid dyes for cytoplasm and aniline blue for connective tissue. Overall, these solutions stain the collagen in blue, the cytoplasm in red, the erythrocytes in yellow and the cell nuclei in black. GAGs and other acidic glycoproteins are strongly anionic due to its high carboxyl and sulfate groups content, which makes them to highly react with AB stain, resulting in turquoise blue coloring [39]. SRP is a particularly good staining to differentiate the collagen with the use of polarized light, where the collagen stains in red [39].

Before staining, native (control) and decellularized tendon tissues were immersed in a 10% (v/v) neutral buffered formalin solution (Thermo Fisher Scientific) for 48 h at room temperature. Then, the tissues were embedded in paraffin and sectioned into 5 μm thickness by using a microtome. The sections

of native and decellularized tissues were deparaffinized, rehydrated and then stained with working solutions of H&E (ThermoScientific), DAPI (VWR), AB (Sigma-Aldrich), SRP staining kit (Bio-optica) and MT staining kit (Bio-optica), according to manufacturer's instructions. In this work, the samples were incubated with DAPI (1:1000, VWR) for 1 hour at RT and then analyzed under a confocal microscope. H&E, AB, and MT samples were observed under an optical microscope, and SRP was analyzed under polarized light microscopy.

II.2.3. Production of dECM hydrogel

The bioink hydrogel was prepared by subjecting the dECM powder to the typical process of enzymatically digestion in an acidic solution, following a previous protocol [40]. To evaluate the impact of matrix concentration and degree of digestion in the rheological properties of the bioink, two different concentrations and digestion time were tested: 1.0 and 2.0 % (w/v) of dECM was digested for 48 and 72h with 1 mg/mL of pepsin (P7012, Sigma-Aldrich) in 0.02 M hydrochloric acid. After digestion, the hydrogel was neutralized with 200 mM NaOH (PanReac) and 10x PBS in proportions of 1:10 and 1:9 of the volume, respectively, while immersed in an ice bath.

To confirm its gelation ability, the neutralized matrix was incubated at 37°C for 15 min.

II.2.3.1. Rheological characterization of dECM

The rheological properties of the hydrogels at concentrations of 1.0 and 2.0 wt.% and subjected to 48 and 72h of digestion were assessed using a Kinexus Pro Rheometer (Malvern Instruments, United Kingdom). All the measurements were performed with a parallel-plate geometry using a 20 mm diameter plate, 1 mm gap size and 320 µL of each precursor solution. Shear viscosity was measured in response to shear rate from 0.001 to 100 s^{-1} and the temperature was set to 4 °C to recreate the bioprinting conditions. After incubation for 15 min at 37 °C to allow gelation of the hydrogel, frequency-dependent oscillatory shear rheology was determined by varying the frequency between 0.01 and 100 Hz (n=3 for all rheological measurements). Mineral oil (Fisher Scientific) was used around the plate as solvent trap to prevent water evaporation from the dECM hydrogel.

II.2.4. Preparation of CNCs support bath for bioprinting

II.2.4.1. Synthesis of cellulose nanocrystals (CNCs)

The colloidal suspension of CNC was produced by acid hydrolysis of microcrystalline cellulose (MCC, Sigma-Aldrich, USA), following a previous protocol [29], [41].

Briefly, sulfuric acid (95-98% from Honeywell, USA) was added to MCC to achieve a final concentration of 62 wt.% in the aqueous solution of microcrystalline cellulose. The reaction was performed under continuous stirring at 60 °C for 40 minutes at 500 rpm and was stopped by adding an excess (5 times the initial volume) of cold water. After decanting, the supernatant was discarded and the remaining suspension was centrifuged (Eppendorf 5810R, Germany) for 10 min at 8603 G and 5 °C until the supernatant becomes turbid. The resulting suspension was collected and dialyzed using a cellulose dialysis tubing membrane (MWCO: 12-14kDa, 0-76mm width, Sigma-Aldrich) against deionized water until neutral pH. The dialyzed suspension was removed from the membranes and subjected to 5 sonication cycles of 5 minutes (VCX 750, Sonics) using an ultrasound probe (Horn ½" REPLACEABLE VCX 750, 630-0220) at 60% amplitude output, under ice-cooling to prevent overheating. Then, the suspension was centrifuged one more time for 10 minutes at 8603 G and 5°C to remove possible big particles remaining. The supernatant was collected and further degassed with a vacuum pump. The final supernatant containing CNC was stored at 4°C until further use and its concentration was determined by gravimetric analysis.

II.2.4.2. Preparation of CNC fluid gel

For the CNC fibrillar support platform, the stock CNC colloidal solution was first diluted to the desired concentration of 2.5 wt.% and then a surface charge screening agent was added, i.e., calcium chloride (Sigma-Aldrich) at concentration of 2.0×10^{-3} M. Then, the colloidal suspension was sonicated for 1 min at 40% of amplitude output to obtain a homogeneous fluid gel, ready to bioprint the living structures. As previously demonstrated in a previous work developed by our group [29], this CNC support bath has the required shear-thinning and self-healing rheological properties, allowing it to be used as suspension media for 3D bioprinting of freeform structures with low viscosity bioinks, holding and maintaining its defined shape. Therefore, this CNC fluid gel will be used here as a microphysiological systems housing material to fabricate our tendon-on-chip constructs.

II.2.5. Preparation of platelet lysate (PL)

PL used in this project was produced from platelet concentrates obtained from healthy human blood donors, provided by "Serviço de Imunohemoterapia do Centro Hospitalar de S. João" (CHSJ, Porto, Portugal) under a previously established cooperation protocol, approved by the Hospital Ethical Committee (approval number 363/18). PL was produced according to a previous established protocol [42]. Briefly, the samples of platelet concentrate were pooled from 12 healthy human donors and subjected to three freeze-thaw cycles by freezing in liquid nitrogen followed by heating at 37 °C in a water bath. The produce PL was aliquoted and stored at -80 °C until further use. These aliquots were then thawed at 37 °C for 5 min, centrifuged at 4000 G for 5 min (Centrifuge 5810 R, Eppendorf) and then filtered with a 0.45 µm sterile filters (TPP, Switzerland), resulting in the final PL bioink ready to encapsulate with cells. All the experimental process was performed under aseptic conditions.

II.2.6. Microphysiological systems development and biological assays

In this work, two different microphysiological systems were developed: a monoculture system intended to recreate the physiological characteristics of healthy tendon microenvironment; and a multicellular system to study the crosstalk between the tendon stroma and cells from the extrinsic compartment namely, vascular cells. The full description of their design and fabrication process is described in this section.

II.2.6.1. Cells employed in the study

II.2.6.1.1. Expansion of human Adipose tissue-derived Stem Cells (hASCs)

Mesenchymal stem cells (MSCs) are characterized as undifferentiated cells having the ability to differentiate into multiple tissue lineages such as cartilage, bone, muscle, ligament, tendon, adipocytes or endothelial phenotypes [43]–[46]. MSCs can be isolated from bone-marrow, umbilical cord blood, brain, liver, dermis, skeletal muscle and adipose tissue [43], [47]. Like bone marrow, adipose tissue is derived from the embryonic mesenchyme and contains a supportive stroma that can be easily isolated [48]. Comparatively with other tissues, adipose tissues can be obtained from less invasive procedures and adipose tissue-derived stem cells (ASCs) can be recovered in high quantities because this tissue is an abundant reservoir of adult MSCs, with approximately >100-fold higher contents than bone marrow

[43]. Because these cells are widely available and easy to obtain, they are a very appealing stem cell source to be used in regenerative medicine strategies. Therefore, hASCs were chosen for this work to be encapsulated in dECM hydrogel. Our aim is that the biophysical and biochemical cues of the tendon dECM will synergistically guide their differentiation towards the tenogenic lineage.

Human adipose-derived stem cells (hASCs) were obtained from lipoaspirate samples of the abdominal region of healthy donors undergoing plastic surgery under the scope of an established protocol with Hospital da Prelada (Porto, Portugal) and with the approval of the Hospital Ethics Committee (approval number 005/2019). The hASCs isolation procedure was performed following a previously optimized protocol [44]. Briefly, human subcutaneous adipose lipoaspirate tissues were extensively washed with PBS at 37 °C to remove erythrocytes and then digested in PBS supplemented with 0.1% collagenase of type I, 1% bovine serum albumin, and 2 mM $CaCl_2$ for 1 h at 37 °C with gentle agitation. Then, the solution was centrifuged at 300 g for 5 min and resuspended in stromal medium. The stromal vascular fraction cell pellet was filtered (40 μm), and the final solution was cultured in T125 flasks until 80-90% confluence [44]. hASCs were maintained in α-MEM (Sigma-Aldrich, USA) supplemented with 10 vol% fetal bovine serum (FBS, Gibco, ThermoFisher Scientific, USA) and 1 vol% antibiotic/antimycotic (A/A, Gibco, ThermoFisher Scientific, USA) and incubated at 37°C in a 5% CO_2 high-humidity environment, with medium replacements every 2 to 3 days. Cells until passage four were used for this study.

II.2.6.1.2. Expansion of human umbilical vein cell line (EA.hy926)

Endothelial cells play critical roles in the control of vascular function, being the interface between blood and tissue, participating in all aspects of the vascular homeostasis and physiological or pathological processes like thrombosis, inflammation or vascular wall remodeling [49].

Tendon is an hypovascular tissue in which blood vessels are mainly present in the endo and epitenon. However, as in the other tissues, cells, GFs, cytokines, nutrients and oxygen are still delivered through the blood supply network [50]. One of the hallmarks of tendinopathy is the observed increased vascularization and scar tissue formation [51]. On the other hand, there is also an increased vascularization and cellularization in tendon development [52]. The incorporation of vascular cell populations should thus be considered when build physiologically relevant *in vitro* models of tendon health and disease [50]. For this reason, endothelial cells namely, human umbilical vein cell line (EA.hy926)

were used here to build a multicellular microphysiological system and study their crosstalk with the tendon core in a biomimetic compartmentalized construct.

EA.hy926 is an immortalized human umbilical vein endothelial cells (HUVECs) line resulting from the fusion of HUVECs with the permanent human cell line A549 derived from a human lung carcinoma [53], [54]. EA.hy926 (ATCC CRL-2922) was obtained from ATCC, LGC Standards, UK, expanded and cultured using DMEM – low glucose (Sigma-Aldrich, USA) with 10 vol% FBS (Gibco, ThermoFisher Scientific, USA) and 1 vol% A/A (Gibco, ThermoFisher Scientific, USA). All cultures were incubated at 37ºC in a 5% CO_2 high-humidity environment, with medium replacements every 2 to 3 days.

II.2.6.2. Preliminary evaluation of dECM hydrogel cytocompatibility by live/dead assay

Before moving toward the actual bioprinting process, the cytocompatibility of the developed dECM hydrogel was assessed to evaluate the potential cytotoxicity of the material after decellularization and enzymatic digestion. Therefore, cell viability was evaluated by a live/dead double cell staining assay using Calcein AM and propidium iodide (PI). Calcein is membrane-permeant and is hydrolyzed by live cells and retained in the cytoplasm, showing a green-fluorescent labeling, allowing to identify live cells. On the other hand, PI cannot cross the intact membranes of live cells, but can penetrate dead or damaged cells, showing a red-fluorescent stain for dead cells.

In a typical assay, the neutralized dECM was encapsulated with hASCs (2×10^6 cells/mL) and 300 µL was poured into each well from a 48 well-plate and cultured for 7 days. The viability was assessed at day 1 and day 7 of culture, to evaluate the cytocompatibility of the hydrogel. At each time point, the hydrogels were rinsed with PBS and incubated with Calcein AM (Invitrogen, USA) 1:500 v/v in α-MEM for 30 min at 37°C. Samples were then rinsed with PBS and incubated in PI (Invitrogen, USA) 1:1000 v/v in PBS for 15 min at 37°C. Finally, samples were washed with PBS and observed using a confocal microscope TCS SP8 (Leica Microsystems, Germany). Each experiment was performed in triplicate.

II.2.6.3. Bioprinting of tendon-on-CNC-chip models

For the bioprinting experiments, a BioX bioprinter (Cellink, Sweden) with pneumatic printheads was used. Computer-aided designs (CAD) were created with the free online software TINKERCAD and

saved as .stl (stereolithography) file format. Cartridges of 3 mL were loaded with bioinks and 25G blunt needles were used as nozzles.

For the printing of the monoculture systems, a pattern with dimensions of 13 x 13 mm was designed as represented in the figure II.4. To print the tendon core constructs, 2.0 % wt. dECM was digested for 72h with 1 mg/mL of pepsin in acidic solution. After neutralized, the hydrogel was encapsulated with hASCs (2×10^6 cells/mL), loaded in a sterile cartridge, and printed immediately. A temperature-controlled print head was used to maintain the temperature of the bioink between 4 and 11 °C to control its viscosity and avoid gelation inside the cartridge.

Figure II.4. CAD design of the tendon monoculture model.

To build the multicellular system with tendon stroma and vascular compartment, the tendon bioink was prepared and processed as described in above. For printing the vascular compartment, PL was encapsulated with endothelial cells (EA.hy926) (6×10^6 cells/mL) and printed as a square around the tendon core composed by dECM encapsulated with hASCs, at a distance of 500 µm from this inner compartment.

The bioinks were directly printed within the support CNC fluid gel (2.5 wt.% with 2.0×10^{-3} M Ca^{2+}) in a 12 well plates, prefilled with 1 mL of CNCs in each well. Few minutes after printing, CNC fluid gel is "locked" and converted into a fibrillar matrix by adding an excess of 7.5×10^{-3} M Ca^{2+} solution on the top of the constructs, becoming stable hydrogels, locking the embedded bioprinted constructs. After 30 min, the Ca^{2+} solution was removed and changed by cells medium [29]. α-MEM with 10% FBS and 1% A/A

was added to the monoculture systems, and 50/50 of α-MEM/DMEM – low glucose with 10% FBS and 1% A/A was added to the multicellular systems. Finally, the samples were incubated at 37 °C in a 5% CO_2 high-humidity environment for 1, 4, 7, 11 and 21 days, with medium replacement every 2 to 3 days. All formulations for each timepoint and assay were produced in quadruplicate.

After locking, this system enables the diffusion of nutrients and long-term *in vitro* maturation, with high cell viability and shape fidelity, as previously demonstrated [29]. Additionally, this system is transparent, which enables real-time optical monitoring during the culture time.

II.2.6.4. Analysis of chip microstructure by high-resolution field scanning electron microscopy (SEM)

The microstructure of dECM hydrogels embedded within CNCs support chip was accessed by high-resolution SEM (Auriga Compact, Zeiss). Before SEM analysis, 2.0 wt.% dECM ink was printed and locked within the CNC fibrillar matrix. After locking, the samples were washed with water and solvent exchanged with ethanol (Thermo Fisher) solutions of increasing concentrations (5%, 15%, 25%, 40%, 70%, 90% and 100% v/v), for 4 h each step. After solvent exchange, ethanol was removed by critical point drying (Autosamdri-815 Series-A, Tousimis) with liquefied CO_2. To expose the dECM microstructure embedded within CNCs, the samples were freeze fractured after immersion in liquid nitrogen and then sputter coated with 1 nm of platinum (EM ACE600 Leica). Samples were observed by SEM with an accelerating voltage of 3 kV.

II.2.6.5. Analysis of cell viability after bioprinting by live/dead assay

Extrusion bioprinting processes causes shear stress in cells, which might lead to cells death if subjected to high pressures. Thus, it is important to evaluate the impact of this process on cell viability. The effects were assessed at day 1 and day 11 of culture after printing on the monoculture systems. At each timepoint, the printed chip samples were rinsed with PBS and incubated with Calcein AM (Invitrogen, USA) 1:500 v/v in α-MEM for 45 min at 37°C. Samples were rinsed with PBS and then incubated in PI (Invitrogen, USA) 1:200 v/v in PBS for 30 min at 37°C. Finally, samples were washed with PBS and observed using a confocal microscope TCS SP8 (Leica Microsystems, Germany). Each experiment was performed in triplicate.

II.2.6.6. Immunocytochemistry and Histology

Immunocytochemistry (ICC) is a commonly used technique for visualization and detection of antigens or proteins in cells, using a specific antibody that binds to the target of interest. In this work, we studied the effect of dECM on the commitment of hASCs toward tenogenic lineage, and also the effect of the presence of endothelial cells in tendon markers expression. For that, we analyzed the expression of Scleraxis (SCX) and Tenomodulin (TNMD), two of the most tendon related markers, and CD31 as a marker of endothelial cells, after 21 days of culture. This labeling and analysis were performed directly on chip and also in histological cuts of this chip to demonstrate the versatility of the proposed concept in terms of processability in cell biology characterization workflows.

For Immunolabelling on chip, monoculture and multicellular samples after 21 days of culture were washed with PBS and fixed with 10% (v/v) neutral buffered formalin at RT. After fixing, samples were washed thoroughly with PBS and kept at 4 °C in PBS until further use. For histological processing, after formalin fixation, the samples were embedded in paraffin for further sectioning using a microtome (HM355S, Microm, Thermo Scientific), obtaining histological cuts of 20 µm thickness. During this process, the epitope of interest is masked and cannot bind to the primary antibody. Therefore, an antigen retrieval is performed, and the masking of the epitope is reversed, enabling to recover the epitope-antibody binding. The histological sections were then deparaffinized and heat-induced epitope retrieval technique was used for the antigen retrieval. Briefly, a solution of citrate buffer (pH=6.0) was heated in the microwave for 2 min. Then, slides were placed inside the buffer and heated for 4 minutes. Thereafter, slides were let to cool down at RT for 30 min and then were washed three times with deionized water.

After this point, both chip and histological cut samples, were permeabilized with 0.2% (v/v) Triton X-100 in PBS for 30 min and then blocked with 3% (w/v) bovine albumin serum (BSA) in PBS for 1h at RT. Thereafter, monoculture and multicellular chips/sections were incubated overnight at 4°C with primary antibody against tenomodulin (TNMD) (rabbit anti-TNMD antibody, 1:100, Abcam ab203676), or against scleraxis (SCX) (rabbit anti-SCX antibody, 1:200, Abcam ab58655) diluted in a solution of 0.2% (v/v) Triton X-100 in PBS with 1% BSA (w/v). Multicellular chips/sections were incubated with the antibody CD31 (APC-conjugated mouse anti-human CD31/PECAM-1 Monoclonal Antibody, R&D Systems, FAB3567A) diluted in a solution of 0.2% (v/v) Triton X-100 in PBS with 1% BSA (w/v), overnight at 4°C and protected from the light. SCX and TNMD chips/cuts were then washed with PBS three times for 15 min and incubated with the corresponding secondary antibody labelled with Alexa Fluor 488 (donkey anti-rabbit IgG (H+L), A21206, ThermoFisher Scientific, 1:200), for 3 h at RT protected from

light. After washing with PBS, nuclei and cytoskeleton of all samples were stained with DAPI (1:1000 in PBS) and phalloidin-TRITC (1:200 in PBS), respectively, for 1h at RT. All the steps for samples preparation were performed under gentle agitation in an orbital shaker. After washing, the samples were kept in PBS and histological cuts were mounted with Vectashield fluorescence mounting medium (Vector Laboratories) and analyzed using a confocal laser scanning microscope TCS SP8 (Leica Microsystems, Germany). Each experiment was performed in triplicate.

The histological sections of the system were also stained with MT and H&E to assess the collagenous structure and ECM spatial distribution after culturing for 21 days.

II.2.6.7. Evaluation of gene expression through Polymerase Chain Reaction

The influence of dECM hydrogel and endothelial cells on tenogenic differentiation of hASCs was evaluated at day 1, 4 and 11 of culture trough reverse transcriptase polymerase chain reaction (RT-PCR) analysis. This technique is extensively used in molecular biology, and combines the process of reverse transcription of ribonucleic acid (RNA) into DNA and the amplification of DNA segments by PCR to study gene expression [55]. First, RNA is isolated from cells and transcribed into complementary DNA (cDNA) trough enzymatic activity of reverse transcriptase. Then the cDNA is amplified trough PCR and, finally, occurs the detection of the amplification product [55].

Briefly, each sample was collected with a biopsy punch of 12 mm diameter, not only to ensure that the size of collected sample was the same for both monoculture and multicellular samples, but also to ensure that no endothelial cells were collected in the multicellular constructs. Samples were crushed into Eppendorf tubes, and 500 µL of TRIReagent (Sigma-Aldrich, Merck, USA) was added in ice bath, and stored at -80 °C until further use. Total RNA was isolated from cells using the TRIReagent, according to the manufacturer´s protocol. The total RNA concentration was quantified at 260 nm using the NanoDrop 1000 spectrophotometer (Thermo Fisher Scientific, USA). Afterwards, cDNA was synthesized using the same amount of isolated RNA (500 ng) and the qScript cDNA Synthesis Kit (Quanta Biosciences, USA) to reverse transcribe it, according to the supplier instructions. Aliquots of each cDNA sample were diluted and frozen (-20°C) until the PCR reactions were carried out.

Real-time PCR was performed for two glyceraldehyde-3-phosphate dehydrogenase (GAPDH) reference gene, and target genes (Table II.1). Real-time PCR was performed in a mastercycler (Realplex, Eppendorf, Germany) using PerfeCTa SYBR Green FastMix (Quanta Biosciences, USA). Each reaction

contained 7 μl of master mix (Perfecta SYBR Green FastMix, Quanta Biosciences, USA), the sense and the antisense specific primers (0.5 μM) and cDNA sample (3 μl) in a final volume of 10 μl. The amplification program consisted of a pre-incubation step for denaturation of the template cDNA (2 min, 95°C), followed by 40 cycles of denaturation (5 s, 95°C), an annealing step (15 s, 60°C) and an extension step (20 s, 72°C). After each cycle, fluorescence was measured at 72°C. A negative control without cDNA template was run in each assay. All samples were normalized by the geometric mean of the expression levels of reference gene GAPDH, and fold changes were related to the control groups using the ΔΔCt method, where Ct is the crossing point of the reaction amplification curves determined by the Realplex 2.2 software (Eppendorf, Germany). The monoculture samples were normalized by day 0, and multicellular samples were normalized by the respective timepoint of monoculture.

Table II.1: Primer sequences for real time PCR. F: forward primer; R: reverse primer.

Gene	Sequence (5'-3')
Glyceraldehyde phosphate dehydrogenase (GAPDH)	F: GGGAGCCAAAAGGGTCATCA
	R: GCATGGACTGTGGTCATGAGT
Alpha-1 type I collagen (COL1A1)	F: CCTGACGCACGGCCAAGAGG
	R: GGCAGGGCTCGGGTTTCCAC
Alpha-1 type III collagen (COL3A1)	F: CCTGAAGCTGATGGGGTCAA
	R: CAGTGTGTTTCGTGCAACCAT
Scleraxis bHLH transcription factor (SCX)	F: AGAACACCCAGCCCAAACAGAT
	R: TCGCGGTCCTTGCTCAACTTT
Tenomodulin (TNMD)	F: CCGCGTCTGTGAACCTTTAC
	R: CACCCACCAGTTACAAGGCA
Tenascin (TNC)	F: ACTGCCAAGTTCACAACAGACC
	R: CCCACAATGACTTCCTTGACTG
Vascular Endothelial growth factor-A (VEGF-A)	F: CCATCCAATCGAGACCCTGG
	R: TCCGCATAATCTGCATGGTG

II.3. Statistical Analysis

All experimental data are expressed as mean ± standard deviation. For statistical analysis, the two-tailed Student's t-test was used for the comparison of two groups, while one-way ANOVA was applied

for the comparison of more than three groups. Statistical analysis was performed using GraphPad Prism version 8.0 (GraphPad Software Inc., USA). The significance for all statistical analysis was defined as $p < 0.05$. All the experiments were performed in triplicates unless otherwise stated.

II.4. References

[1] C. Liu, M. Pei, Q. Li, and Y. Zhang, "Decellularized extracellular matrix mediates tissue construction and regeneration," *Front. Med.*, vol. 16, no. 1, pp. 56–82, 2022, doi: 10.1007/s11684-021-0900-3.

[2] C. Lee, "Tendon physiology and repair," *Orthop. Trauma*, vol. 35, no. 5, pp. 274–281, Oct. 2021, doi: 10.1016/j.mporth.2021.07.003.

[3] B. S. Kim, S. Das, J. Jang, and D.-W. Cho, "Decellularized Extracellular Matrix-based Bioinks for Engineering Tissue- and Organ-specific Microenvironments," *Chem. Rev.*, vol. 120, no. 19, pp. 10608–10661, Oct. 2020, doi: 10.1021/acs.chemrev.9b00808.

[4] J. Chakraborty, S. Roy, and S. Ghosh, "Regulation of decellularized matrix mediated immune response," *Biomater. Sci.*, vol. 8, no. 5, pp. 1194–1215, 2020, doi: 10.1039/C9BM01780A.

[5] F. Kabirian and M. Mozafari, "Decellularized ECM-derived bioinks : Prospects for the future," vol. 171, no. February 2019, pp. 108–118, 2020, doi: 10.1016/j.ymeth.2019.04.019.

[6] T. W. Gilbert, T. L. Sellaro, and S. F. Badylak, "Decellularization of tissues and organs," *Biomaterials*, vol. 27, no. 19, pp. 3675–3683, 2006, doi: https://doi.org/10.1016/j.biomaterials.2006.02.014.

[7] L. T. Saldin, M. C. Cramer, S. S. Velankar, L. J. White, and S. F. Badylak, "Extracellular matrix hydrogels from decellularized tissues: Structure and function," *Acta Biomater.*, vol. 49, pp. 1–15, Feb. 2017, doi: 10.1016/j.actbio.2016.11.068.

[8] A. J. Vernengo, S. Grad, D. Eglin, M. Alini, and Z. Li, "Bioprinting Tissue Analogues with Decellularized Extracellular Matrix Bioink for Regeneration and Tissue Models of Cartilage and Intervertebral Discs," vol. 1909044, 2020, doi: 10.1002/adfm.201909044.

[9] G. Schulze-Tanzil, O. Al-Sadi, W. Ertel, and A. Lohan, "Decellularized Tendon Extracellular Matrix—A Valuable Approach for Tendon Reconstruction?," *Cells*, vol. 1, no. 4, pp. 1010–1028, Nov.

2012, doi: 10.3390/cells1041010.

[10] A. Gilpin and Y. Yang, "Decellularization Strategies for Regenerative Medicine : From Processing Techniques to Applications," vol. 2017, 2017, doi: 10.1155/2017/9831534.

[11] M. A. Bhat *et al.*, "Preparation and Functional Characterization of Decellularized Bovine Tendon Scaffolds for Tendon Tissue Engineering," *J. Anim. Res.*, vol. 5, no. 4, p. 921, 2015, doi: 10.5958/2277-940X.2015.00152.7.

[12] T. Tu *et al.*, "Tendon ECM modified bioactive electrospun fibers promote MSC tenogenic differentiation and tendon regeneration," *Appl. Mater. Today*, vol. 18, p. 100495, 2020, doi: 10.1016/j.apmt.2019.100495.

[13] B. Toprakhisar, A. Nadernezhad, E. Bakirci, N. Khani, G. A. Skvortsov, and B. Koc, "Development of Bioink from Decellularized Tendon Extracellular Matrix for 3D Bioprinting," *Macromol. Biosci.*, vol. 18, no. 10, p. 1800024, Oct. 2018, doi: 10.1002/mabi.201800024.

[14] X. Yao *et al.*, "Stem Cell Extracellular Matrix-Modified Decellularized Tendon Slices Facilitate the Migration of Bone Marrow Mesenchymal Stem Cells," *ACS Biomater. Sci. Eng.*, vol. 5, no. 9, pp. 4485–4495, Sep. 2019, doi: 10.1021/acsbiomaterials.9b00064.

[15] A. Dede Eren *et al.*, "Decellularized Porcine Achilles Tendon Induces Anti-inflammatory Macrophage Phenotype In Vitro and Tendon Repair In Vivo," *J. Immunol. Regen. Med.*, vol. 8, no. January, p. 100027, Jun. 2020, doi: 10.1016/j.regen.2020.100027.

[16] F. Zhao *et al.*, "Digestion degree is a key factor to regulate the printability of pure tendon decellularized extracellular matrix bio-ink in extrusion-based 3D cell printing," *Biofabrication*, vol. 12, no. 4, p. 045011, Jul. 2020, doi: 10.1088/1758-5090/aba411.

[17] F. Zhao *et al.*, "Comparison of three different acidic solutions in tendon decellularized extracellular matrix bio-ink fabrication for 3D cell printing," *Acta Biomater.*, vol. 131, no. xxxx, pp. 262–275, Sep. 2021, doi: 10.1016/j.actbio.2021.06.026.

[18] G. Jones, A. Herbert, H. Berry, J. H. Edwards, J. Fisher, and E. Ingham, "Decellularization and Characterization of Porcine Superflexor Tendon: A Potential Anterior Cruciate Ligament Replacement," *Tissue Eng. Part A*, vol. 23, no. 3–4, pp. 124–134, Feb. 2017, doi: 10.1089/ten.tea.2016.0114.

[19] S. Chae, Y. Sun, Y.-J. Choi, D.-H. Ha, I. Jeon, and D.-W. Cho, "3D cell-printing of tendon-bone

interface using tissue-derived extracellular matrix bioinks for chronic rotator cuff repair," *Biofabrication*, vol. 13, no. 3, p. 035005, Jul. 2021, doi: 10.1088/1758-5090/abd159.

[20] A. Lohan, B. Kohl, C. Meier, and G. Schulze-tanzil, "Tenogenesis of Decellularized Porcine Achilles Tendon Matrix Reseeded with Human Tenocytes in the Nude Mice Xenograft Model," pp. 1–18, 2018, doi: 10.3390/ijms19072059.

[21] D. Choudhury, H. W. Tun, T. Wang, and M. W. Naing, "Organ-Derived Decellularized Extracellular Matrix : A Game Changer for Bioink Manufacturing ?," *Trends Biotechnol.*, vol. 36, no. 8, pp. 787–805, 2018, doi: 10.1016/j.tibtech.2018.03.003.

[22] H. Hanai, G. Jacob, S. Nakagawa, R. S. Tuan, and D. E. Heath, "Potential of Soluble Decellularized Extracellular Matrix for Musculoskeletal Tissue Engineering – Comparison of Various Mesenchymal Tissues," vol. 8, no. November, pp. 1–15, 2020, doi: 10.3389/fcell.2020.581972.

[23] C. Brigham, *Biopolymers: Biodegradable Alternatives to Traditional Plastics*. Elsevier Inc., 2017.

[24] Y. Habibi, L. A. Lucia, and O. J. Rojas, "Cellulose Nanocrystals: Chemistry, Self-Assembly, and Applications," *Chem. Rev.*, vol. 110, no. 6, pp. 3479–3500, Jun. 2010, doi: 10.1021/cr900339w.

[25] O. M. Vanderfleet and E. D. Cranston, "Production routes to tailor the performance of cellulose nanocrystals," *Nature Reviews Materials*, vol. 6, no. 2. Springer US, pp. 124–144, 2021, doi: 10.1038/s41578-020-00239-y.

[26] E. Prince and E. Kumacheva, "Design and applications of man-made biomimetic fibrillar hydrogels," *Nat. Rev. Mater.*, doi: 10.1038/s41578-018-0077-9.

[27] R. Ajdary, B. L. Tardy, B. D. Mattos, L. Bai, and O. J. Rojas, "Plant Nanomaterials and Inspiration from Nature : Water Interactions and Hierarchically Structured Hydrogels," vol. 2001085, 2020, doi: 10.1002/adma.202001085.

[28] M. Gomez-Florit *et al.*, "Natural-Based Hydrogels for Tissue Engineering Applications," *Molecules*, vol. 25, no. 24, p. 5858, Dec. 2020, doi: 10.3390/molecules25245858.

[29] S. M. Bakht, M. Gomez-Florit, T. Lamers, R. L. Reis, R. M. A. Domingues, and M. E. Gomes, "3D Bioprinting of Miniaturized Tissues Embedded in Self-Assembled Nanoparticle-Based Fibrillar Platforms," *Adv. Funct. Mater.*, vol. 31, no. 46, 2021, doi: 10.1002/adfm.202104245.

[30] M. Matsui and Y. Tabata, "Enhanced angiogenesis by multiple release of platelet-rich plasma contents and basic fibroblast growth factor from gelatin hydrogels," *Acta Biomater.*, vol. 8, no. 5, pp. 1792–1801, 2012, doi: 10.1016/j.actbio.2012.01.016.

[31] V. E. Santo, A. R. C. Duarte, E. G. Popa, M. E. Gomes, J. F. Mano, and R. L. Reis, "Enhancement of osteogenic differentiation of human adipose derived stem cells by the controlled release of platelet lysates from hybrid scaffolds produced by supercritical fluid foaming," *J. Control. Release*, vol. 162, no. 1, pp. 19–27, 2012, doi: 10.1016/j.jconrel.2012.06.001.

[32] R. Costa-Almeida *et al.*, "The effects of platelet lysate patches on the activity of tendon-derived cells," *Acta Biomater.*, vol. 68, pp. 29–40, 2018, doi: 10.1016/j.actbio.2018.01.006.

[33] P. Babo *et al.*, "Platelet lysate membranes as new autologous templates for tissue engineering applications," *Inflamm. Regen.*, vol. 34, 2014, doi: 10.2492/inflammregen.34.033.

[34] T. M. Fortunato, C. Beltrami, C. Emanueli, P. A. De Bank, and G. Pula, "Platelet lysate gel and endothelial progenitors stimulate microvascular network formation in vitro: Tissue engineering implications," *Sci. Rep.*, vol. 6, no. April, pp. 1–15, 2016, doi: 10.1038/srep25326.

[35] B. B. Mendes, M. Gómez-Florit, P. S. Babo, R. M. Domingues, R. L. Reis, and M. E. Gomes, "Blood derivatives awaken in regenerative medicine strategies to modulate wound healing," *Adv. Drug Deliv. Rev.*, vol. 129, pp. 376–393, 2018, doi: 10.1016/j.addr.2017.12.018.

[36] J. Kurita *et al.*, "Enhanced vascularization by controlled release of platelet-rich plasma impregnated in biodegradable gelatin hydrogel," *Ann. Thorac. Surg.*, vol. 92, no. 3, pp. 837–844, 2011, doi: 10.1016/j.athoracsur.2011.04.084.

[37] K. M. Hirpara, O. Abouazza, B. O'Neill, and M. O'Sullivan, "A TECHNIQUE FOR PORCINE FLEXOR TENDON HARVEST," *J. Musculoskelet. Res.*, vol. 10, no. 04, pp. 181–186, Dec. 2006, doi: 10.1142/S0218957706001856.

[38] F. Pati *et al.*, "Printing three-dimensional tissue analogues with decellularized extracellular matrix bioink," *Nat. Commun.*, vol. 5, pp. 1–11, 2014, doi: 10.1038/ncomms4935.

[39] L. C. Junqueira and J. Carneiro, *Basic Histology*, 3rd ed. Rio de Janeiro: Guanabara, 1974.

[40] S. Farnebo *et al.*, "Design and Characterization of an Injectable Tendon Hydrogel: A Novel Scaffold for Guided Tissue Regeneration in the Musculoskeletal System," *Tissue Eng. Part A*, vol. 20, no. 9–10, pp. 1550–1561, May 2014, doi: 10.1089/ten.tea.2013.0207.

[41] D. Bondeson, A. Mathew, and K. Oksman, "Optimization of the isolation of nanocrystals from microcrystalline cellulose by acid hydrolysis," *Cellulose*, vol. 13, no. 2, pp. 171–180, 2006, doi: 10.1007/s10570-006-9061-4.

[42] B. B. Mendes *et al.*, "Human platelet lysate-based nanocomposite bioink for bioprinting hierarchical fibrillar structures," *Biofabrication*, vol. 12, no. 1, p. 015012, Nov. 2019, doi: 10.1088/1758-5090/ab33e8.

[43] Y. W. Eom *et al.*, "Rapid isolation of adipose tissue-derived stem cells by the storage of lipoaspirates," *Yonsei Med. J.*, vol. 52, no. 6, pp. 999–1007, 2011, doi: 10.3349/ymj.2011.52.6.999.

[44] P. P. Carvalho *et al.*, "The Effect of Storage Time on Adipose-Derived Stem Cell Recovery from Human Lipoaspirates," *Cells Tissues Organs*, vol. 194, no. 6, pp. 494–500, 2011, doi: 10.1159/000324892.

[45] S. Kern, H. Eichler, J. Stoeve, H. Klüter, and K. Bieback, "Comparative Analysis of Mesenchymal Stem Cells from Bone Marrow, Umbilical Cord Blood, or Adipose Tissue," *Stem Cells*, vol. 24, no. 5, pp. 1294–1301, 2006, doi: 10.1634/stemcells.2005-0342.

[46] A. I. Gonçalves, A. D. Eren, J. De Boer, R. L. Reis, and M. E. Gomes, "Evaluation of tenogenic differentiation potential of selected subpopulations of human adipose - derived stem cells," no. September 2019, pp. 1–14, 2020, doi: 10.1002/term.2967.

[47] G. Yu, Z. E. Floyd, X. Wu, Y. C. Halvorsen, and J. M. Gimble, "Isolation of Human Adipose-Derived Stem Cells from Lipoaspirates," in *Methods*, vol. 702, no. 9, J. M. Gimble and B. A. Bunnell, Eds. Totowa, NJ: Humana Press, 2011, pp. 17–27.

[48] P. A. Zuk *et al.*, "Human Adipose Tissue Is a Source of Multipotent Stem Cells," *Mol. Biol. Cell*, vol. 13, no. 12, pp. 4279–4295, Dec. 2002, doi: 10.1091/mbc.e02-02-0105.

[49] C. Michiels, "Endothelial cell functions," *J. Cell. Physiol.*, vol. 196, no. 3, pp. 430–443, Sep. 2003, doi: 10.1002/jcp.10333.

[50] M. Meeremans, G. R. Van de Walle, S. Van Vlierberghe, and C. De Schauwer, "The Lack of a Representative Tendinopathy Model Hampers Fundamental Mesenchymal Stem Cell Research," *Front. cell Dev. Biol.*, vol. 9, p. 651164, May 2021, doi: 10.3389/fcell.2021.651164.

[51] M. Gomez-Florit, C. J. Labrador-Rached, R. M. A. Domingues, and M. E. Gomes, "The Tendon

Microenvironment: Engineered In Vitro Models to Study Cellular Crosstalk," *Adv. Drug Deliv. Rev.*, vol. 185, p. 114299, 2022, doi: 10.1016/j.addr.2022.114299.

[52] N. Maffulli, P. Renström, and W. B. Leadbetter, *Tendon Injuries*. London: Springer-Verlag, 2005.

[53] C. J. Edgell, C. C. McDonald, and J. B. Graham, "Permanent cell line expressing human factor VIII-related antigen established by hybridization," *Proc. Natl. Acad. Sci. U. S. A.*, vol. 80, no. 12, pp. 3734–3737, Jun. 1983, doi: 10.1073/pnas.80.12.3734.

[54] M. Boerma, G. Burton, J. Wang, L. Fink, R. Mcgehee, and M. Hauer-Jensen, "Comparative expression profiling in primary and immortalized endothelial cells: Changes in gene expression in response to hydroxy methylglutaryl-coenzyme A reductase inhibition," *Blood Coagul. Fibrinolysis*, vol. 17, pp. 173–180, 2006, doi: 10.1097/01.mbc.0000220237.99843.a1.

[55] J. Jozefczuk and J. Adjaye, "Quantitative Real-Time PCR-Based Analysis of Gene Expression," in *Methods in Systems Biology*, vol. 500, D. Jameson, M. Verma, and H. V. B. T.-M. in E. Westerhoff, Eds. Academic Press, 2011, pp. 99–109.

Chapter III.

Writing 3D *in vitro* models of human tendon within a biomimetic fibrillar support platform

This chapter is based on the following publication:

Rosa F. Monteiro, Syeda M. Bakht, Manuel Gomez-Florit, Rui L. Reis, Rui M. A. Domingues, Manuela E. Gomes, "Writing 3D *in vitro* models of human tendon within a biomimetic fibrillar support platform", submitted.

Chapter III. Writing 3D *in vitro* models of human tendon within a biomimetic fibrillar support platform

Rosa F. Monteiro[1,2], Syeda M. Bakht[1,2], Manuel Gomez-Florit[1,2], Rui L. Reis[1,2], Rui M. A. Domingues[1,2], Manuela E. Gomes[1,2]

[1] 3B's Research Group, I3Bs – Research Institute on Biomaterials, Biodegradables and Biomimetics, University of Minho, Headquarters of the European Institute of Excellence on Tissue Engineering and Regenerative Medicine, AvePark, Parque de Ciência e Tecnologia, Zona Industrial da Gandra, 4805-017 Barco, Guimarães, Portugal;

[2] ICVS/3B's–PT Government Associate Laboratory, Braga/Guimarães, Portugal;

III.1. Abstract

Tendon pathologies are highly debilitating diseases, for which current treatments remains challenging, and have poor recovery outcomes. Therefore, relevant *in vitro* models allowing to study tendinopathies and test new regenerative approaches to develop better treatments are highly needed. Here we propose the automated fabrication of 3D bioprinted microphysiological systems (MPS) embedded into a biomimetic fibrillar support platform based on self-assembling of cellulose nanocrystals (CNCs). Tendon decellularized extracellular matrix (dECM) was used to produce a bioink that closely recapitulate the biophysical and biochemical cues of tendon cell niche, and thus self-induce the tenogenic differentiation of human adipose derived stem cells (hASCs). Two MPS were developed: a monoculture system that recreates the cellular patterns and phenotype of tendon core; and a multicellular system, incorporating endothelial cells to study the crosstalk between the tendon and the vascular compartments, which plays critical roles in tendinopathy and tendon development. Both MPS showed high cell viability, proliferation, and alignment during culture up to 21 days, and the dECM hydrogel induced stem cell differentiation towards tenogenic lineage, as shown by the expression of tendon-related markers such as Scleraxis (SCX) and Tenomodulin (TNMD). Remarkably, endothelial cells migrate towards tendon compartment, showing the existing chemoattraction between the two compartments, but did not invaded it. The crosstalk with endothelial cells seem to boost hASCs tenogenesis. Overall, the proposed system might be promising for the automated fabrication of organotypic tendon-on-chip models that will be a valuable new tool to study tendon physiology and pathologies, as well as the effect of drugs for the treatment of tendinopathy.

Keywords: Decellularized extracellular matrix, cellulose nanocrystals, tendon-on-chip, tendinopathy, microphysiological systems

III.2. Introduction

Tendon is a highly and dense organized tissue that connects the muscle to the bone and is subjected to extreme mechanical forces during its activity [1]. The extracellular matrix (ECM) of tendons represents around 80% of the tendon composition, whose most abundant constituent is collagen (60-85% of its dry-weight) , where type I collagen is the most abundant (≈95%), followed by type III collagen (3%) and other collagen types in small quantities (2%) [2]. The ground substance that surrounds collagen consists of proteoglycans, glycoproteins and glycosaminoglycans (GAGs) which are highly viscous and hydrophilic, giving tendon the viscoelastic properties to resist compressive forces [2], [3]. Elastic fibers allow long-range deformability and passive recoil, ensuring the flexibility and extensibility of tendons [3].

Mature and healthy tendons are characterized by low cellular density (20%), composed mainly by tenoblasts and tenocytes, specialized fibroblast-like cells that produce collagen [2], [3]. Structurally, the tendon unit is formed by collagen organized from the nano to the microscale into microfibrils, fibrils, fibers and fascicles [2]. The fascicles are packed together and separated by the endotenon or interfascicular matrix, a fine connective tissue that contains the blood vessels, lymphatics and nerves, and are all enclosed by the epitenon [4]. These fascicles represents the commonly named intrinsic compartment of the tendon, also known as tendon core, while the extrinsic tendon compartment connects the vascular, immune and nervous systems, trough synovium-like tissues [5].

Tendinopathy describes a complex multifaceted pathology of the tendon, and is characterized by induction of pain, loss of function, and reduce exercise tolerance [6]. A diseased tendon is characterized by fragmented collagen fibers, disorganized collagen bundles, accumulation of GAGs and increased microvasculature associated with neoinnervation, leading to adverse changes in the material properties of the tendon [6]. To the date, treatment of tendinopathy remains challenging and has poor recovery outcomes, resulting in prolonged patient suffering and substantial loss of personal productivity [5]. Therefore, there is a need to develop new and effective treatments to bring a better life for patients that suffer from tendinopathy. Although animal models sound appealing for the study of tendon repair, as they have interplay between tissues and cell-system interaction like lymph, nerve and vessel, these models are limited in their availability and ability to capture human features of tendon disease, as they fail to mimic the intrinsic repair capacity of adult human tendon tissue, and they also represent a high cost approach with low throughput, with the addition of considerable ethical and time constraints [4], [7]. On the other

hand, 2D cell culture models are commonly used to study cell behavior due to their practicability, high throughput and cost-effectiveness, but they are oversimplified systems that fail in represent the biomechanical and biophysical environment of native tendons [4], [8]. Tendon explant models have been used as another approach to study tendon tissue, where intact native tissue samples are dissected and cultured *ex vivo* to study cell-ECM interactions in a near-physiological environment within intact tissue architecture [7]. However, these models are limited by the loss of homeostasis, time-dependent viability, difficulty in standardization, and poor translatability to human [7]. Mimicking the tendon environment and tendinopathy situation remains challenging, and the lack of representative models have been leading to the demand for new representative models, where 3D *in vitro* models has been pointed as the main solution. 3D *in vitro* models can recreate the physiological context of the tissue, and adequately recreate neo-tendon formation after an acute injury, study the interactions between recruited tendon cells and a potentially implanted biomaterial, or the crosstalk between tenocytes and other cell types such as immune and stem cells [7].

Bioengineered microphysiological systems (MPS) are proposed as an improved tools to recapitulate the physiology of human organs or tissues *in vitro*, which might help to better predict *in vivo* responses using *in vitro* assays [9]. One of the type of MPS that are gaining increased attention by the scientific community and pharmaceutical industry are organs-on-chip (OoC) models, dynamic systems that have been widely used for diseases modeling and test of new drugs [10]. OoC are usually built on plastic microfluidic platforms. However, according to its recent definition, platforms that have a significant engineering component and spatially guides cell confinement can also be considered an OoC device, even if the system lacks of microfluidic flow [11], [12]. Microfluidic devices are commonly made of polydimethylsiloxane (PDMS), a material easy to mold, biocompatible and transparent. However, its soft lithography-based microfabrication process involves the stacking and bonding different layers together, which limits the 3D complexity of the constructs and increases the final cost [13]. 3D Bioprinting has emerging as an alternative to solve the fabrication barrier associated with MPS, allowing low-cost, rapid, one-step, and truly 3D fabrication of microfluidic devices, which may result into more complex multicellular *in vitro* models [10]. Bioprinting in suspension baths followed by its annealing/crosslinking has been proposed for the direct 3D writing of different free-form MPS house in hydrogel materials, as this baths prevent the bioinks from settling, collapse, and dehydration of the embedded material [14]. For example, a modular platform of self-healing and annealable granular support bath was proposed for the direct embedded 3D printing of human stem cells, and was used to bioengineer models of neuronal networks [15]. This platform provided physical support for high fidelity printing, and allowed healthy

cellular growth, maturation and activity [15]. Our group has also proposed a self-assembled nanoparticle-based fibrillar platform for the embedded 3D bioprinting of miniaturized tissues [16]. This system allows the 3D free-from bioprinting by controlling the self-assembling of plant-derived cellulose nanocrystals (CNCs), resulting into a fibrillar matrix platform that allows more biomimetic cell-cell and cell-matrix crosstalk [16]. Overall, these platform doesn't need specific microfabrication processes, equipment or skills, and has several implementation advantages such as high throughput, reproducibility, and scalability for the manufacturing of miniaturized multicellular systems with complex bioinspired 3D architectures, and can be a promising platform for the automated biofabrication of *in vitro* tissue/organ models [16]. To build these bioprinted MPS, the bioinks must be selected, designed, and prepared according to the target tissue or organ. Many hydrogel polymers have been proposed for bioprinting e.g. alginate [17], [18], agarose [19], hyaluronic acid (HA) [20], [21], chitosan [22], [23], gelatin [24], [25], collagen [26], [27], silk [28], [29] and gelatin methacryloyl (GelMA) [30], [31], but their potential to closely mimic the rich cell microenvironment is limited [32]. Decellularized extracellular matrix (dECM) hydrogels are emerging as a valuable approach for bioink formulation as dECM bioinks exhibit higher levels of biofunctionality for the generation of inherent environmental niches than other available polymeric hydrogel, preserving the main biochemical and biophysical cues of the respective niches [33]. A few works have proposed tendon dECM to formulate bioinks, as this material can retain the main biochemical and biophysical cues of the native tendon niche after decellularization and self-induce stem cell differentiation towards the tenogenic lineage [34]–[36].

Tenocytes are fibroblast-like mature elongated cells that are aligned along the collagen fibers, and are responsible for the synthesis and remodeling of tendon ECM [4]. Although tenocytes seem an obvious choice as a cell source, the *in vitro* expansion of these cells remains challenging due to rapid tenogenic phenotype drift, and an alternative cell source should thus be considered [37]. Human adipose derived stem cells (hASCs) are becoming an important cell source for the development of tendon engineering approaches, as these cells have multipotent capacity properties, are widely available, can be harvested with minimally invasive procedures from an autologous source, are available in great quantities, and its differentiation towards the tenogenic phenotype can be promoted by topographical and chemical cues [37], [38]

In this work, we propose the development of tendon MPS by combining the concept of 3D bioprinting within suspension media with the unique features of tendon dECM hydrogels for the freeform 3D writing of humanized tendon-on-chip models. For that, we successfully decellularized porcine tendons

and developed a tendon dECM hydrogel, suitable for 3D bioprinting. The use of the CNCs platform allowed the printing of desired patterns and sustains the maturation of the construct. Two tendon-on-CNC-chip models were developed: a tendon core monoculture system and a multicellular system including endothelial cell structures to study the interaction between these cell populations in tendon development and disease, where an increased vascularization play important roles. The schematic representation of the systems development can be seen in figure III.1.

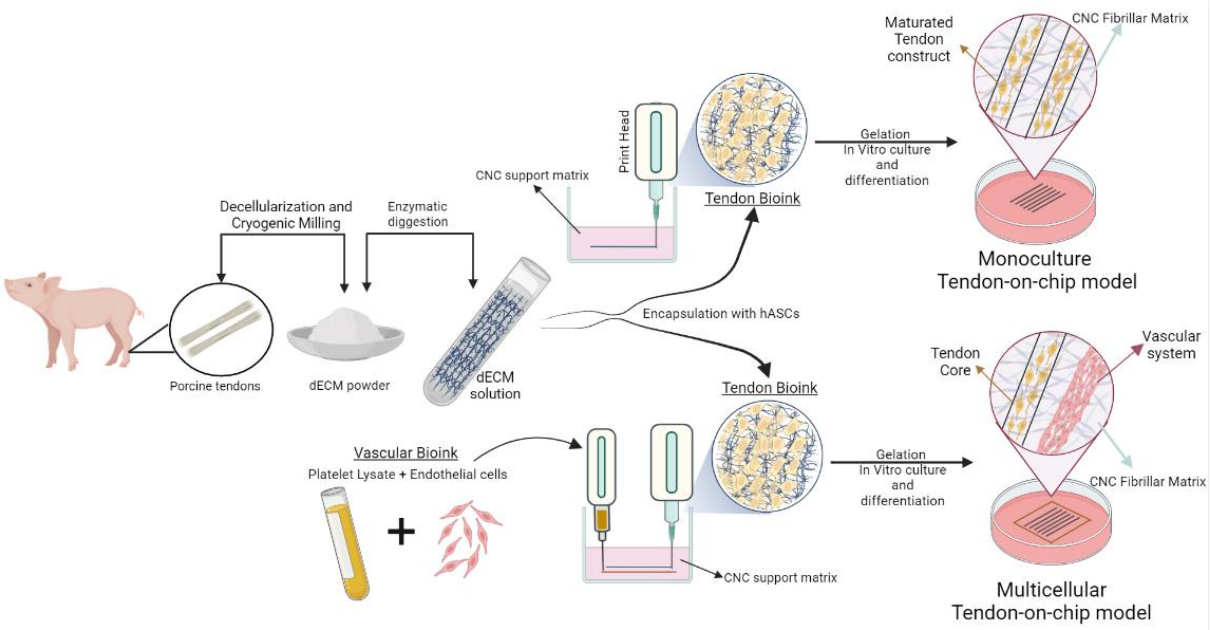

Figure III.1. Schematic representation of the monoculture and multicellular tendon-on-chip development. Porcine tendons were harvested, decellularized and milled to obtain a homogeneous dECM powder that was enzymatically digested to form the dECM ink solution. This dECM solution was encapsulated with hASCs and printed within CNCs support matrix to represent the tendon core compartment. For the multicellular systems, a square of PL encapsulated with endothelial cells was printed around the tendon core compartment to represent the vascular system. After printing, both systems were allowed to jellify and cultured up to 21 days.

III.3. Materials and Methods

III.3.1. Porcine tendons decellularization and processing

Porcine trotters were obtained from a local slaughterhouse and the flexor *profundus* tendons were immediately harvested under aseptic conditions, following a previously optimized harvesting protocol [39].

After dissection, the tendons were cut in small pieces and frozen at -80 °C for further decellularization. The decellularization procedure followed the protocol proposed by B. Toprakhisar et. al. [40], with some modifications. In general, it consisted of successive washing cycles performed under sterile conditions and kept in an orbital shaker at 4 °C, unless otherwise is referred. Tendons were first subjected to five cycles of freeze-thaw in liquid nitrogen and PBS (Sigma-Aldrich) at 37 °C, respectively, and then incubated in a solution of 50 mM Tris/ 1.5 M NaCl (Sigma-Aldrich) (pH=7.6) overnight. The tendons were then incubated at 37 °C in a solution of 0.5% (v/v) Trypsin/ 5 mM EDTA (Sigma-Aldrich) (in PBS) (pH=7.6), and finally placed in a 2% SDS (Sigma-Aldrich) + 2% Triton X-100 (Sigma-Aldrich) solution (w/v and v/v respectively, in PBS) for 2 days. The tendons were rinsed with PBS and then incubated in 10 mM Tris + 1% Triton X-100 for 1 day. Next, samples were incubated in DNase (200 U/mL) (VWR) at 37 °C overnight, and finally washed with PBS containing antibiotic for one week to remove any remaining detergent or enzyme.

After decellularization, the tendons were freeze-dried and milled in a cryogenic grinder (SPEX SamplePrep) during 2 min, with a rate of 20 cps (cycles per second), resulting in a homogeneous powder of porcine tendon decellularized extracellular matrix. The dECM was then stored at -20 °C until further use.

III.3.2. Characterization of tendon decellularized extracellular matrix

DNA quantification. To measure the double-stranded DNA (dsDNA), both native and decellularized tendon pieces were freeze dried and then cryogenic milled as previously described, to obtain a homogeneous powder. The powder was digested for 6h at 56 °C with proteinase K and the remaining DNA extraction was performed using DNeasy blood and tissue kit (Qiagen) according to manufacturer's instructions. Each sample (N=3) was derived from different decellularization batches and weighed before the digestion step. The extracted DNA was measured using Nanodrop spectrophotometer (Thermo Fisher Scientific).

Histology and Immunohistochemistry. To fully characterize the dECM, the decellularized tissue was analyzed by microscopy imaging methods, and the native tissue was used as control. Native and decellularized tendon tissues were immersed in a 10% (v/v) neutral buffered formalin solution (Thermo Fisher Scientific) for 48h at room temperature. Then, the tissues were embedded in paraffin and sectioned into 5 μm thickness sections by using a microtome. The sections of native and decellularized tissues

were deparaffinized, rehydrated and then stained with different dyes. Hematoxylin and eosin (H&E) (ThermoScientific) and 6-diamidino-2-phenylindole (DAPI) (VWR) staining were used to assess the efficiency of nuclear material removal by the decellularization process. Masson's Trichrome (MT) (Bio-Optica) and Alcian Blue (AB) (Sigma-Aldrich) were used to analyze the preservation of the collagenous and glycosaminoglycans (GAGs) content after decellularization, respectively. Finally, Sirius Red Picrate (SRP) (Bio-Optica) was used to stain collagen type I and type III fibrils. H&E, AB, and MT samples were observed under an optical microscope, DAPI with confocal microscope, and SRP under polarized light microscopy.

III.3.3. Production of dECM hydrogel

The bioink hydrogel was prepared by subjecting the dECM powder to the typical process of enzymatically digestion in acidic conditions [41]. To evaluate the impact of decellularization process on cell viability (see assay description below), 2.0 % (w/v) of dECM was first digested for 72h with 1 mg/mL of pepsin (P7012, Sigma-Aldrich) in 0.02 M hydrochloric acid solution. To evaluate the impact of matrix concentration and degree of digestion in the rheological properties of the bioink, two different concentrations and digestion time were tested: 1.0 and 2.0 % (w/v) of dECM was digested for 48 and 72h with 1 mg/mL of pepsin (P7012, Sigma-Aldrich) in 0.02 M hydrochloric acid. After digestion, the hydrolyzed dECM was neutralized with 200 mM NaOH (PanReac) and 10x PBS in proportions of 1:10 and 1:9 of the volume, respectively, while immersed in an ice bath. To confirm its gelation ability, the neutralized matrix was incubated at 37 °C for 15 min.

Rheological characterization of dECM. The rheological properties of the precursor solutions and resulting hydrogels at concentrations of 1.0 and 2.0 wt.% and subjected to 48 and 72h of digestion were assessed using a Kinexus Pro Rheometer (Malvern Instruments, United Kingdom). All the measurements were performed with a parallel-plate geometry using a 20 mm diameter plate, 1 mm gap size and 320 µL of each precursor solution. Shear viscosity was measured in response to shear rate from 0.001 to 100 s^{-1} and the temperature was set to 4 °C to recreate the bioprinting conditions. After incubation at 37 °C for 30 min, in order to allow gelation of the dECM hydrogel, frequency-dependent oscillatory shear rheology was determined by varying the frequency between 0.01 and 100 Hz (n=3 for all rheological

measurements). Mineral oil (Fisher Scientific) was used around the plate as solvent trap to prevent water evaporation from the dECM hydrogel.

III.3.4. Preparation of CNCs support media for bioprinting

Synthesis of cellulose nanocrystals (CNCs). The colloidal suspension of CNC was produced by acid hydrolysis of microcrystalline cellulose (MCC, Sigma-Aldrich, USA), following a previous protocol [16], [42]. Briefly, sulfuric acid (95-98% from Honeywell, USA) was added to MCC to achieve a final concentration of 62 wt.% in the aqueous solution of microcrystalline cellulose. The reaction was performed under continuous stirring at 60 °C for 40 minutes at 500 rpm and was stopped by adding an excess (5 times the initial volume) of cold water. After decanting, the supernatant was discarded and the remaining suspension was centrifuged (Eppendorf 5810R, Germany) for 10 min at 8603 G and 5 °C until the supernatant becomes turbid. The resulting suspension was collected and dialyzed using a cellulose dialysis tubing membrane (MWCO: 12-14 kDa, 0-76 mm width, Sigma-Aldrich) against deionized water until neutral pH. The dialyzed suspension was removed from the membranes and subjected to 5 sonication cycles of 5 minutes (VCX 750, Sonics) using an ultrasound probe (Horn ½" REPLACEABLE VCX 750, 630-0220) at 60% amplitude output, under ice-cooling to prevent overheating. Then, the suspension was centrifuged one more time for 10 minutes at 8603 G and 5 °C to remove possible big particles remaining. The supernatant was collected and further degassed with a vacuum pump. The final supernatant containing CNC was stored at 4 °C until further use and its concentration was determined by gravimetric analysis.

Preparation of CNC fluid gel. For preparation of the CNC fibrillar support platform, the stock CNC colloidal suspension was first diluted to the desired concentration of 2.5 wt.% and then a surface charge screening agent, i.e., calcium chloride (Sigma-Aldrich) at concentration of 2.0×10^{-3} M, was added to induce de formation of a fluid gel [16]. Then, the colloidal suspension was sonicated for 1 min at 40% of amplitude output for homogenization before bioprinting the living structures. Therefore, this CNC fluid gel will be used here as a microphysiological systems housing material to fabricate our tendon-on-chip constructs.

III.3.5. Microphysiological systems development and biological assays

Cell Isolation and Culture. Human adipose-derived stem cells (hASCs) were obtained from lipoaspirate samples of the abdominal region of healthy donors undergoing plastic surgery under the scope of an established protocol with Hospital da Prelada (Porto, Portugal) and with the approval of the Hospital Ethics Committee (approval number 005/2019). The hASCs isolation procedure was performed following a previously optimized protocol [43]. hASCs were maintained in α-MEM (Sigma-Aldrich, USA) supplemented with 10 vol% fetal bovine serum (FBS, Gibco, ThermoFisher Scientific, USA) and 1 vol% antibiotic/antimycotic (A/A, Gibco, ThermoFisher Scientific, USA) and incubated at 37°C in a 5% CO_2 high-humidity environment, with medium replacements every 2 to 3 days. Cells until passage four were used for this study. Human umbilical vein cell line (EA.hy926) (ATCC CRL-2922) was obtained from ATCC, LGC Standards, UK, expanded and cultured using DMEM – low glucose (Sigma-Aldrich, USA) with 10 vol% FBS (Gibco, ThermoFisher Scientific, USA) and 1 vol% A/A (Gibco, ThermoFisher Scientific, USA). All cultures were incubated at 37ºC in a 5% CO_2 high-humidity environment, with medium replacements every 2 to 3 days.

Preliminary evaluation of dECM hydrogel cytocompatibility by live/dead assay. Cell viability was evaluated by a live/dead double cell staining assay using Calcein AM and propidium iodide (PI). In a typical assay, the neutralized dECM was encapsulated with hASCs (2×10^6 cells/mL) and 300 µL was poured into each well from a 48 well-plate and cultured for 7 days. The viability was assessed at day 1 and day 7 of culture, to evaluate the cytocompatibility of the hydrogel. At each time point, the hydrogels were rinsed with PBS and incubated with Calcein AM (Invitrogen, USA) 1:500 v/v in α-MEM for 30 min at 37°C. Samples were then rinsed with PBS and incubated in PI (Invitrogen, USA) 1:1000 v/v in PBS for 15 min at 37°C. Finally, samples were washed with PBS and observed using a confocal microscope TCS SP8 (Leica Microsystems, Germany). Each experiment was performed in triplicate.

Preparation of Bioinks. Two bioinks solutions were used for the development of the microphysiological system: dECM, representing the tendon bioink, and platelet lysate (PL), representing the vascular bioink. To develop the tendon bioink, 1.0 and 2.0 % wt. dECM was digested for 48 and 72h, respectively, with 1 mg/mL of pepsin in 0.02 M HCl, neutralized, encapsulated with hASCs (2×10^6 cells/mL), loaded in a sterile cartridge, and printed immediately. PL used in this project was produced

from platelet concentrates obtained from healthy human blood donors, provided by "Serviço de Imunohemoterapia do Centro Hospitalar de S. João" (CHSJ, Porto, Portugal) under a previously established cooperation protocol, approved by the Hospital Ethical Committee (approval number 363/18). PL was produced according to a previous established protocol [44]. Briefly, the samples of platelet concentrate were pooled from 12 healthy human donors and subjected to three freeze-thaw cycles by freezing in liquid nitrogen followed by heating at 37 °C in a water bath. The produced PL was aliquoted and stored at -80 °C until further use. These aliquots were then thawed at 37 °C for 5 min, centrifuged at 4000 G for 5 min (Centrifuge 5810 R, Eppendorf) and then filtered with a 0.45 μm sterile filters (TPP, Switzerland), resulting in the final PL bioink that was encapsulated with endothelial cells (EA.hy926) (6×10^6 cells/mL).

Bioprinting of tendon-on-CNC-chip models. For the bioprinting experiments, a BioX bioprinter (Cellink, Sweden) with pneumatic printheads was used. Computer-aided designs (CAD) were created with the free online software TINKERCAD and saved as .stl (stereolithography) file format. Cartridges of 3 mL were loaded with bioinks and 25G blunt needles were used as nozzles. For the printing of the monoculture systems, a pattern with dimensions of 13 x 13 mm (rectilinear pattern, without perimeter, 25 % infill, 0.25 mm height) was designed. To develop the tendon core constructs, the tendon bioink was placed into a temperature-controlled print head that was used to maintain the temperature of the bioink between 4 and 11 °C and avoid its gelation inside the cartridge. To build the multicellular system, the tendon bioink was printed as described in above, and the vascular bioink was printed as a square at a distance of 500 μm from the tendon core compartment. The bioinks were directly printed within the support CNC fluid gel (2.5 wt.% with 2.0×10^{-3} M Ca^{2+}) in a 12 well plates, prefilled with 1 mL of CNCs in each well. Few minutes after printing, CNC fluid gel is "locked" and converted into a fibrillar matrix by adding an excess of 7.5×10^{-3} M Ca^{2+} solution on the top of the constructs, becoming stable hydrogels, locking the embedded bioprinted constructs. After 30 min, the Ca^{2+} solution was removed and changed by cell culture medium [16]. α-MEM with 10% FBS and 1% A/A was added to the monoculture systems, and 50/50 of α-MEM/DMEM – low glucose with 10% FBS and 1% A/A was added to the multicellular systems. Finally, the samples were incubated at 37 °C in a 5% CO_2 high-humidity environment for up to 21 days, with medium replacement every 2 to 3 days. All formulations for each timepoint and assay were produced in quadruplicate.

Analysis of chip microstructure by high-resolution field scanning electron microscopy (SEM). The microstructure of dECM hydrogels embedded within CNCs support chip was accessed by high-resolution SEM (Auriga Compact, Zeiss). Before SEM analysis, 2.0 wt.% dECM ink was printed and locked within the CNC fibrillar matrix. After locking, the samples were washed with water and solvent exchanged with ethanol (Thermo Fisher) solutions of increasing concentrations (5%, 15%, 25%, 40%, 70%, 90% and 100% v/v), for 4 h each step. After solvent exchange, ethanol was removed by critical point drying (Autosamdri-815 Series-A, Tousimis) with liquefied CO_2. To expose the dECM microstructure embedded within CNCs, the samples were freeze fractured after immersion in liquid nitrogen and then sputter coated with 1 nm of platinum (EM ACE600 Leica). Samples were observed by SEM with an accelerating voltage of 3 kV.

Cell Viability, Morphology and Immunocytochemistry of developed MPS. The impact of printing process in cell viability were assessed at day 1 and day 11 of culture after printing on the monoculture systems by live/dead assay. At each timepoint, the printed chip samples were rinsed with PBS and incubated with Calcein AM (Invitrogen, USA) 1:500 v/v in α-MEM for 45 min at 37°C. Samples were rinsed with PBS and then incubated in PI (Invitrogen, USA) 1:200 v/v in PBS for 30 min at 37°C. Finally, samples were washed with PBS and observed using a confocal microscope TCS SP8 (Leica Microsystems, Germany). Each experiment was performed in triplicate. For Immunolabelling on chip, monoculture and multicellular samples after 21 days of culture were washed with PBS and fixed with 10% (v/v) neutral buffered formalin at RT. After fixing, samples were washed thoroughly with PBS and kept at 4 °C in PBS until further use. For histological processing, after formalin fixation, the samples were embedded in paraffin for further sectioning using a microtome (HM355S, Microm, Thermo Scientific), obtaining histological sections of 20 µm thickness. The histological sections were then deparaffinized and heat-induced epitope retrieval technique was used for the antigen retrieval. Briefly, a solution of citrate buffer (pH=6.0) was heated in the microwave for 2 min. Then, slides were placed inside the buffer and heated for 4 minutes. Thereafter, slides were let to cool down at RT for 30 min and then were washed three times with deionized water. After this point, both chip and histological sections, were permeabilized with 0.2% (v/v) Triton X-100 in PBS for 30 min and then blocked with 3% (w/v) bovine albumin serum (BSA) in PBS for 1h at RT. Thereafter, monoculture and multicellular chips/sections were incubated overnight at 4°C with primary antibody against tenomodulin (TNMD) (rabbit anti-TNMD antibody, 1:100, Abcam ab203676), or against scleraxis (SCX) (rabbit anti-SCX antibody, 1:200, Abcam ab58655) diluted in a solution of 0.2% (v/v) Triton X-100 in PBS with 1% BSA (w/v). Multicellular chips/sections were incubated

with the antibody CD31 (APC-conjugated mouse anti-human CD31/PECAM-1 Monoclonal Antibody, R&D Systems, FAB3567A) diluted in a solution of 0.2% (v/v) Triton X-100 in PBS with 1% BSA (w/v), overnight at 4°C and protected from the light. SCX and TNMD chips/sections were then washed with PBS three times for 15 min and incubated with the corresponding secondary antibody labelled with Alexa Fluor 488 (donkey anti-rabbit IgG (H+L), A21206, ThermoFisher Scientific, 1:200), for 3 h at RT protected from light. After washing with PBS, nuclei and cytoskeleton of all samples were stained with DAPI (1:1000 in PBS) and phalloidin-TRITC (1:200 in PBS), respectively, for 1h at RT. All the steps for samples preparation were performed under gentle agitation in an orbital shaker. After washing, the samples were kept in PBS and histological sections were mounted with Vectashield fluorescence mounting medium (Vector Laboratories) and analyzed using a confocal laser scanning microscope TCS SP8 (Leica Microsystems, Germany). Each experiment was performed in triplicate.

Gene expression. The gene expression of Tenomodulin (TNMD), Scleraxis (SCX), Tenascin C (TNC), type I collagen (COL-1), type III collagen (COL-3) and Vascular Endothelial Growth Factor A (VEGF-A) were determined by real-time polymerase chain reaction (RT-PCR) analysis. The samples were washed twice with PBS, crushed into Eppendorfs, and the total RNA was extracted with Trizol reagent (TRIzol Reagent – Thermo Fisher Scientific), according to manufacturer's instructions. The extracted RNA was analyzed with NanoDrop ND-100 spectrophotometer (NanoDrop, ThermoScientific, USA). For the reverse transcription to cDNA, qScript cDNA SuperMix kit (Thermo Fisher Scientific) was used. The quantitative polymerase chain reaction (qPCR) was carried out for the quantification of the transcripts using the PerfeCTA SYBR Green FastMix kit following the manufacturer's protocol, in a Real-Time Mastercycler Realplex thermocycler (Eppendorf, Germany). The primers were pre-designed with PerlPrimer v1.1.21 software and synthesized by MWG Biotech. GAPDH (Glyceraldehyde 3-phosphate dehydrogenase) was used as the housekeeping gene. The ΔΔCt Method was selected to evaluate the relative expression level for each target gene. All values were first normalized against GAPDH values. Then, the monoculture values were normalized by day 1, and multicellular values were normalized by the respective day of monoculture (n = 3, independent experiments).

III.3.6. Statistical Analysis

All experimental data are expressed as mean ± standard deviation. For statistical analysis, the two-tailed Student's t-test was used for the comparison of two groups, while one-way ANOVA was applied for the comparison of more than three groups. Statistical analysis was performed using GraphPad Prism

version 8.0 (GraphPad Software Inc., USA). The significance for all statistical analysis was defined as $p < 0.05$. All the experiments were performed in triplicates unless otherwise stated.

III.4. Results and Discussion

III.4.1. Porcine tendons decellularization

To access the efficiency of the decellularization process, the cellular content and retention of ECM structural components were evaluated in both native and decellularized tendon tissues. The typically decellularization criteria defines that a tissue is considered properly decellularized when its DNA content is <50 ng dsDNA per mg dry weight, and the absence of nuclear material in the dECM should be further proved by histological or other cell staining analysis [28], [45], [46]. As can be observed by H&E and DAPI staining, in the native tissue (figure III.2 B, D) cells are shown aligned between the crimp pattern of the collagenous ECM, being more densely packed between the fascicles in the endotenon regions. After decellularization, these stainings revealed the absence of nucleus (figure III.2 C, E) in the matrix, results that are corroborated by DNA quantification (figure III.2 L), where the residual DNA content detected in the dECM was 16.08 ± 13.74 ng/mg, lower than the limit of 50 ng/mg of dry weight of tissue. Moreover, MT staining also demonstrates complete removal of cytoplasmic residues (red) while preserving most of the collagenous structure (blue) (figure III.2 F, G). Similarly, despite some loss of glycosaminoglycans (GAGs) and other acidic glycoproteins can be noticed after decellularization compared to the native tissue, AB staining (figure III.2 H, I) show a good preservation of these components in the dECM. As expected, Sirius Red Picrate (SRP) staining shows that the fibrillar and crimped collagen type I (red) is the prevalent collagen type identified in both samples (figure III.2 J, K). Overall, the decellularization process revealed to be effective in removing the cellular content while preserving the general biochemical and structural signature of the native ECM.

To exclude potential cytotoxic effect of the dECM derived to the presence of remanent detergents or enzymes from the decellularization process [47], the cytocompatibility of the developed dECM hydrogel was preliminarily evaluated before the bioprinting steps. dECM hydrogels (2.0 wt.%) were encapsulated with hASCs and tested by live/dead assay at day 1 (figure III.2 M) and day 7 (figure III.2 N) of culture. Overall, the hydrogels show good cell viability and increased proliferation over time. Macroscopically, the hydrogel suffers a significant volume contraction along the culture time (figure III.2 O, P), suggesting the

ability of cells to attach and remodel the hydrogel, reshaping the surrounding matrix environment, an effect that is in accordance with previous studies on dECM hydrogels [35], [47], [48].

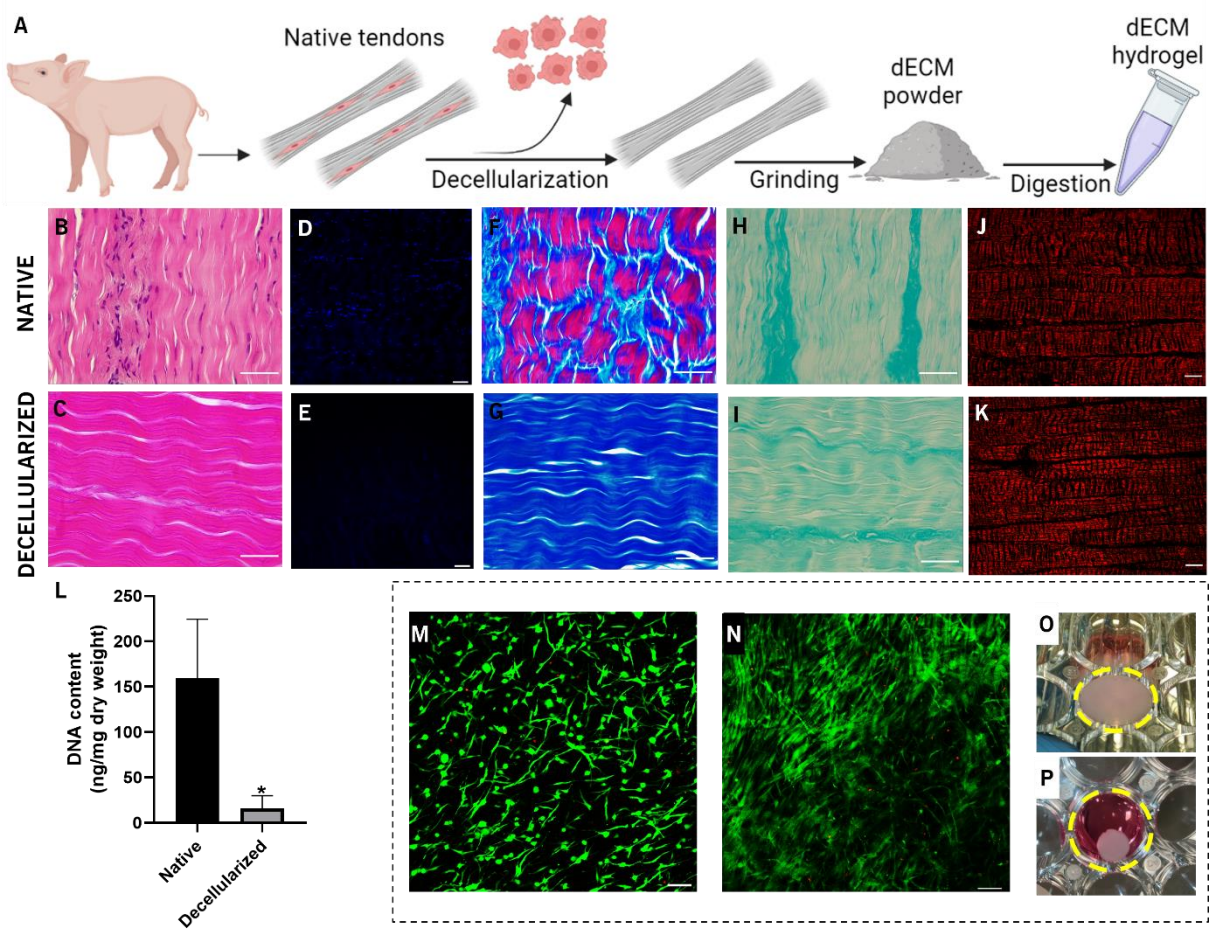

Figure III.2. Tendon dECM development. (A) Schematic representation of dECM hydrogel solutions preparation. The process starts with harvesting and dissection of porcine tendons, followed by decellularization, grinding and digestion of dECM powder, resulting in a homogenous hydrogel precursor solution. (B-L) Removal of genetic material and preservation of tendon ECM after decellularization: histological sections of native (B, D, F, H, J) and decellularized (C, E, G, I, K) tendons were stained with nuclear stainings H&E (B, C) (nucleus in purple) and DAPI (D, E) (nucleus in blue), MT staining (F, G) for collagenous structure (blue) and cytoplasmic components (red), AB staining (H, I) for GAGs and PSR staining (J, K) for collagen type I (red) and III (green), under polarized light; DNA quantification (L) was assessed after decellularization, and native tissues were used as control. (M-P) Preliminary evaluation of dECM hydrogel cytocompatibility by live/dead assay at day 1 (M) and day 7 (N) of culture (green: live cells; red: dead cells), and respective images depicting their volume contraction from day 1 (O) until day

7 (P) of culture. Scale Bar: (B-I) 50 μm; (J, K) 200 μm; (M, N) 100 μm. Values are plotted as mean ± standard deviation. $*p < 0.05$.

III.4.2. dECM ink development and characterization

The general protocol of dECM hydrogel production involves enzymatic digestion of dECM powder, neutralization (figure III.3 A), and gelation of the hydrogel after incubation at 37 °C (figure III.3 B). After digestion, dECM gelation ability was confirmed by visual inspection, observing the solution color changing from clear to cloudy, as well as by an inversion test confirming the formation of a non-flowing semi-solid hydrogel at the bottom of the flask.

The rheological properties of hydrogels bioinks are key parameters to access their printability in extrusion-based 3D bioprinting systems [49]. Thus, the rheological behavior of dECM hydrogels at two different concentrations (1.0 and 2.0 wt. %) and digestion times (48 and 72 h) was characterized. Shear viscosity measurements of precursor dECM solutions (figure III.3 C) showed that all formulations exhibit a clear shear-thinning behavior at 4 °C, a characteristic which is known to favor cell viability in extrusion bioprinting application [49]. Higher dECM concentration results in solutions with increased zero-shear rate viscosity, while the increase of digestion time leads to less viscous solutions.

dECM-based hydrogels have abundant collagenous proteins that facilitate its self-assembly into crosslinked networks under physiological pH and temperature conditions, which is a particular advantage of these systems [36], [50]. Frequency-dependent oscillatory test showed the typical solid-like behavior of these type of dECM hydrogels, independently of its concentration (storage modulus (G') higher than loss modulus (G'') (figure III.3 D), indicating their ability to retain the shape after printing [34]–[36]. On the other hand, while the increasing of dECM concentration results in hydrogels with higher storage modulus, increasing of digestion time logically decreases it (figure III.3 E), being in accordance with previous works with tendon dECM bioinks that compare different digestion times and hydrogel concentrations to achieve the best condition for bioprinting [34], [35], [40].

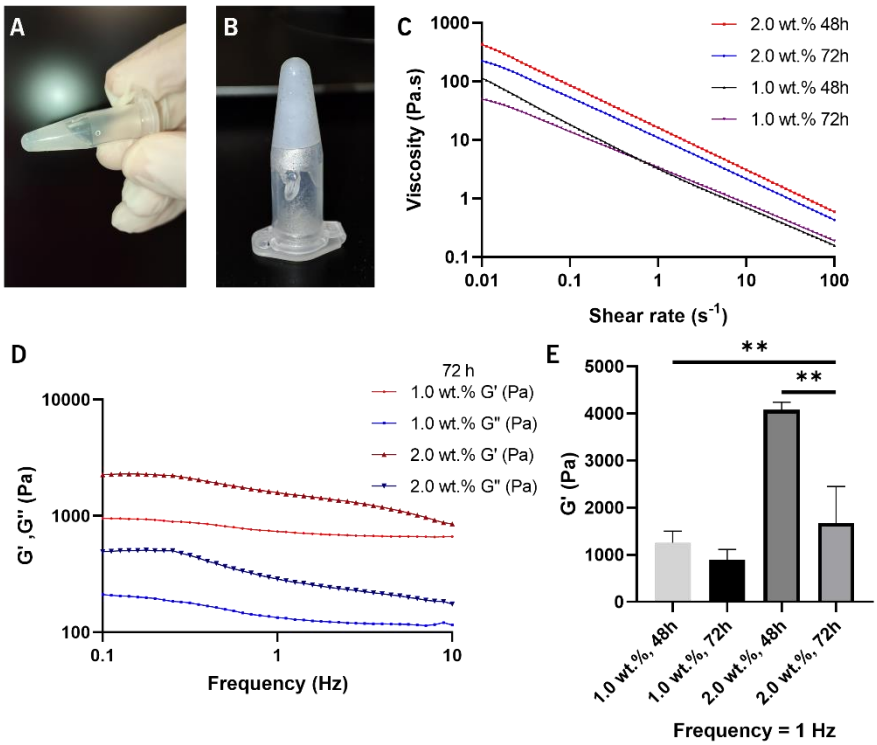

Figure III.3. Characterization of tendon dECM solution. Representation of dECM solution (A) before, and (B) after gelation, forming a consistent hydrogel. (C) Shear viscosity of 1.0 and 2.0 wt. % dECM, digested for 48 h and 72 h, at 4 °C. (D) Frequency-dependent oscillatory shear rheology of 1.0 and 2.0 wt. % dECM digested for 72h and incubated at 37 °C (G': storage modulus, G'': loss modulus). (E) Storage modulus (G') of 1.0 and 2.0 wt. % dECM digested for 48 and 72h, incubated at 37 °C at 1 Hz of frequency (** denotes significance, $p<0.01$).

III.4.3. Tendon-on-CNC-Chip system development

After characterization of the hydrogel formulation, we moved to the development of the microphysiological systems. In this work, two different microphysiological systems were developed: a monoculture system intended to recreate the physiological characteristics of healthy tendon microenvironment; and a multicellular system to study the crosstalk between the tendon stroma and cells from the extrinsic compartment namely, vascular cells.

In extrusion bioprinting processes, the higher the viscosity of the bioink precursor solution, the higher are the pressures required to extrude it, leading to increased shear stresses that can negatively affects cells viability [49]. Thus, a compromise between dECM concentration and digestion time should be achieved to allow bioprinting without exerting excessive cell stress and, at the same time, the bioink

should provide a proper cell niche to sustain cells growth and proliferation. The first sept to fabricate the monoculture tendon core system (figure III.4 A) was to test and select the ink formulation that would be more appropriate to enable the proposed concept. Based on the rheological characterization of the inks, the 2.0 wt. % dECM digested for 48 h was judge to be too viscus to be extruded without harming cells, while the 1.0 wt. % dECM digested for 72 h resulted in soft hydrogels with very low mechanical integrity. These two formulations were therefore excluded from further testing. For a first assessment on the structural integrity of bioprinted structures, hASCs were suspended in the other two dECM inks, printed within the CNCs fluid gel and then locked into the CNC fibrillar matrix, where they were maintained in culture for 7 days. As show in figure III.4 B, 1.0 wt. % dECM bioink filaments broke and retracted to the corners of the construct, demonstrating that this low dECM concentration hydrogels were unable to support the contractile forces resulting from cells attachment, proliferation and remodeling activity while maintaining the shape fidelity of printed structures. In contrast, the structures printed with the 2.0 wt. % dECM bioink showed no contraction or retraction, maintaining its shape during the culture time (figure III.4 C). To assess the chip microstructure and evaluate if the dECM was able to fibrillate within the CNC support matrix, the acellular dECM ink was printed and locked in this material following the same conditions of the cellular constructs. Their cross-sections were then analyzed by SEM after critical point drying and cryogenic fracturing. The exposed cross-section of the chip (figure III.4 D) shows a hierarchical fibrous arrangement, with the fibrillated dECM embedded within a nanoscale CNC fibrillar network. The interface between these two materials (figure III.4 E) shows some physical entanglement that occurs during the simultaneous gelation of dECM and the self-assembling of CNCs. As demonstrated in a previous work developed by our group, this CNC support media successfully embedded the printed material, and presented a well-developed hierarchical fibrillar architecture with entangled fibrils, mimicking the native ECM [16].

The viability in the monoculture system was assessed by live/dead assay, showing high cell viability after the printing process (figure III.4 F) and during culture up to 11 days (figure III.4 G, H). To confirm the ability of this system to support cells growth and proliferation, the system was cultured for 21 days. As CNCs platform is transparent, it allows to optical monitoring the samples throughout the culture time. At day 0 (figure III.4 I), the printed cells look homogenously distributed throughout the hydrogel. After 7 days of culture (figure III.4 J) the cells started to stretch, showing elongated morphology, and stablished cell-to-cell contacts. At the end of the 21 days of culture (figure III.4 K), the printed patterns are densely filled with cells, nicely stretched and aligned along the filament direction without visible contraction of dECM bioink within CNCs, in contrast with what happens when the dECM bioink is directly

cultured on well-plates (figure III.2 P), or a lower concentration of dECM hydrogel is applied in the system (figure III.4 B). This marked cell elongation and alignment along the filament direction shows that the synergy between dECM cues and printed patterns is able to induce anisotropic cells organization resembling tenocytes morphology in tendon tissues [36], [40].

Next, we aimed to demonstrate the versatility of the proposed tendon-on-CNC-chip platform in terms of processability in cell biology characterization workflows. Standard staining and immunohistochemistry labeling can be directly performed and analyzed by microscopy techniques on chip without disturbing the printed constructs. However, these systems can also undergo typical histological sectioning protocols without requiring the previous release of the cultured structures, which is an advantage over general organ/tissue-on-chip housed on plastic microfluidic devices [16]. To demonstrate this versatility, histological sections of the tendon-on-CNC-chip cultured for 21 days were stained with MT (figure III.4 L, M) and H&E (figure III.4 N) to assess the collagenous structure and ECM organization of the tendon core. Interestingly, a recent study has compared the behavior of cell-seeded high density collagen gels when unclamped or clamped to provide uniaxial tension [48]. As expected, when unclamped the gels suffered significant volume contraction, and the structure remained unorganized, while clamped constructs developed hierarchical collagen organizations similar to native juvenile tendon tissue [48]. Similarly, our dECM hydrogel also suffers significant contraction with unorganized cells when unclamped, as shown above for the dECM hydrogels cultured in well-plates (figure III.2 N, P), while when printed within CNCs fluid gel, the constructs remodel into highly organized and dense collagen (blue) filaments showing high cell density (red) (figure III.4 L, M). In these systems, the fixed path in the CNCs matrix act as “anchors” that contributes to maintain the bioink under tension during culture, allowing the densification of the collagen structure (figure III.4 L, M). MT staining also shows that the cells and the collagenous structure establish close connection with the CNCs fibrillar material (arrow: figure III.4 M), while H&E sating of cross sections of embedded filaments (figure III.4 N) confirms that dECM hydrogel do not undergo extensive volume contraction, remaining entangled with the CNCs network (arrows) and demonstrating interfacial integration between the two materials. Moreover, the high uniaxial alignment and elongated cell morphology was also confirmed by directionality analysis of cell cytoskeleton in the constructs (figure III.4 O, P), suggesting the adoption of a tendon lineage-specific morphology.

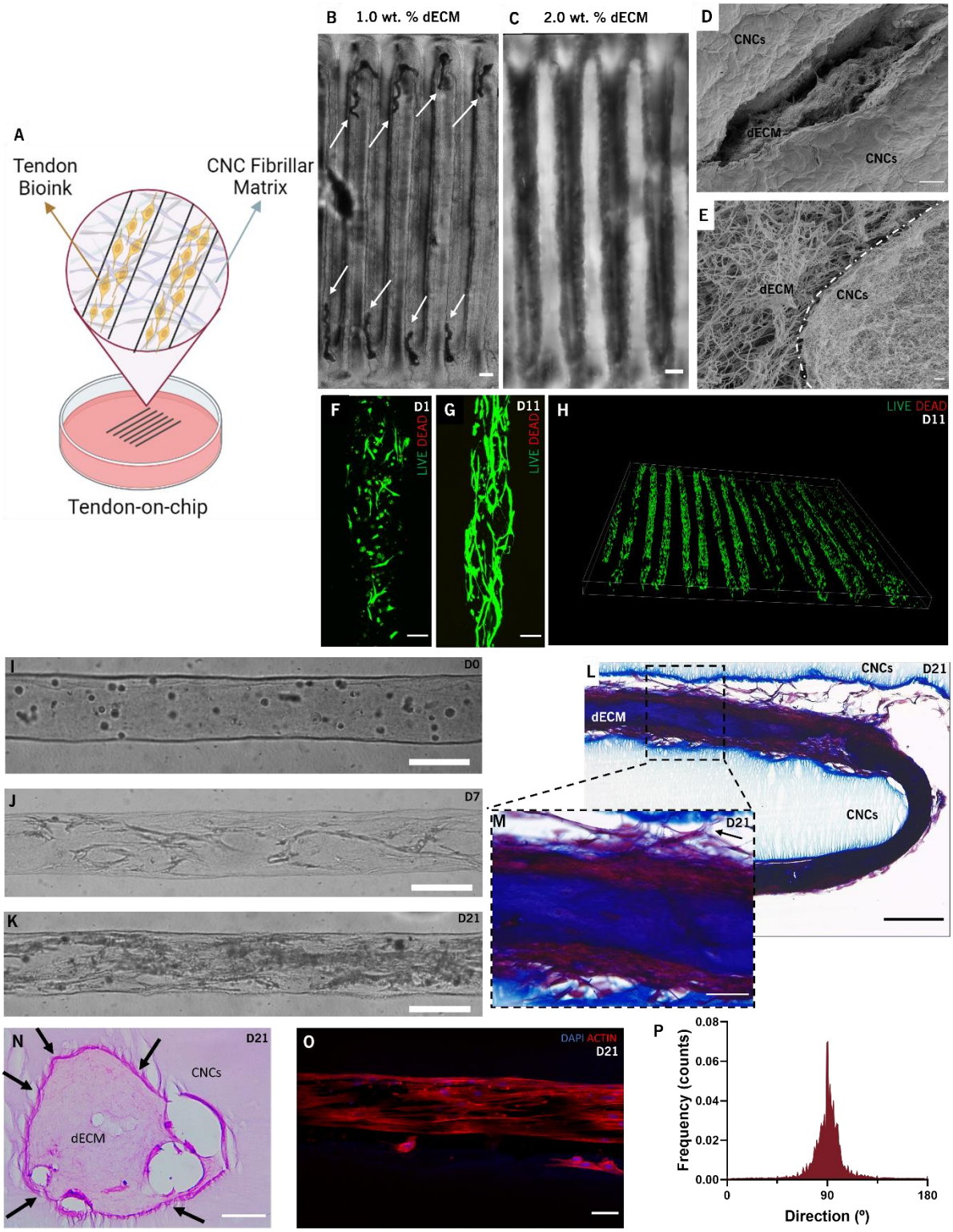

Figure III.4. Development of the monoculture tendon-on-chip model. (A) Schematic representation of the monoculture system development. Brightfield confocal laser microscopy (CLM) images of (B) 1.0 wt. % dECM bioink after 7 days of culture, showing contraction and retraction of the hydrogel (arrows) and (C) of 2.0 wt. % dECM bioink, showing no contraction after 7 days of culture. SEM images of (D) dECM

hydrogel embedded within CNCs fibrillar matrix, and (E) interface between dECM (left) and CNCs fibrillar matrix (right). Evaluation by CLM of Bioprinting process in cells viability by Live/Dead staining at day 1 (F) and day 11 (G, H) of culture, with the 3D reconstruction of the full tile of the system (H) (green: live cells, red: dead cells). Transmitted light microscopy images of the optical monitoring of cellular behavior at day 0 (I), day 7 (J), and day 21 (K) of culture. (L, M) Histological longitudinal section of the monoculture construct after 21 days of culture stained with MT. (N) Histological cross section of the monoculture system after 21 days of culture, stained with H&E. (O) CLM image of cellular cytoskeleton organization after 21 days of culture, and (P) respective directionality analysis. (D, N, O, M) scale bar: 50 µm. (E) scale bar: 1 µm. (B, C) scale bar: 1 mm. (F, G) scale bar: 100 µm. (I, J, K, L) scale bar: 200 µm.

As mentioned before, human tenocytes are scarce, difficult to obtain from a healthy donor, and hard to maintain its phenotype *in vitro*, which limits their application in tendon tissue engineering strategies [37]. On the other hand, mesenchymal stem cells (MSCs) are characterized as undifferentiated cells having the ability to differentiate into multiple tissue lineages such as cartilage, bone, muscle, ligament, tendon, adipocytes or endothelial phenotypes [43], [51]–[53]. A commonly used type of MSCs are hASCs, which are widely available and easy to obtain, making them a very appealing stem cell source to be used in tissue engineering and regenerative medicine strategies [38]. Following the strategy of previous studies [34]–[36], [54], our hypothesis was that the biophysical and biochemical cues of the tendon dECM would synergistically guide hASCs differentiation towards the tenogenic lineage without requiring additional supplementation with biological factors. To assess the tenogenic commitment of hASCs in our MPS, both gene expression and immunolabeling of the system was performed. Gene expression analysis (figure III.5 A) show a significant increase in the expression of TNMD along the culture time, while the expression of SCX significantly increases until day 4 of culture, followed by a slight decrease. The variation of COL-III expression is not significant during the culture time, while the COL-I significantly increases along the time, suggesting an increase in the maturation of the construct, as in mature tendons, where the collagen type I is predominant [2]. For the immunolabeling, the protein expression of Scleraxis (SCX) and Tenomodulin (TNMD), two of the most tendon related markers, were assessed in both the CNC embedded constructs and their histological sections after 21 days of culture. As expected, the monoculture system showed the expression of both markers (figure III.5 B-E), demonstrating that the synergistic effects of the tendon dECM and construct architecture are able to successfully induce the commitment of hASCs toward the tenogenic lineage.

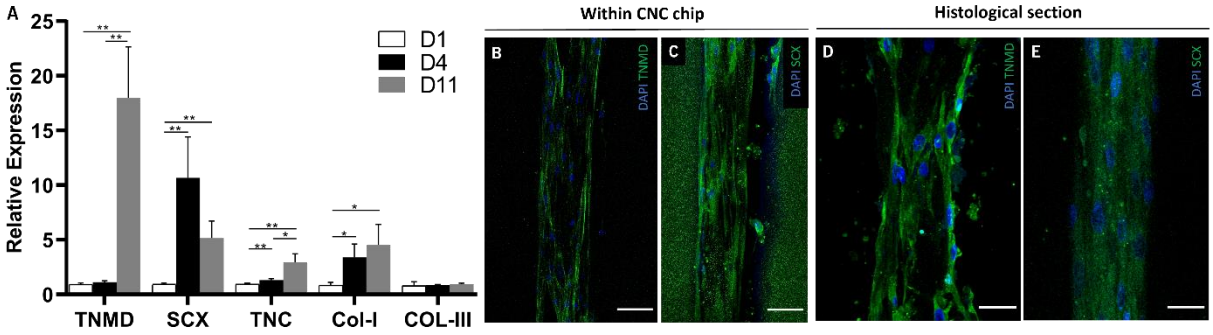

Figure III.5. *In vitro* evaluation and gene expression of monoculture systems. (A) Gene expression of monoculture systems. Evaluation of protein expression of SCX (C, E) and TNMD (B, D), by directly staining the chip (B, C) or on their respective histological sections (D, E). Scale Bar: (B, C) 75 µm; (D, E) 25 µm. Statistical significance: * $p \leq 0.1$, ** $p \leq 0.01$, *** $p \leq 0.001$, and **** $p \leq 0.0001$.

Tendon is an hypovascular tissue in which blood vessels are mainly present in the endo and epitenon. However, as in the other tissues, cells, GFs, cytokines, nutrients and oxygen are still delivered through the blood supply network [55]. One of the hallmarks of tendinopathy is the observed increased vascularization and scar tissue formation [4]. On the other hand, there is also an increased vascularization and cellularization in tendon development [56]. The incorporation of vascular cell populations should thus be considered when build physiologically relevant *in vitro* models of tendon health and disease [55]. For this reason, endothelial cells were used here to build a multicellular MPS and study their crosstalk with the tendon core in a biomimetic compartmentalized construct (figure III.6 A). Unexpectedly, during culture time endothelial cells started to migrate towards the tendon compartment, showing the existence of a chemoattraction effect between these two systems and the ability of endothelial cells to physically remodel the CNC network. However, these cells seemed to accumulate and stop migrate at the interface of tendon lines as soon as it achieved the tendon compartment (figure III.6 B). To better understand the behavior and positioning of the endothelial cells, multicellular systems were stained for CD31 (red) as an endothelial marker, while F-actin (green) was stained to visualize the cytoskeleton of whole cells in the system. Fluorescence confocal microscopy images showed that although endothelial cells migrate towards the tendon compartment, there is not a significant invasion of these structures (figure III.6 C, D), as they accumulate in the interface of the tendon core compartment instead of crossing the barrier (figure III.6 E). On the other hand, the tendon compartment is filled with hASCs, nicely stretched and aligned along the constructs (figure III.6 F). To evaluate the potential effects stemming from this cellular crosstalk on the tenogenic commitment of hASCs, changes on gene expression of tendon core compared to monoculture were assessed and histological sections of the multicellular MPS were immunolabeled for

tenogenic markers. We first evaluated the expression of vascular endothelial growth factor (VEGF) by hASCs. VEGF is one of the most vital angiogenic factors that regulate blood vessel formation in tendon healing [57]. From the protein family of VEGF, VEGF-A is among the most potent stimulators of angiogenesis, and is not only expressed during tendon development, but also during tendinopathic diseased states or tendon healing [57]. While in the monoculture system VEGF-A expression was below the detection limit, in the multicellular system it is significantly increased after 11 days of culture (Figure III.6 I). This suggests that soluble biochemical factors secreted by endothelial cells activate VEGF signaling on the core hASCs. Like in the monoculture constructs, cells of the tendon compartment in this multicellular system also shows the expression of SCX (figure III.6 G) and TNMD (figure III.6 H) after 21 days of culture. Moreover, gene expression assays demonstrated that the expression of tenogenic markers (figure III.6 J) was upregulated, in comparison to the monoculture system, showing that the crosstalk with the vascular compartment favors the tenogenesis and maturation of the tendon construct. Interestingly, similar effects have been previously reported when tenocytes were co-cultured together with HUVECs on fibrous scaffolds [58]. TNMD is known to be positively regulated by the transcription factor SCX in a tendon cell-lineage-dependent manner [59]. Here, an increase on the expression of SCX is also followed by a significant increase of TNMD. TNMD is a type II transmembrane glycoprotein containing a C-terminal antiangiogenic domain [60]. This antiangiogenic characteristic of TNMD, combined with its strong presence in the multicellular system might explain the fact that the endothelial cells start to accumulate at the interface with the tendon core (figure III.6 E), instead of invading it. However, this hypothesis remains to be proved in future works. Besides these two tenogenic markers, the gene of the main tendon matrix-related markers where also upregulated namely, the fibrillar COL-1 and COL-3, and glycoprotein TNC. The specific role of TNC in tendon development and healing still needs to be clarified, but high levels of TNC expression have been found in both development and diseased tendons [60]. Although not entirely conclusive, these results suggest that endothelial cell can establish a compartmentalized biochemical crosstalk with the tendon core constructs but do not hinder their tenogenic commitment. It is likely that this MPS is recreating a state of tendon development, although its evolution to a disease situation for longer culture periods cannot be excluded and should be tested in future works.

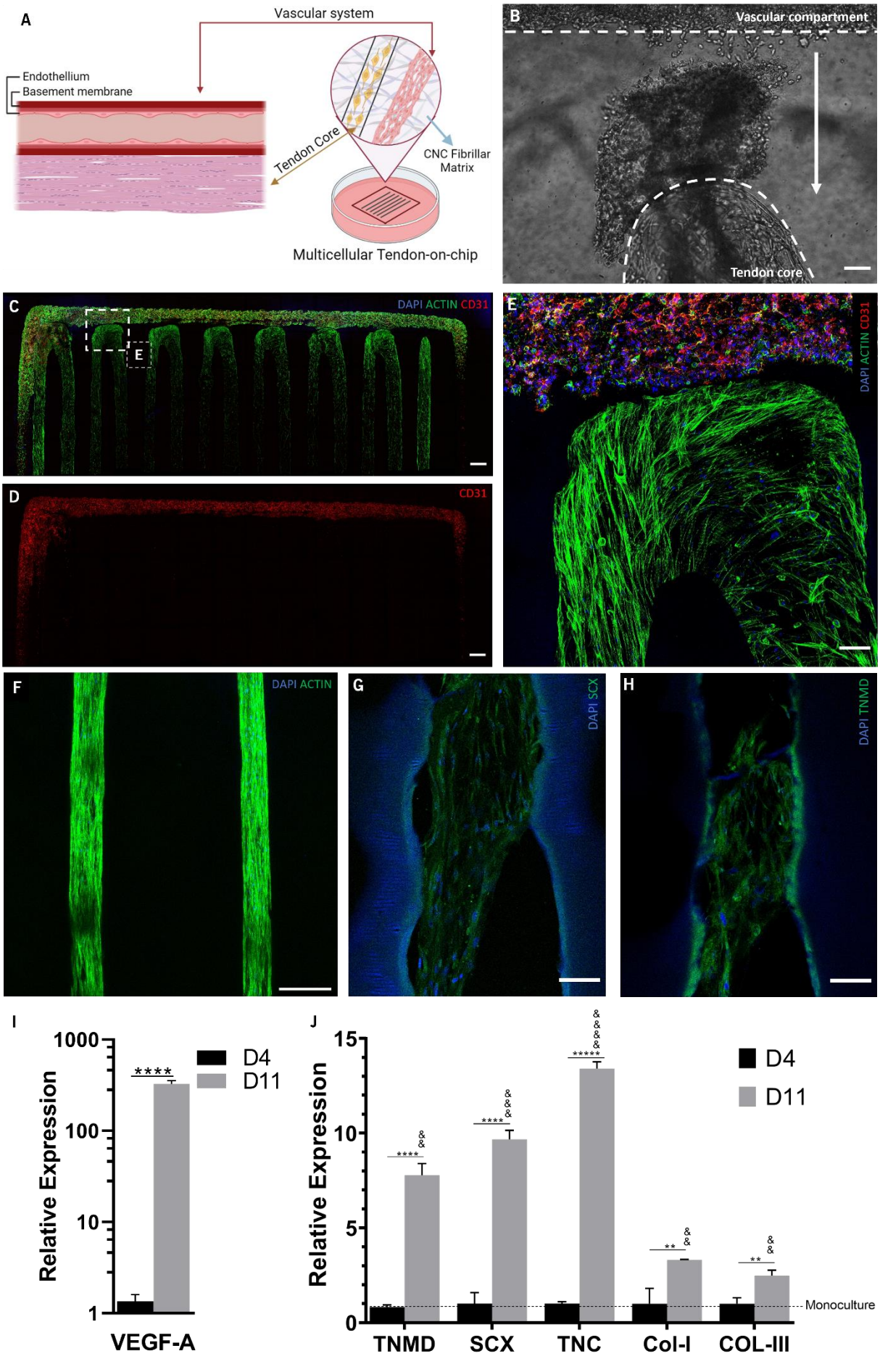
A
Vascular system
Endothellium
Basement membrane
Tendon Core
CNC Fibrillar Matrix
Multicellular Tendon-on-chip
B
Vascular compartment
Tendon core
C
DAPI ACTIN CD31
E
D
CD31
E
DAPI ACTIN CD31
F
DAPI ACTIN
G
DAPI SCX
H
DAPI TNMD
I
Relative Expression
1000
100
10
1
****
D4
D11
VEGF-A
J
Relative Expression
15
10
5
0
D4
D11
Monoculture
TNMD
SCX
TNC
Col-I
COL-III

Figure III.6. *In vitro* evaluation and gene expression of the multicellular systems. Schematic representation of multicellular constructs design (A). Transmitted light microscopy images of endothelial cells migrating towards the tendon compartment at day 11 of culture (B). CLM image of the multicellular construct (C), with focus on endothelial cells spatial distribution (D) in the system, at day 21 of culture. CLM image of the interface between the vascular compartment and the tendon core compartment (E). CLM image of tendon core compartment at day 21 (F). Evaluation of tenogenic differentiation of hASCs after 21 days of culture by immunolabeling of SCX (G) and TNMD (H) in histological section. Scale bar: (C, D) 1 mm; (B, E) 100 µm; (F) 250 µm; (G, H) 75 µm. Gene expression of VEGF-A (I) and tenogenic (J) markers in multicellular systems. & indicate statistical significance relative to monoculture. * indicate statistical significance relative to time. Statistical significance: * $p \leq 0.1$, ** $p \leq 0.01$, *** $p \leq 0.001$, and **** $p \leq 0.0001$; & $p \leq 0.1$, && $p \leq 0.01$, &&& $p \leq 0.001$, and &&&& $p \leq 0.0001$.

The two models developed in this work can be useful, not only to study tendon physiology and pathophysiology, but also to study the effect of new drugs, and predict its effect *in vivo*. For example, a synthetic microRNA (miR) mimic to miR-29a initiated a phase I clinical study, as the reduction of this molecule leads to development of tendinopathy by influencing the expression of collagen type III, over-expressing it, and its reintroduction reverse the collagen switch [61], [62]. The effect of miR-29a could be predicted with our tendon-on-CNC-chip models, predicting more accurate results, and avoiding the excessive tests in animals in pre-clinical tests. Adding to this, anti-inflammatory and systematic drugs in tendinopathy treatments only have been demonstrated in the short term, but still remains a lack in the long term studies that could be overtaken by using tendon-on-chip models [62].

III.5. Conclusions

In this work, we were able to successfully develop two tendon-on-chip systems. First, we developed a tendon dECM solution, suitable for bioprinting from porcine derived tendons. Then, we developed a monoculture system to not only evaluate the effect of tendon dECM in the tenogenic commitment of stem cells, but also to mimic the tendon microenvironment. This monoculture system proved to represent a mature tendon tissue, by expressing two of the main tendon related markers (TNMD and SCX), and by expressing increasing values of mature collagen (COL-I), while the immature collagen type (COL-III) remained stable along the culture time. Secondly, we increased the complexity of our system and made it multicellular by adding endothelial cells, to study the interaction between the tendon tissue and the vascular system. Remarkably, the endothelial cells migrated towards the tendon compartment,

without invading it, suggesting an antiangiogenic effect from the tendon core compartment, that should be further studied in detail. On the other hand, the presence of endothelial cells improved the tenogenic commitment of stem cells by significantly increasing the expression of both tenogenic and matrix deposition markers, and also showed a significant increase of VEGF–A, responsible for angiogenesis in tendon development and healing in a tendinopathy situation. Further tests need to be performed to understand the mechanism beyond this system, to better define if we face a tendon development or a tendinopathy model. In the future work, the complexity of the system can be increased by incorporating other relevant tendon cell populations that could be useful for the study of tendon physiology and pathophysiology. When completely understood, these models can be useful for testing new drugs for the treatment of tendinopathy.

III.6. References

[1] T. Stauber *et al.*, "Extrinsic Macrophages Protect While Tendon Progenitors Degrade: Insights from a Tissue Engineered Model of Tendon Compartmental Crosstalk," *Adv. Healthc. Mater.*, vol. 10, no. 20, p. 2100741, Oct. 2021, doi: 10.1002/adhm.202100741.

[2] C. Lee, "Tendon physiology and repair," *Orthop. Trauma*, vol. 35, no. 5, pp. 274–281, Oct. 2021, doi: 10.1016/j.mporth.2021.07.003.

[3] D. Docheva, S. A. Müller, M. Majewski, and C. H. Evans, "Biologics for tendon repair," *Adv. Drug Deliv. Rev.*, vol. 84, pp. 222–239, Apr. 2015, doi: 10.1016/j.addr.2014.11.015.

[4] M. Gomez-Florit, C. J. Labrador-Rached, R. M. A. Domingues, and M. E. Gomes, "The Tendon Microenvironment: Engineered In Vitro Models to Study Cellular Crosstalk," *Adv. Drug Deliv. Rev.*, vol. 185, p. 114299, 2022, doi: 10.1016/j.addr.2022.114299.

[5] J. G. Snedeker and J. Foolen, "Tendon injury and repair – A perspective on the basic mechanisms of tendon disease and future clinical therapy," *Acta Biomater.*, vol. 63, pp. 18–36, Nov. 2017, doi: 10.1016/j.actbio.2017.08.032.

[6] N. L. Millar *et al.*, "Tendinopathy," *Nat. Rev. Dis. Prim.*, vol. 7, no. 1, p. 1, Dec. 2021, doi: 10.1038/s41572-020-00234-1.

[7] S. L. Wunderli, U. Blache, and J. G. Snedeker, "Tendon explant models for physiologically relevant in vitro study of tissue biology – a perspective biology – a perspective," *Connect. Tissue Res.*, vol.

61, no. 3–4, pp. 262–277, 2020, doi: https://doi.org/10.1080/03008207.2019.1700962.

[8] L. Yao, C. S. Bestwick, L. A. Bestwick, N. Maffulli, and R. M. Aspden, "Phenotypic Drift in Human Tenocyte Culture," *Tissue Eng.*, vol. 12, no. 7, pp. 1843–1849, Jul. 2006, doi: 10.1089/ten.2006.12.1843.

[9] J. Parrish, K. Lim, B. Zhang, and M. Radisic, "New Frontiers for Biofabrication and Bioreactor Design in Microphysiological System Development," *Trends Biotechnol.*, vol. 37, no. 12, pp. 1327–1343, 2019, doi: 10.1016/j.tibtech.2019.04.009.

[10] V. Mehta and S. N. Rath, "3D printed microfluidic devices: a review focused on four fundamental manufacturing approaches and implications on the field of healthcare," *Bio-Design Manuf.*, vol. 4, no. 2, pp. 311–343, Jun. 2021, doi: 10.1007/s42242-020-00112-5.

[11] B. Zhang, A. Korolj, B. F. L. Lai, and M. Radisic, "Advances in organ-on-a-chip engineering," *Nat. Rev. Mater.*, vol. 3, no. 8, pp. 257–278, 2018, doi: 10.1038/s41578-018-0034-7.

[12] Y. Zhao *et al.*, "Engineering microenvironment for human cardiac tissue assembly in heart-on-a-chip platform," *Matrix Biol.*, vol. 85–86, pp. 189–204, 2020, doi: 10.1016/j.matbio.2019.04.001.

[13] S. Piluso *et al.*, "Mimicking the Articular Joint with In Vitro Models," *Trends Biotechnol.*, vol. 37, no. 10, pp. 1063–1077, Oct. 2019, doi: 10.1016/j.tibtech.2019.03.003.

[14] A. McCormack, C. B. Highley, N. R. Leslie, and F. P. W. Melchels, "3D Printing in Suspension Baths: Keeping the Promises of Bioprinting Afloat," *Trends Biotechnol.*, vol. 38, no. 6, pp. 584–593, 2020, doi: https://doi.org/10.1016/j.tibtech.2019.12.020.

[15] J. Kajtez *et al.*, "Embedded 3D Printing in Self-Healing Annealable Composites for Precise Patterning of Functionally Mature Human Neural Constructs," *Adv. Sci.*, vol. 2201392, p. 2201392, Jun. 2022, doi: 10.1002/advs.202201392.

[16] S. M. Bakht, M. Gomez-Florit, T. Lamers, R. L. Reis, R. M. A. Domingues, and M. E. Gomes, "3D Bioprinting of Miniaturized Tissues Embedded in Self-Assembled Nanoparticle-Based Fibrillar Platforms," *Adv. Funct. Mater.*, vol. 31, no. 46, 2021, doi: 10.1002/adfm.202104245.

[17] T. Jiang *et al.*, "Engineering bioprintable alginate/gelatin composite hydrogels with tunable mechanical and cell adhesive properties to modulate tumor spheroid growth kinetics," *Biofabrication*, vol. 12, no. 1, p. 15024, 2019, doi: 10.1088/1758-5090/ab3a5c.

[18] C. Antich *et al.*, "Bio-inspired hydrogel composed of hyaluronic acid and alginate as a potential bioink for 3D bioprinting of articular cartilage engineering constructs," *Acta Biomater.*, vol. 106, pp. 114–123, 2020, doi: https://doi.org/10.1016/j.actbio.2020.01.046.

[19] G. R. López-Marcial, A. Y. Zeng, C. Osuna, J. Dennis, J. M. García, and G. D. O'Connell, "Agarose-Based Hydrogels as Suitable Bioprinting Materials for Tissue Engineering," *ACS Biomater. Sci. Eng.*, vol. 4, no. 10, pp. 3610–3616, Oct. 2018, doi: 10.1021/acsbiomaterials.8b00903.

[20] M. E. Prendergast, M. D. Davidson, and J. A. Burdick, "A biofabrication method to align cells within bioprinted photocrosslinkable and cell-degradable hydrogel constructs via embedded fibers," *Biofabrication*, vol. 13, no. 4, 2021, doi: 10.1088/1758-5090/ac25cc.

[21] D. Petta, U. D'Amora, L. Ambrosio, D. W. Grijpma, D. Eglin, and M. D'Este, "Hyaluronic acid as a bioink for extrusion-based 3D printing," *Biofabrication*, vol. 12, no. 3, p. 32001, 2020, doi: 10.1088/1758-5090/ab8752.

[22] A. Sadeghianmaryan *et al.*, "Extrusion-based printing of chitosan scaffolds and their in vitro characterization for cartilage tissue engineering," *Int. J. Biol. Macromol.*, vol. 164, pp. 3179–3192, 2020, doi: https://doi.org/10.1016/j.ijbiomac.2020.08.180.

[23] F. Pahlevanzadeh *et al.*, "Three-Dimensional Printing Constructs Based on the Chitosan for Tissue Regeneration: State of the Art, Developing Directions and Prospect Trends," *Materials (Basel).*, vol. 13, no. 11, 2020, doi: 10.3390/ma13112663.

[24] N. Contessi Negrini, N. Celikkin, P. Tarsini, S. Farè, and W. Święszkowski, "Three-dimensional printing of chemically crosslinked gelatin hydrogels for adipose tissue engineering," *Biofabrication*, vol. 12, no. 2, p. 25001, 2020, doi: 10.1088/1758-5090/ab56f9.

[25] A. Leucht, A.-C. Volz, J. Rogal, K. Borchers, and P. J. Kluger, "Advanced gelatin-based vascularization bioinks for extrusion-based bioprinting of vascularized bone equivalents," *Sci. Rep.*, vol. 10, no. 1, p. 5330, 2020, doi: 10.1038/s41598-020-62166-w.

[26] N. Diamantides, C. Dugopolski, E. Blahut, S. Kennedy, and L. J. Bonassar, "High density cell seeding affects the rheology and printability of collagen bioinks," *Biofabrication*, vol. 11, no. 4, p. 45016, 2019, doi: 10.1088/1758-5090/ab3524.

[27] S. Zhang, D. Huang, H. Lin, Y. Xiao, and X. Zhang, "Cellulose Nanocrystal Reinforced Collagen-Based Nanocomposite Hydrogel with Self-Healing and Stress-Relaxation Properties for Cell

Delivery," *Biomacromolecules*, vol. 21, no. 6, pp. 2400–2408, Jun. 2020, doi: 10.1021/acs.biomac.0c00345.

[28] A. J. Vernengo, S. Grad, D. Eglin, M. Alini, and Z. Li, "Bioprinting Tissue Analogues with Decellularized Extracellular Matrix Bioink for Regeneration and Tissue Models of Cartilage and Intervertebral Discs," vol. 1909044, 2020, doi: 10.1002/adfm.201909044.

[29] S. Gupta, H. Alrabaiah, M. Christophe, M. Rahimi-Gorji, S. Nadeem, and A. Bit, "Evaluation of silk-based bioink during pre and post 3D bioprinting: A review," *J. Biomed. Mater. Res. Part B Appl. Biomater.*, vol. 109, no. 2, pp. 279–293, Feb. 2021, doi: https://doi.org/10.1002/jbm.b.34699.

[30] P. N. Bernal *et al.*, "Volumetric Bioprinting of Organoids and Optically Tuned Hydrogels to Build Liver-Like Metabolic Biofactories," *Adv. Mater.*, 2022, doi: 10.1002/adma.202110054.

[31] H. Ravanbakhsh *et al.*, "Freeform cell-laden cryobioprinting for shelf-ready tissue fabrication and storage," *Matter*, vol. 5, no. 2, pp. 573–593, 2022, doi: 10.1016/j.matt.2021.11.020.

[32] C. Mota, S. Camarero-Espinosa, M. B. Baker, P. Wieringa, and L. Moroni, "Bioprinting: From Tissue and Organ Development to in Vitro Models," *Chem. Rev.*, vol. 120, no. 19, pp. 10547–10607, Oct. 2020, doi: 10.1021/acs.chemrev.9b00789.

[33] B. Kang *et al.*, "Facile Bioprinting Process for Fabricating Size-Controllable Functional Microtissues Using Light-Activated Decellularized Extracellular Matrix-Based Bioinks," *Adv. Mater. Technol.*, vol. 2100947, pp. 1–13, 2021, doi: 10.1002/admt.202100947.

[34] F. Zhao *et al.*, "Digestion degree is a key factor to regulate the printability of pure tendon decellularized extracellular matrix bio-ink in extrusion-based 3D cell printing," *Biofabrication*, vol. 12, no. 4, p. 045011, Jul. 2020, doi: 10.1088/1758-5090/aba411.

[35] F. Zhao *et al.*, "Comparison of three different acidic solutions in tendon decellularized extracellular matrix bio-ink fabrication for 3D cell printing," *Acta Biomater.*, vol. 131, no. xxxx, pp. 262–275, Sep. 2021, doi: 10.1016/j.actbio.2021.06.026.

[36] S. Chae, Y. Sun, Y.-J. Choi, D.-H. Ha, I. Jeon, and D.-W. Cho, "3D cell-printing of tendon-bone interface using tissue-derived extracellular matrix bioinks for chronic rotator cuff repair," *Biofabrication*, vol. 13, no. 3, p. 035005, Jul. 2021, doi: 10.1088/1758-5090/abd159.

[37] W. Liu, B. Wang, and Y. Cao, "Engineered Tendon Repair and Regeneration," in *Tendon Regeneration*, M. E. Gomes, R. L. Reis, and M. T. B. T.-T. R. Rodrigues, Eds. Boston: Elsevier,

2015, pp. 381–412.

[38] A. I. Gonçalves, R. Costa-Almeida, P. Gershovich, M. T. Rodrigues, R. L. Reis, and M. E. Gomes, "Cell-Based Approaches for Tendon Regeneration," in *Tendon Regeneration*, M. E. Gomes, R. L. Reis, and M. T. B. T.-T. R. Rodrigues, Eds. Boston: Elsevier, 2015, pp. 187–203.

[39] K. M. Hirpara, O. Abouazza, B. O'Neill, and M. O'Sullivan, "A TECHNIQUE FOR PORCINE FLEXOR TENDON HARVEST," *J. Musculoskelet. Res.*, vol. 10, no. 04, pp. 181–186, Dec. 2006, doi: 10.1142/S0218957706001856.

[40] B. Toprakhisar, A. Nadernezhad, E. Bakirci, N. Khani, G. A. Skvortsov, and B. Koc, "Development of Bioink from Decellularized Tendon Extracellular Matrix for 3D Bioprinting," *Macromol. Biosci.*, vol. 18, no. 10, p. 1800024, Oct. 2018, doi: 10.1002/mabi.201800024.

[41] S. Farnebo *et al.*, "Design and Characterization of an Injectable Tendon Hydrogel: A Novel Scaffold for Guided Tissue Regeneration in the Musculoskeletal System," *Tissue Eng. Part A*, vol. 20, no. 9–10, pp. 1550–1561, May 2014, doi: 10.1089/ten.tea.2013.0207.

[42] D. Bondeson, A. Mathew, and K. Oksman, "Optimization of the isolation of nanocrystals from microcrystalline cellulose by acid hydrolysis," *Cellulose*, vol. 13, no. 2, pp. 171–180, 2006, doi: 10.1007/s10570-006-9061-4.

[43] P. P. Carvalho *et al.*, "The Effect of Storage Time on Adipose-Derived Stem Cell Recovery from Human Lipoaspirates," *Cells Tissues Organs*, vol. 194, no. 6, pp. 494–500, 2011, doi: 10.1159/000324892.

[44] B. B. Mendes *et al.*, "Human platelet lysate-based nanocomposite bioink for bioprinting hierarchical fibrillar structures," *Biofabrication*, vol. 12, no. 1, p. 015012, Nov. 2019, doi: 10.1088/1758-5090/ab33e8.

[45] S. F. Badylak, "Xenogeneic extracellular matrix as a scaffold for tissue reconstruction," *Transpl. Immunol.*, vol. 12, no. 3, pp. 367–377, 2004, doi: https://doi.org/10.1016/j.trim.2003.12.016.

[46] P. M. Crapo, T. W. Gilbert, and S. F. Badylak, "An overview of tissue and whole organ decellularization processes," *Biomaterials*, vol. 32, no. 12, pp. 3233–3243, 2011, doi: https://doi.org/10.1016/j.biomaterials.2011.01.057.

[47] J. Fernández-Pérez and M. Ahearne, "The impact of decellularization methods on extracellular matrix derived hydrogels," *Sci. Rep.*, vol. 9, no. 1, p. 14933, 2019, doi: 10.1038/s41598-019-

49575-2.

[48] J. L. Puetzer, T. Ma, I. Sallent, A. Gelmi, and M. M. Stevens, "Driving Hierarchical Collagen Fiber Formation for Functional Tendon, Ligament, and Meniscus Replacement," *Biomaterials*, vol. 269, no. August, p. 120527, Feb. 2021, doi: 10.1016/j.biomaterials.2020.120527.

[49] M. E. Cooke and D. H. Rosenzweig, "The rheology of direct and suspended extrusion bioprinting," *APL Bioeng.*, vol. 5, no. 1, p. 011502, Mar. 2021, doi: 10.1063/5.0031475.

[50] J. Jang, J. Y. Park, G. Gao, and D.-W. Cho, "Biomaterials-based 3D cell printing for next-generation therapeutics and diagnostics," *Biomaterials*, vol. 156, pp. 88–106, Feb. 2018, doi: 10.1016/j.biomaterials.2017.11.030.

[51] Y. W. Eom *et al.*, "Rapid isolation of adipose tissue-derived stem cells by the storage of lipoaspirates," *Yonsei Med. J.*, vol. 52, no. 6, pp. 999–1007, 2011, doi: 10.3349/ymj.2011.52.6.999.

[52] S. Kern, H. Eichler, J. Stoeve, H. Klüter, and K. Bieback, "Comparative Analysis of Mesenchymal Stem Cells from Bone Marrow, Umbilical Cord Blood, or Adipose Tissue," *Stem Cells*, vol. 24, no. 5, pp. 1294–1301, 2006, doi: 10.1634/stemcells.2005-0342.

[53] A. I. Gonçalves, A. D. Eren, J. De Boer, R. L. Reis, and M. E. Gomes, "Evaluation of tenogenic differentiation potential of selected subpopulations of human adipose - derived stem cells," no. September 2019, pp. 1–14, 2020, doi: 10.1002/term.2967.

[54] A. Dede Eren *et al.*, "Decellularized Porcine Achilles Tendon Induces Anti-inflammatory Macrophage Phenotype In Vitro and Tendon Repair In Vivo," *J. Immunol. Regen. Med.*, vol. 8, no. January, p. 100027, Jun. 2020, doi: 10.1016/j.regen.2020.100027.

[55] M. Meeremans, G. R. Van de Walle, S. Van Vlierberghe, and C. De Schauwer, "The Lack of a Representative Tendinopathy Model Hampers Fundamental Mesenchymal Stem Cell Research," *Front. cell Dev. Biol.*, vol. 9, p. 651164, May 2021, doi: 10.3389/fcell.2021.651164.

[56] N. Maffulli, P. Renström, and W. B. Leadbetter, *Tendon Injuries*. London: Springer-Verlag, 2005.

[57] X. Liu *et al.*, "The Role of Vascular Endothelial Growth Factor in Tendon Healing.," *Front. Physiol.*, vol. 12, p. 766080, 2021, doi: 10.3389/fphys.2021.766080.

[58] S. Wu, Y. Wang, P. N. Streubel, and B. Duan, "Living nanofiber yarn-based woven biotextiles for

tendon tissue engineering using cell tri-culture and mechanical stimulation," *Acta Biomater.*, vol. 62, pp. 102–115, 2017, doi: https://doi.org/10.1016/j.actbio.2017.08.043.

[59] C. Shukunami, A. Takimoto, M. Oro, and Y. Hiraki, "Scleraxis positively regulates the expression of tenomodulin, a differentiation marker of tenocytes," *Dev. Biol.*, vol. 298, no. 1, pp. 234–247, 2006, doi: https://doi.org/10.1016/j.ydbio.2006.06.036.

[60] B. Rothrauff, G. Yang, and R. Tuan, "Tendon Resident Cells—Functions and Features in Section I—Developmental Biology and Physiology of Tendons," in *Tendon Regeneration: Understanding Tissue Physiology and Development to Engineer Functional Substitutes*, 2015, pp. 41–76.

[61] N. L. Millar, G. A. C. Murrell, and I. B. Mcinnes, "Inflammatory mechanisms in tendinopathy – towards translation," *Nat. Publ. Gr.*, vol. 13, no. 2, pp. 110–122, 2017, doi: 10.1038/nrrheum.2016.213.

[62] B. John *et al.*, "Review : Emerging concepts in the pathogenesis of tendinopathy ScienceDirect The Surgeon , Journal of the Royal Colleges of Surgeons of Edinburgh and Ireland Review : Emerging concepts in the pathogenesis of tendinopathy," *Surg.*, no. June, 2017, doi: 10.1016/j.surge.2017.05.005.

Chapter IV.

General Conclusions

Chapter IV. General conclusions

Tendon pathologies are highly debilitating diseases for which current treatments remains challenging and have poor recovery outcomes. Thus, the development of reliable models for the study of tendon physiology and pathophysiology are highly needed. Numerous strategies have been proposed, including 2D cell cultures, tendon explants or animal models. However, these models have limited predictability and physiological relevance on their extrapolations to human physiology, and animal experimentation are additionally associated with ethical issues. Thus, bioengineered 3D *in vitro* models are emerging as alternative solution to recreate the physiological context of human tissues and organs. Among these models, microphysiological systems such as organs-on-chip are gaining increased interest by the scientific community and pharmaceutical industry.

In this work, we developed a new strategy for the automated biofabrication of tendon microphysiological systems that circumvents the need for the use of microfluidic platforms or microfabrication technologies, which we termed tendon-on-CNC-chip. First, we successfully decellularized porcine tendons, and then developed a tendon dECM hydrogel to be used in bioinks for 3D bioprinting. For the development of a monoculture tendon core system, tendon dECM solution was encapsulated with hASCs and printed embedded within a CNCs fluid gel. This fluid gel can then be solidified by inducing the self-assembly of CNC, locking the embedded freeform structures in a nanofibrillar material. Next, in order to study the interaction between the tendon compartment and the vascular system, endothelial cell structures were printed around the tendon core, creating multicellular systems where cell compartmentalization is made by an ECM mimetic CNC matrix that allows cell communication. The monoculture system showed the commitment of hASCs towards the tenogenic phenotype, as confirmed by the increased expression of the main tendon related markers such as TNMD and SCX over time. In the multicellular system, the presence of endothelial cells upregulated the expression of the main tenogenic markers, comparatively to the monoculture system. Remarkably, the endothelial cells migrated towards the tendon compartment, showing chemoattraction between the two compartments, but the endothelial cells didn't invade the tendon compartment, which can be possibly explained by the antiangiogenic effect of TNMD that was upregulated in this system. The biological data from this multicellular microphysiological system suggest that it might be recreating *in vitro* a situation of tendon development. However, on longer culture time beyond those studied here, this behavior might also progress toward the cell and matrix signature of tendon healing or tendinopathy. Thus, further studies should be developed in order to better characterize our system.

Overall, the biofabrication platform proposed here allows the automated replication of humanized tendon-on-CNC-chip models directly on standard *in vitro* culture supports. We have shown how the fate of hASCs could be successfully guided toward the tenogenic phenotype by the synergy between the biochemical cues of the tendon dECM and the printed patterns, being thus an attractive alternative for tendon *in vitro* modelling. This platform was forward explored to create microphysiological systems that include the tendon core and vascular compartments, allowing to study the crosstalk between these two cell populations of tendon tissue. The work started here opens multiple prospects for future *in vitro* studies aiming at better understating tendon physiology and pathophysiology. For example, the mechanisms of the antiangiogenic effect of TNMD, which remain elusive to date, could be studied in more detail. It would also be interesting to increase the complexity of the system and incorporate other relevant tendon cell populations that could be useful for the study of tendon physiology and pathophysiology. These systems could certainly be useful in the future for testing new therapeutic drugs for the treatment of tendinopathy, like, for example, the treatment miR-29a which is currently in clinical trials [1].

IV.1. References

[1] N. L. Millar, G. A. C. Murrell, and I. B. Mcinnes, “Inflammatory mechanisms in tendinopathy – towards translation,” *Nat. Publ. Gr.*, vol. 13, no. 2, pp. 110–122, 2017, doi: 10.1038/nrrheum.2016.213.